DM

Laponite-based Nanogels for Bone Tissue Regeneration

Optimization and efficacy studies

MASTER DISSERTATION

Fátima José Mendes Ferreira

MASTER IN APPLIED BIOCHEMISTRY

UNIVERSIDADE da MADEIRA

A Nossa Universidade

www.uma.pt

February | 2020

Laponite-based Nanogels for Bone Tissue Regeneration

Optimization and efficacy studies

MASTER DISSERTATION

Fátima José Mendes Ferreira
MASTER IN APPLIED BIOCHEMISTRY

ORIENTATION
Helena Maria Pires Gaspar Tomás

CO-ORIENTATION
Ana Rute de Azevedo Pina Neves

Laponite®-based nanogels for bone tissue regeneration: optimization and efficacy studies

Dissertation submitted to the University of Madeira in fulfilment of the requirements for the degree of Master in Applied Biochemistry

By Fátima José Mendes Ferreira

Work developed under the supervision of

Professor Dr. Helena Maria Pires Gaspar Tomás and

Co-supervised by Dr. Ana Rute de Azevedo Pina Neves

Faculdade de Ciências Exatas e da Engenharia

Centro de Química da Madeira

Universidade da Madeira

Funchal – Portugal

2020

Acknowledgements

Firstly, I would like to thank Professor Helena Tomás for the opportunity to work on this project under her supervision, and to present it in the various conferences, for all the support, assistance and guidance given to me throughout the development of this dissertation.

A sincere thank you to my co-supervisor Dr. Ana Rute Neves. Your patience, advice, teachings and support were crucial in this project and allowed me to gain and improve skills that made me grow professionally and that will be valuable in my future. Thank you for readiness to help, for your comforting and motivating words and for challenging me.

I am profoundly grateful to Master Filipe Olim, without whom this project would have taken longer and been quite more difficult. For his endless patience and constant availability to lend a helping hand and guide me, for his uplifting presence and his friendship.

Thank you to the laboratory technician Paula Andrade, for the patience, attention and availability in providing me the necessary tools for developing this work.

I would like to thank the professors and colleagues from CQM, especially the LBCC colleagues, namely Mariana Vieira, Ana Olival, and Teresa de Abreu for their assistance, availability, advice and contributions to this dissertation as well as their friendship throughout this year.

Thank you to Tiago Henriques for the assistance in the last stages of the laboratory work.

A special thanks to my dear friends, whose support was essential during this year: Emídio Pontes, Francisca Costa, Helena Chá-Chá, Onofre Figueira, Andreia Luís, Sara Fernandes and Rubina Maciel. For their help, patience, support, for listening and for advising in times of need, and celebrating when the opportunities came, for their valuable friendship and company through these years and making this journey far more enjoyable and memorable.

Lastly, I'm deeply grateful to my family: my sister-in-law Ana, and, above all, my mother and my brothers Jorge and Celso. For their endless love and support, their patience, their encouragement and for their kind, calming and comforting words much needed during this year of work, and for the sacrifices and all the efforts they made through the years so I could achieve this, and all my other goals. Thank you so very much. I love you.

Finally, I would like to thank CQM for the tools and the support provided to me during the development of this Master's Dissertation.

This work was supported by *FCT-Fundação para a Ciência e a Tecnologia* (project PEst-OE/QUI/UI0674/2019, CQM, Portuguese Government Funds) and *ARDITI - Agência Regional para o Desenvolvimento da Investigação, Tecnologia e Inovação* (project M1420-01-0145-FEDER-000005-Centro de Química da Madeira-CQM+, Madeira 14-20 Programme).

Presentations in scientific meetings in the scope of this master project:

- Neves, RA., Olim, F., Luís, A., Mendes, F., Rodrigues J., Tomás H. (2018). Marine-based nanomaterials for tissue engineering. MAD-NANO18: Madeira International Conference on Emerging Trends and Future of Nanomaterials for Human Health, Funchal, Madeira.

- Mendes, F. Olim, F., Neves, AR., Rodrigues, J., Tomás, H. (2018). Development of laponite-based nanogels for bone tissue regeneration. MAD-NANO18: Madeira International Conference on Emerging Trends and Future of Nanomaterials for Human Health, Funchal, Madeira.

- Mendes, F., Olim, F., Neves, AR., Rodrigues, J., Tomás., H. (2019). Laponite®-based nanogels for Bone Tissue Regeneration. 6th CQM Annual Meeting, Porto Moniz, Madeira.

- Mendes, F. Olim, F., Neves, AR., Rodrigues, J., Tomás, H. (2019). Laponite®-based nanogels for the treatment of osteoporosis. XXVI Encontro Nacional da SPQ – XXVIENSPQ, Porto.

Abstract

Osteoporosis is the most prevalent disease of the skeletal system, currently affecting millions of people worldwide, causing painful fractures that lead to costly treatments and often to morbidity and loss of independence. With life expectancies gradually increasing and a growing elder population, the incidence of the illness and cost of the treatments associated is expected to rise in the next decades. Out of the therapies currently available, bisphosphonates are the most prescribed, particularly alendronate, for their efficacy and their affordability. However, these drugs are associated with complicated drug regimens and adverse side effects that often discourage patients from correctly following the treatment, as well as low gastrointestinal absorption and bioavailability. Hence, Laponite®-based nanogels conjugated to bisphosphonates are here proposed as new targeted drug delivery systems to overcome the disadvantages associated with bisphosphonates, namely increasing their bioavailability and minimizing their side effects in the organism. The nanogels synthetized displayed high entrapment efficiency of alendronate, with the constituting nanoparticles measuring approximately 180 nm (hydrodynamic diameter), with polydispersity index of 0.4 and a zeta potential of about -51 mV. That size increases drastically when the nanogels are frozen and lyophilized, though it returns to values close to the initial ones, highlighting the nanogel's restructuring properties. Alendronate was successfully conjugated to FITC and used to synthetize fluorescent-labelled nanogels to evaluate the kinetics of cellular uptake and internalization pathways. The preliminary results indicate a maximum uptake after 24 hours of incubation and internalization mainly through the macropinocytosis pathway. The conjugation to the nanogels decreased alendronate's cytotoxicity in Human Mesenchymal Stem Cells and maintained its hemocompatibility. The osteogenic differentiation assays also revealed promising results, with improvements in all assays with exposure to the nanogel, which were also enhanced by the presence of Laponite®.

Keywords: Osteoporosis, Bisphosphonates, Alendronate, Laponite®, Nanotechnology.

Resumo

A osteoporose é a doença do sistema ósseo mais prevalente, afetando atualmente milhões de pessoas mundialmente, causando fraturas dolorosas que requerem tratamentos dispendiosos e, frequentemente, morbidez e perda de autonomia. Com a esperança média de vida a aumentar gradualmente e uma população cada vez mais envelhecida, prevê-se um aumento da sua incidência bem como dos custos associados aos tratamentos. Dos tratamentos atualmente disponíveis, os bisfosfonatos são os mais prescritos, especialmente o alendronato, pela sua eficácia e acessibilidade de custo. No entanto, estes medicamentos estão associados a regimes de toma complexos e efeitos secundários desagradáveis que frequentemente dissuadem os pacientes de seguirem corretamente o tratamento, além de que apresentam uma baixa absorção gastrointestinal e biodisponibilidade. Assim, nanogéis à base de Laponite®são aqui propostos como um novo sistema de entrega direcionada de bisfosfonatos para colmatar os obstáculos a eles associados, nomeadamente aumentando a biodisponibilidade e minimizando os efeitos secundários no organismo. Os nanogéis sintetizados exibiram elevadas eficiências de encapsulação de alendronato, com nanopartículas de aproximadamente 180 nm (diâmetro hidrodinâmico), com índice de polidispersão de 0.4 e carga superficial de cerca de -51 mV. Esse tamanho sofre um aumento drástico quando os nanogéis são congelados e liofilizados, no entanto retorna a valores próximos dos originais, evidenciando a sua capacidade de reestruturação. O alendronato foi também conjugado ao fluoróforo FITC com sucesso e utilizado para sintetizar nanogéis marcados com fluorescência, usados para avaliar a cinética e vias de internalização celular, com resultados preliminares indicando um máximo de uptake após 24 horas de incubação e internalização preferencial através da via macropinocitose. A conjugação aos nanogéis reduziu a citotoxicidade do alendronato em células estaminais mesenquimais humanas, mantendo a sua hemocompatibilidade. A diferenciação osteogénica revelou também resultados promissores, com melhorias em todos os ensaios com incubação com o nanogel, favorecidos também pela presença de Laponite®.

Palavras-Chave: Osteoporose, Bisfosfonatos, Alendronato, Laponite®, Nanotecnologia.

Index

Figures Index

Tables Index

Abreviations

%EE Entrapment Efficiency

α-MEM α-Minimum Essential Medium

AA Antibiotic-antimycotic 100x solution

ACN Acetonitrile

ALD Alendronate

ALP Alkaline Phosphatase

ASTM American Society for Testing and Materials

ATP Adenosine triphosphate

BCA Bicinchoninic Acid

BMD Bone Mineral Density

BMP-2 Bone Morphogenetic Protein 2

BP Bisphosphonate

CD Cyclodextrin

CHCA α-cyano-hydroxy-cinnamic Acid

CHMP Committee for Medicinal Products for Human Use

CLSI Clinical and Laboratory Standards Institute

CRP C-reactive Protein

D_2O Deuterium Oxide

DIVA Dosing Intravenous Administration

DLS Dynamic Light Scattering

DMSO Dimethyl Sulfoxide

DNFB 4-chloro-nitrobenzufurazan

DSPE Distearoylphosphoethanolamine

DXA Dual energy X-ray absorptiometry

ELISA Enzyme Linked Immunosorbent Assay

ELS Electrophoretic Light Scattering

EMA European Medicine Agency

ERETIC Electronic Reference to access *in vivo* Concentrations

ERT Estrogen Replacement Therapy

FACTS Fosamax Actonel Comparison Trial international study

FBS Fetal Bovine Serum

FIT Fracture Intervention Trial

FITC Fluorescein Isothiocyanate

FLEX FIT-Long Term Extension Trial

GI Gastrointestinal

GTP Guanosine trisphosphate

ICSH International Council for Standardization in Hematology

IU International Units

IV Intravenous

HA Hydroxyapatite

HCl Hydrogen Chloride

hMSCs Human Mesenchymal Stem Cells

HRT Hormone Replacement Therapy

IU International units

MALDI-TOF/TOF MS Matrix-Assisted Laser Desorption and Ionization (Time-of-Flight) Mass Spectrometry

MOBILE Monthly Oral Ibandronate in Ladies

MOTION Monthly Oral Therapy with Ibandronate for Osteoporosis INtervention trial

MRI Magnetic Resonance Imaging

NLC Nanostructured Lipid carriers

NMR Nuclear Magnetic Resonance

ONJ Osteonecrosis of the Jaw

OPG Osteoprotegerin

PAMAM Polyamidoamine

PBS Phosphate Buffered Saline

PdI Polydispersity Index

PEG Polyethylene Glycol

PGA Polyglycolic Acid

PLA Polylactic Acid

PLGA Poly(lactic-co-glycolic acid)

PTH Parathyroid Hormone

PTHrP Parathyroid Hormone-related Peptide

qNMR Quantitative Nuclear Magnetic Resonance

RANK Receptor Activator of Nuclear Factor Kappa B

RANKL Receptor Activator of Nuclear Factor Kappa B Ligand

SERM Selective Estrogen Receptor Modulator

SLN Solid-Lipid Nanoparticles

^{99m}Tc Technetium-99m

TEM Transmission Electron Microscopy

TFA Trifluoroacetic Acid

THF Tetrahydrofuran

WHO World Health Organization

1. INTRODUCTION

1.1. Osteoporosis

Osteoporosis is the most common disease of the skeletal system, being characterized by a low bone mineral density (BMD) and microarchitectural deterioration of the bones (Figure 1) that results from a disruption of the bone remodeling process, in which the bone resorption by osteoclasts occurs at a higher rate than the bone formation by osteoblasts (1–3). This leads to an increased vulnerability of the bones to fracture, frequently as a consequence of low energy trauma or in atypical sites, like the vertebrae, whose incidence increases with age after 50 years old (2,4).

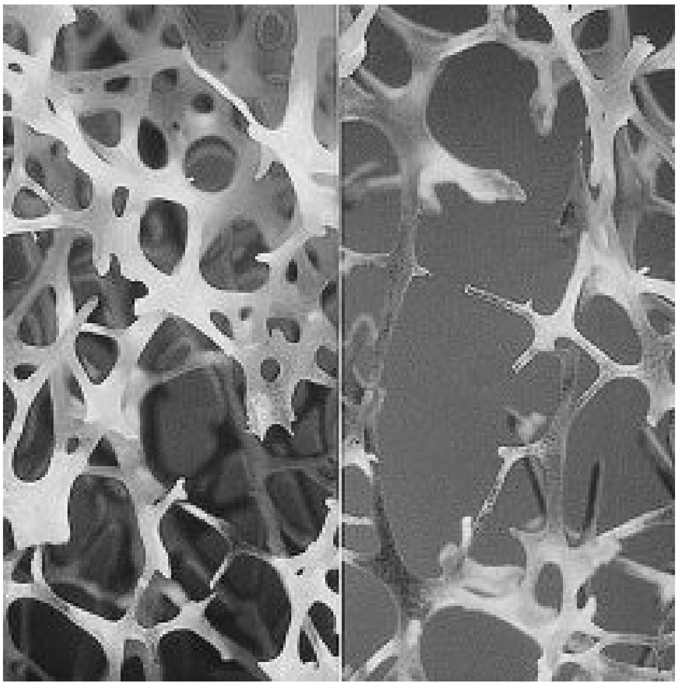

Figure 1 – Normal bone (left) and Osteoporotic bone (right). The progression of the deterioration of the bone microarchitecture with the loss of bone density is clearly visible (5).

In its early stages, this is most commonly asymptomatic, being only diagnosed when a fracture occurs. To facilitate the diagnosis and allow for an earlier treatment, the World Health Organization (WHO) defined four categories that classify the change in BMD when compared to the mean of the healthy reference population (T-score), based on dual energy X-ray absorptiometry (DXA), when applied to sites of relevance, mainly lumbar spine, hip or femoral neck (Figure 2): normal (T-score ≥ -1), osteopenia or low bone mass (T-score < -1 and > -2.5), osteoporosis (T-score ≤ -2.5) and severe osteoporosis (T-score ≤ -2.5 with one or more fragility fractures) (6).

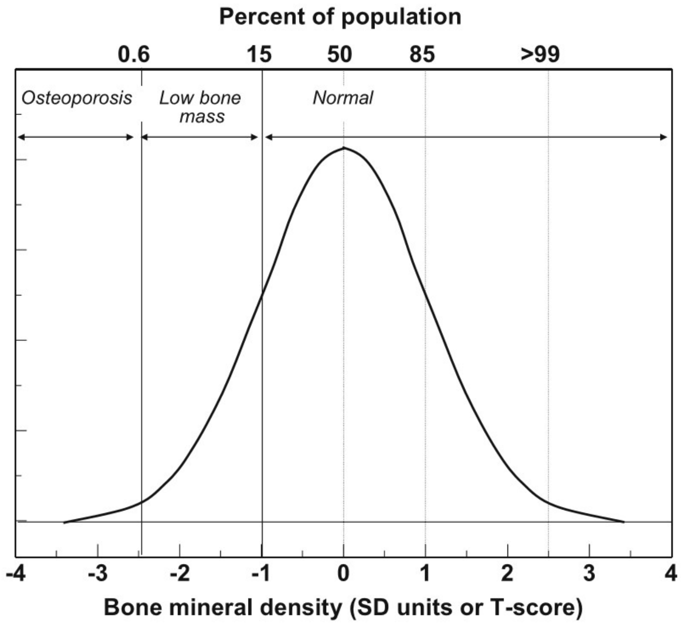

Figure 2 - Distribution of BMD in young healthy women in SD units and threshold values for osteoporosis and low bone mass (osteopenia) (6).

Osteoporosis can be divided into two types: primary and secondary. Primary osteoporosis includes postmenopausal, derived from the significant decrease in estrogen levels associated with menopause, and senile osteoporosis, associated with aging (7). Secondary osteoporosis consists of the disease caused by any factor other than postmenopausal status or aging, mainly deriving from medical conditions, such as celiac disease and hyperparathyroidism, or certain medications, particularly glucocorticoids (1,2,8). Besides these, other factors that contribute to the disease are genetics, as BMD, bone turnover, architecture and skeletal geometry are highly heritable, but also nutritional and vitamin deficiencies, especially calcium and vitamin D, and lifestyle choices such as smoking, alcohol consumption and physical inactivity (6,9).

It was estimated in 1994 that osteoporosis affected approximately 75 million people in the EU, USA and Japan and the more recent estimatives point to 27.6 million people in the EU and 10.2 million in the USA suffering with the disease (10–12). These numbers are predicted to rise in the next decades as life expectancy and the prevalence of elders over 60 years old increase. The number of people over that age is projected to rise between 1990 and 2025 from 30% to 50% in Europe and North America, however that increase will be greater in Africa, Asia and South America, as life conditions improve, thus shifting the burden of the disease to those areas. Osteoporosis is more common in women, with the prevalence being 3 to 4 times greater in women over 50 years old compared to men. The higher risk is partially caused by the peak bone density at skeletal maturity, which is lower than men's, and the loss of bone density resultant from the menopause. It is also due to the fact that women live longer than men, thus living with reduced bone density and subject to other risk factors for longer periods (11,13). Men, however, are more prone to suffer with morbidity and mortality due to osteoporotic fractures than women (14,15).

The main clinical consequence of osteoporosis, and the one that leads to the diagnostic, is the occurrence of fractures, which can be quite detrimental to the patient's life. Osteoporosis causes more than 8.9 million fractures annually worldwide, with estimates pointing to 1 in 3 women over the age of 50 years and 1 in 5 men will experience osteoporotic fractures in their lifetime (16–18). The most common fractures are those of wrist, hip and spinal vertebrae, and frequently the occurrence of an osteoporotic fracture poses a very strong risk factor for the occurrence of future fractures (6,19). Wrist fractures usually result from a fall onto an outstretched hand and, although they most commonly do not require hospitalization and induce lower morbidity, rarely being fatal, they are associated with a high incidence of algodystrophy (20–22). Hip fractures happen usually due to a fall from standing position, though some occur spontaneously. There is a notable increase in mortality related to these fractures, with up to 20% of patients dying in the first year after the surgery, typically due to serious underlying medical conditions, such as embolism and pneumonia. They are also associated with high morbidity with over half of the patients needing assistance in their everyday life (19,23–25). Hip fractures throughout the world are predicted to rise from 1.66 million in 1990 to 6.26 million in 2050 (26). Vertebrae fractures are a most often a consequence of minimal to moderate trauma, that arises from daily activities, for example lifting light objects. The epidemiology of these fractures is not yet well documented due to the lack of consensus on the definition of vertebrae facture as well as due their asymptomatic nature that often causes them to go undiagnosed. Vertebrae fractures often cause pain, loss of height and kyphosis, that when severe can lead to respiratory and gastrointestinal (GI) difficulties, thus being associated with increased mortality and a morbidity increase similar to that of hip fractures (27–32). The majority of fractures occur in elder women, and they have approximately a twice higher risk of sustaining a fracture when compared to men, although there are variations in the difference related to the fracture site.

The cost of osteoporosis, comprising the treatment of incident fractures, pharmacological prevention and long-term fracture care were estimated at an annual cost of €37 billion in the EU, $20 billion dollar in the USA, $4.6 billion in Canada, $1.7 billion in Australia, $11 billion in China and $8 billion in Japan, and similar values are seen in other parts of the world. Hip fractures account for most of the costs of the disease, with over a third of the overall cost, reflecting the constant medical care and nursing home care of patients that is often needed (1,11,33–36). But the expenditures for osteoporotic fractures are rising faster than the general rate of inflation in most countries, and with life expectancy and prevalence of elders steadily increasing worldwide, these costs are expected to rise in the following decades, representing a source of concern for governments. The estimated economic burden of osteoporotic fractures is expected to rise in the next decades to $25 billion in the USA, €46.8 billion in the EU, AUD$3.84 billion in Australia, $20 billion in China (1,11,33,35).

1.2. Currently available Therapies

For the prevention, management and treatment of the disease, the pharmacological therapies currently available are divided into two categories: anabolic drugs, that stimulate bone formation by stimulating osteoblast activity, and antiresorptive drugs, that inhibit osteoclast activity and, consequently, the process of bone resorption (37). These can be preceded and complemented by non-pharmacological approaches, including nutrient supplementation.

Calcium and Vitamin D are essential in the maintenance of skeletal health. Low serum levels of calcium, either due to low calcium intake or vitamin D deficiency, increase parathyroid hormone (PTH) secretion which leads to bone remodeling and bone turnover (9,38). Vitamin D_3 is synthetized in skin tissue when exposed to ultraviolet light. However, that conversion is affected by several factors such as latitude, weather conditions, use of sunscreens, etc., and decreases with aging, particularly in elders who are no longer fully independent and, consequently, less exposed to sunlight. Vitamin D regulates calcium homeostasis, being essential for its absorption in the gastrointestinal tract (9,39). Usually, the recommended daily intake of calcium is 1000 mg for men age 51 to 70 and 1200 mg for women over age 50 as well as men older than 71 years old. For vitamin D, the recommended daily intake is 600 international units (IU) for adults between 51 and 70 years old, and 800 IU over 71 years (6,40). The supplementation with calcium and vitamin D, separately or combined, and its effects on BMD and osteoporotic fracture risk have been widely evaluated with conflicting results, possibly due to different methodologies, diet and living condition of patients and compounds used. Calcium supplementation has been reported to induce a slight benefit in BMD, though the reduction of fracture risk is still debated, as results have not been consistent (41–43). The same was verified for vitamin D, shown to improve BMD, however its benefits on fracture risk have been disputed, due to the varying results obtained (44,45). Its deficiency has also been linked with atrophy of skeletal muscle which increases the risk of falls and, thus, the risk of fractures (20). The effects of combined supplementation have been subject of discussion as well, with contradictory results being reported (45,47,48). Some concerns have been raised for a possible association of calcium supplementation and increased risk of cardiovascular events, reported in some trials while no alteration in risk is described in others, though gastrointestinal side effects, hypercalcemia and kidney stones are reported in various randomized control trials (45,49,50). Despite the conflicting results, and as adequate levels of calcium are required for the efficacy of some pharmacological treatments, calcium and vitamin D supplementation, usually in combination, is still recommended as baseline treatment in situations of deficiency, but also as a complement to those treatments (6,51).

The only anabolic drugs offered at present time are the PTH and its analogues (1-34). PTH is an 84-amino acid polypeptide secreted by the parathyroid gland that regulates calcium homeostasis by stimulating the release of calcium from bone by osteoclasts when its extracellular levels are low, as well as distal renal tubular calcium reabsorption and intestinal calcium absorption. Parathyroid hormone-related peptide (PTHrP) is a 34-amino acid polypeptide produced by various tissues that also regulates calcium homeostasis through the same mechanisms, although it likely does not partake the intestinal calcium absorption. While persistently elevated levels of PTH stimulate osteoclast activity and thus bone resorption by stimulating Receptor Activator of Nuclear Factor Kappa B Ligand (RANKL) and its binding to the Receptor Activator of Nuclear Factor κ B (RANK), and inhibiting Osteoprotegerin (OPG) in the RANKL/RANK/OPG signaling pathway, its intermittent administration causes recurrent rises in serum concentration that mostly enhance bone formation through modulation of the Wnt signaling pathway, resulting in an overall improvement of bone mass and microarchitecture (52–54). The PTH analogues are known as teriparatide, that contains the first 34 amino-acids of the N-terminal part of PTH, and abalobaparatide, a synthetic analogue of PTH related peptide (PTHrP), both acting on PTH1 receptor to stimulate bone formation and remodeling, with the latter being only available in the USA (55–57). Both are administered in low doses through daily subcutaneous injections, in patients with severe osteoporosis, glucorticoid-induced osteoporosis, or when the antiresorptive drugs are not efficient, not tolerated and cases of contraindication, although a recent phase III clinical trial of a once-weekly administration of a 56.5 μg dose of teriparatide exhibited similar efficiency in the reduction of the risk of new vertebral fractures in patients with primary osteoporosis, which could help in the compliance to the treatment from the patients. The use of either drugs is limited to a two-year period, due to concerns of a potential increased risk of osteosarcoma. Afterwards, it should be followed by treatment with an antiresorptive drug in order to maintain the bone density gain previously achieved, and the treatment should not be repeated. Despite their advantages, teriparatide and abalobaratide are not used as a first line treatment due to their high cost and for being contraindicated for other bone diseases, cases of skeletal malignancy and of prior skeletal radiotherapy (9,55,58,59).

Romosozumab is a monoclonal antibody that blocks the effect of sclerostin, a protein that negatively regulates bone formation. It is secreted by osteocytes and inhibits Wnt and bone morphogenic protein (BMP) signaling pathways and, consequently, osteoblast proliferation and activity, causing a decrease in bone formation. By attaching to sclerostin and preventing its action, romosozumab increases formation of new bone and reduces bone resorption, improving bone strength and lessening the risk of fractures (60–62). It is recommended as a subcutaneous injection once a month, to treat postmenopausal osteoporosis in women at high risk of fracture, although it should not be prescribed to patients that have suffered cardiovascular events in the previous year, as one clinical trial suggests an increased risk of serious effects in the cardiovascular system, namely of heart attacks and strokes. Romosozumab was recently approved in the USA, as well as in Japan, South Korea and Canada. In the EU however, the European Medicine Agency's (EMA) Committee for Medicinal Products for Human Use (CHMP) has refused its approval, due to the association with increased risk of serious cardiovascular events (63,64).

Antiresorptive drugs are more numerous and more prescribed than anabolic drugs. Currently available drugs included in this category are Hormone Replacement Therapy, Selective Estrogen Receptor Modulators, Strontium ranelate, Denosumab, Calcitonin and Bisphosphonates (11,65).

In women, the main cause for osteoporosis is the decrease in estrogen production that causes the loss of bone by increasing bone turnover and the rate of bone resorption to higher levels than the rate of formation, and, therefore, the suppression of osteoclast activity through the replacement of estrogen in the system has been used as a treatment, both alone (Estrogen Replacement Therapy, ERT) and in combination with progestrin (Hormone Replacement Therapy, HTR), which resulted in reduction of fractures in vertebrae and hip by 34% and other osteoporotic fractures by 23% in the Women's Health Initiative Randomized Controlled Trial using HRT consisting of a tablet of conjugated equine estrogens, 0.625 mg/day, plus medroxyprogesterone acetate, 2.5 mg/day (66). Similar results were found through a meta-analysis of randomized trials, including fractures trials (67). The effect of HRT on BMD declines after cessation of therapy at an unpredictable rate, though some degree of protection may remain (68). However, it has been reported that ERT and HRT can increase the risk of breast cancer, thromboembolic disease and cardiac events and stroke (66,69,70). Hence it is recommended only for women in early menopause until around 50 years old to prevent bone loss and in post-menopausal women until the age of 60 in the absence of risk factors for breast and endometrial cancer, cardiovascular and thromboembolic disease, in small doses and for a short period of time, and not as a first-line treatment (71). HRT is also recommended for men, as one of the main causes for male osteoporosis is hypogonadism. Testosterone replacement therapy was reported to increase BMD at spine by 5%, although no studies have adequately assessed its clinical impact on fracture prevention. It is best suited for osteoporotic men with symptomatic hypogonadism at fracture risk, not simultaneously with other fracture-preventing medication, though this therapy has shown adverse side effects on the prostate (72–74).

Selective Estrogen Receptor Modulators (SERMs) are non-steroidal synthetic drugs that interact with the estrogen receptor, acting as agonists in some tissues, like bone tissue, and antagonists in others, such as breast and brain tissue, having a similar effect to ERT and HRT on bone tissue, with fewer adverse side effects on breast and endometrium tissue. The SERMs available in the market at present time are Raloxifene and Bazedoxifene. Raloxifene suppresses the bone turnover, thought to a lesser degree comparing to estrogen therapies, resulting in the prevention of bone loss and a small increase in BMD, effectively reducing the risk of vertebral fractures by 30% to 35% compared to the placebo, without significant effect on non-vertebral fractures (75–77). It is recommended at a dose of 60 mg/day for post-menopausal women in the prevention of osteoporosis and in the treatment of less severe osteoporosis and can be safely used for 8 years, according to the clinical trials. Raloxifene has also been found to reduce the risk of breast cancer, although it can increase menopausal symptoms, like hot flushes, and has been associated with an increase in the risk of stroke, thromboembolism, leg cramp, and postmenopausal vasomotor symptoms (78). Bazedoxifene is an indole-based SERM that has similar effect to raloxifene, and has been shown to produce a mild reduction in bone turnover and bone loss, preserving BMD, and, at the recommended dose of 20 mg/day, reduced the risk for new vertebral fractures by 42% in post-menopausal women with osteoporosis and non-vertebral fractures by 50% in post-menopausal women at high fracture risk (79,80). Bazedoxifene caused an increased risk of vasomotor symptoms, leg cramps and deep vein thrombosis (81). Both SERMs are contraindicated for pre-menopausal women as it competes with estrogen, blocking its action and, consequently, increasing bone loss (82).

Strontium ranelate consists of two molecules of stable strontium complexed by a molecule of ranelic acid. It shows both antiresorptive and anabolic activity, increasing the number of osteoblast and reducing the number of osteoclasts, hence being known as a “dual acting bone agent”. The exact mechanism of action of strontium ranelate is not yet clear, however a minor antiresorptive effect and small benefit of bone formation have been noted through the reduced concentration of bone resorption markers and increased concentration of bone formation markers. It reduced vertebral fractures by 41% compared to a placebo, but showed no effect on non-vertebral fractures (83). It is recommended, under strict restrictions, if treatment with other pharmacological therapies is not effective or unsuited due to contraindications or intolerance, at a dose of 2 g/day, for women and men with severe osteoporosis at high risks of fracture, with no history of heart or circulatory disease, as it caused an increased risk of myocardial infection and thromboembolic events. Severe allergic reactions, namely the drug reaction with eosinophilia and systemic symptoms (DRESS syndrome), have also been reported (83,84).

Denosumab is a human monoclonal antibody that binds selectively and with high affinity to RANKL, an important mediator of bone remodeling, preventing the binding of RANKL to RANK on osteoclast membranes, consequently inhibiting their differentiation, activation and survival (85,86). This inhibition effectively suppressed the progression of bone resorption, resulting in an increase in BMD at lumbar spine, hip, femoral neck and distal radius, and reductions in vertebral, hip and nonvertebral fractures of 68%, 40% and 20%, respectively, compared to a placebo, in a phase III clinical trial (85,87,88). The effects of this therapy are reversible once treatment is discontinued, with a rapid increase in bone turnover markers and a decline in BMD taking place, indicating that its activity is sustained by continuous administration (89). The conservation of the beneficial effects of the treatment after its discontinuation is still under investigation. Denosumab is generally well tolerated, though some adverse effects were reported such as musculoskeletal pain, hypercholesterolemia, serious cellulitis and hypocalcemia, thus requiring correction of vitamin D and calcium levels previous and during the treatment (85,90–92). As RANKL and RANK are also expressed in T-lymphocytes, B cells and dendritic cells, an increased risk of infection and dermatological reactions was reported (85,89). Osteonecrosis of the jaw and atypical fractures were also reported with prolonged use of the drug, though at a very low incidence (85,93). It is administered at a dose of 60 mg once every 6 months, through a subcutaneous injection, and can be used as a first-line treatment for men and post-menopausal women with osteoporosis who are intolerant to other treatments, for example, to patients with renal impairment who cannot take bisphosphonates, as denosumab’s clearance happens through the reticuloendothelial system (94).

Calcitonin is a peptide hormone produced by the parafollicular cells (C cells) of the thyroid gland and this is secreted as a response to increase serum levels of calcium (95). The calcitonin therapy, particularly salmon calcitonin for its high affinity to the human calcitonin receptor, was shown to have an antiresorptive effect through the increase of osteoblast activity, resulting in a mild increase in BMD at the spine and a decrease in biomarkers of bone turnover, however its effects on the prevention of fractures are disputed, causing a reduction of vertebral fracture risk in some studies, with no effect on non-vertebral fractures, while no efficiency in the prevention of fractures is reported in others (96–98). Calcitonin's adverse side effects include nausea, vomits and allergic reactions, as well as an increased risk of cancer with long term use. Due to its limited efficacy compared to other therapies, as well as the increased risk of cancer associated, it is recommended only as a second-line treatment, if other pharmacological approaches are ineffective or unsuited, to women at more than 5 years after menopause, usually to relieve from acute pain from fractures, for a period of time not superior to 6 months. Afterwards, it should be followed by treatment with other pharmacological drugs to maintain the effects (98).

Bisphosphonates (BPs) are the most prescribed for the prevention and treatment of osteoporosis due to their high affinity to bone mineral, long safety record, inexpensiveness, and effectiveness in multiple types of the disease, such as post-menopausal, male and steroid-induced (37). Their history, characteristics, available formulations and pharmacokinetics are discussed in the sections ahead.

1.3. BISPHOSPHONATES

1.3.1. History of bisphosphonates

BPs, originally denominated disphosphonates, were firstly synthetized in mid-19th century in Germany, being only commercialized in 1960, initially used in industrial processes as corrosion inhibitors, complexing agents in textiles, fertilizers, in the oil industries and as water softeners as they were able to capture calcium by acting as sequestering agents and inhibited the precipitation of calcium carbonate, making them useful in the prevention of scaling in water pipes and other installations (99–101).

They have been used clinically to treat disorders of the calcium metabolism since the 1970s, after the discovery that etidronate could control the formation and dissolution of calcium phosphate *in vitro* and also the processes of bone mineralization and resorption *in vivo*, in a dose dependent manner, with the first use in humans being that of Etidronate on a child with fibrodysplasia ossificans progressiva, formerly known as myositis ossificans (100,102,103). Clodronate was then shown to prevent bone loss following spinal cord injury in humans (104). Afterwards, it was demonstrated that Etidronate was highly effective in the treatment of Paget's disease, being later approved by the regulatory agency, not only for this treatment but also for the prevention and treatment of heterotopic calcification and ossification caused by hip replacement surgeries or injuries of the spinal cord and the intravenous treatment of hypercalcemia of malignancy (105). Afterwards, research continued to develop other BPs with more potent antiresorptive capacity, as well as a larger difference between the dose that inhibited mineralization and the dose that reduced bone resorption, since the difference between the doses was of only about 10-fold with Etidronate. This was achieved through variations in the substituents in the R_2 chain bonded to the central carbon atom, maintaining the hydroxyl group in the R_1 chain (Figure 3), originating two new generations of BPs (100). BPs were also used as bone scanning agents, for the detection of abnormal metabolic activity of bones, for example bone metastases, Paget's disease of the bone and calcification of soft tissues (101,106). Simultaneously, BPs started being used in oncology, especially Clodronate and Pamidronate, and are now established for prevention and treatment of bone metastases, especially breast and prostate, and skeletal complications derived from multiple myeloma (100). In the 1980s, Etidronate was studied by Procter & Gamble Company as a treatment for post-menopausal osteoporosis, producing a significant increase in BMD and a reduction of vertebral fractures in patients at high risk of fracture (107). Other BPs were then developed and studied for the treatment of this disease, namely Alendronate, Risedronate, Ibandronate and Zoledronate, and further clinical studies established BPs' long-term efficacy and relatively safe profile for the prevention of both vertebral and non-vertebral osteoporotic fractures. BPs were also shown to be effective in the treatment of glucocorticoid-induced and male osteoporosis (108–115).

Currently, bisphosphonates remain the first-line treatment for post-menopausal, glucocorticoid-induced and male osteoporosis, and in the treatment of other diseases of the skeletal system, specifically Paget's disease, osteogenesis imperfecta in children and bone metastases, combined with the standard anti-neoplastic therapy, where BPs may exert a synergistic anti-tumor effect with those drugs, as well as to prevent damages to the skeletal system due to myeloma. They are also still used as bone scanning agents (100,116–119).

1.3.2. Chemical structure and properties of bisphosphonates

BPs (Figure 3) are chemically stable synthetic analogues of inorganic pyrophosphates, in which the geminal oxygen is replaced by a carbon, forming a P-C-P bond that is resistant to enzymatic hydrolysis by pyrophosphatases in the gastrointestinal tract, unlike the P-O-P bond of pyrophosphates that made them inactive when given orally (100,120,121). The central carbon atom confers stability to the molecule, and has also two other covalent bonds (R_1 and R_2 chains) that, depending on the functional group attached, give the BPs molecule different binding activity to the bone mineral, hydroxyapatite (HA), and varying physicochemical, biological, therapeutic and toxicological characteristics (9,100). The substituent in the R_1 chain mainly influences the binding affinity of the BPs to the calcium crystals in bone mineral and the substituent in R_2 affects the mechanism of action and the antiresorptive potency. Generally, a hydroxyl group in R_1 enhances the mineral binding properties through tridentate binding to calcium and the presence of a Nitrogen atom in R_2 enhances the BPs' potency (100,101).

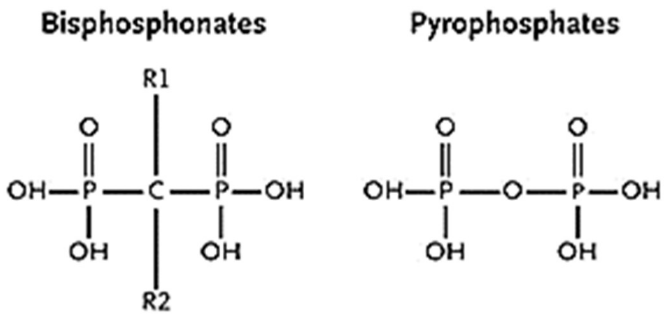

Figure 3 - Schematic representation of the structure of Bisphosphonates and Pyrophosphates (122).

They are commonly divided into two categories based on the presence or absence of Nitrogen in the R_2 chain (Figure 4), but can be also categorized on their generation. First generation BPs do not contain nitrogen in the R_2 substituent, hence being also denominated Non-Nitrogen containing BPs, and were the first to be tested in animals and to be clinically used. These include Etidronate, Clodronate and Tiludronate. Second and third generation BPs contain at least one Nitrogen atom in the R_2 chain, either in an amino group or in a nitrogenous ring, consequently being known as Nitrogen-containing BPs, and include Alendronate, Ibandronate, Pamidronate, Risedronate, Zolandronate (100).

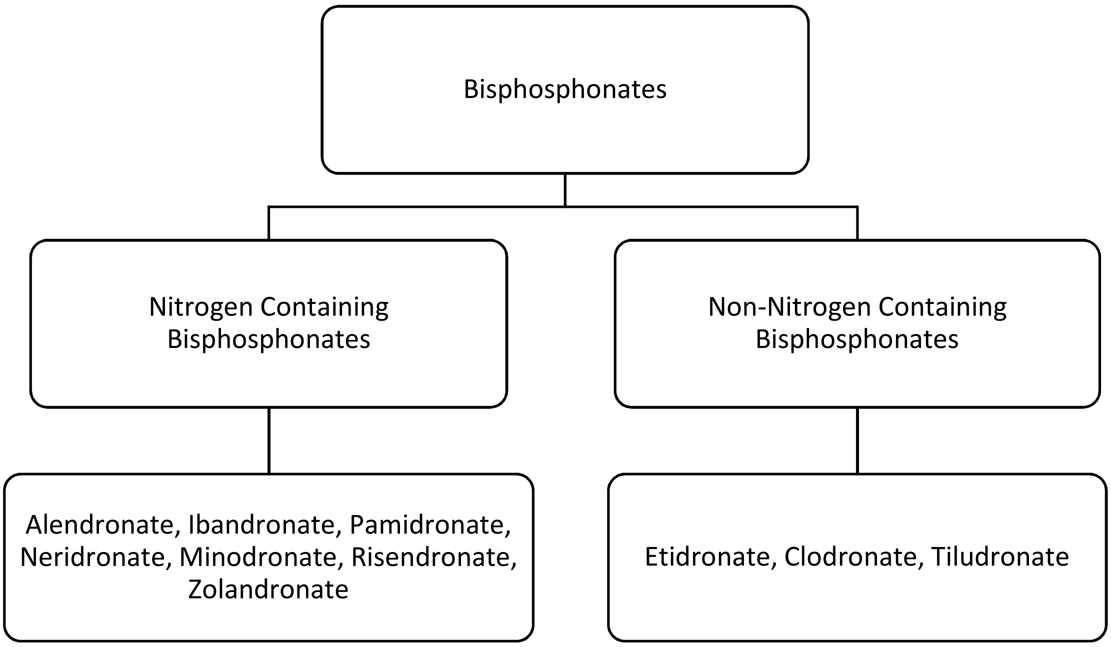

Figure 4 - Classification based on the presence of Nitrogen and Examples of Bisphosphonates.

BPs have very high affinity to HA, the main mineral constituent of the bone tissue, due to the P-C-P moiety, and were found to prevent the formation and aggregation of calcium phosphate crystals. The affinity for HA results in them being deposited near to osteoclasts in newly formed bone, forming a thin layer on the bone surface. Their remarkable selectivity for the bone tissue is also one of the main factors responsible for their efficacy and safety. The P-C-P moiety is also required for them to be pharmacologically active. Later, during the resorption phase of the cycle, the subcellular space beneath the osteoclast becomes more acidic, causing the dissolution of HA, while the extracellular bone matrix is broken down by proteolytic enzymes. Consequently, the BPs are released from the bone mineral and osteoclasts are exposed to a higher BPs concentration, that will be internalized by the cells, where they will exert their effect (100,123).

The antiresorptive potency of BPs is derived from two main factors: their affinity to calcium ions in hydroxyapatite and their mechanism of action. Nitrogen-containing BPs are more potent as they display higher affinity to the bone mineral, for their capacity to chelate the calcium ions in HA by tridentate binding while non-Nitrogen-containing BPs bind to calcium through bidentate binding, having the efficacy of Nitrogen-containing BPs been improved between 10 and 100 times in the case of alkyl-amino BPs, and up to 10 000 times with heterocyclic BPs, in animal models, in comparison to non-nitrogen containing BPs (124,125). Risedronate and Zoledronate are the most potent of the Nitrogen-containing BPs due to the nitrogen in the heterocyclic ring, which allows for that group to be in a critical distance to the P-

C-P bond and in a specific spatial configuration that favors maximum potency, followed by Ibandronate with the highly substituted nitrogen moiety and, lastly, Alendronate and Pamidronate, with a simpler structure and a primary Nitrogen atom (Figure 5) (125–127). Etidronate, Clodronate and Tiludronate present similar potency, which is comparatively lower than their Nitrogen-containing counterparts (125).

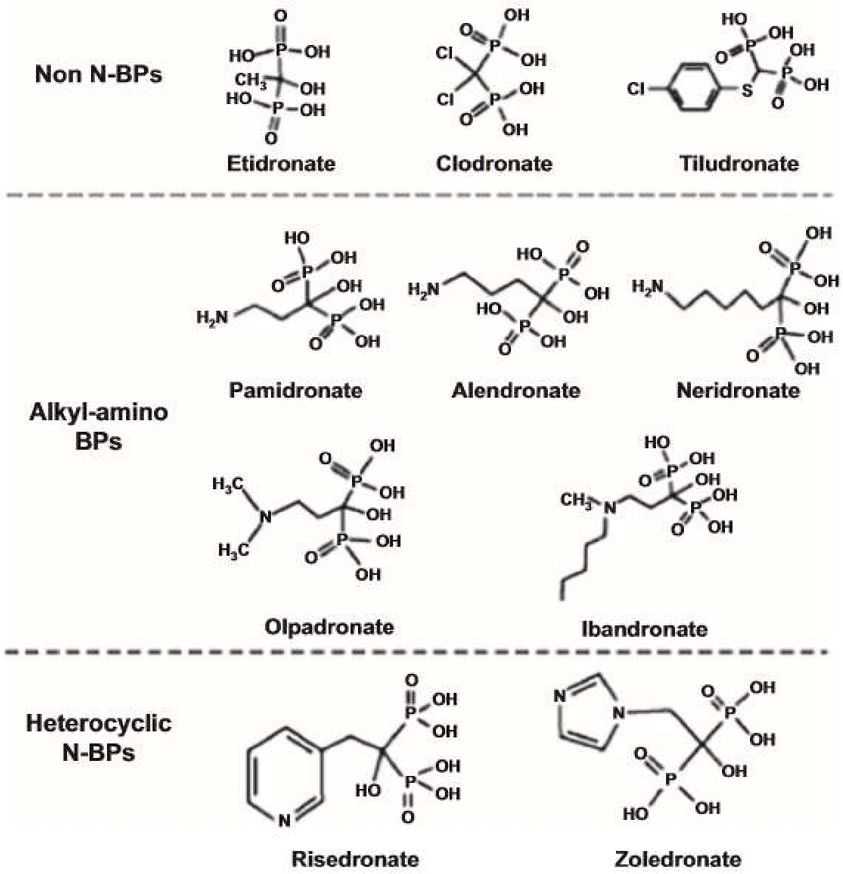

Figure 5 - Chemical structure of bisphosphonates, categorized by the presence of a Nitrogen-containing substituent, coinciding with the generations of BPs: Non Nitrogen-containing BPs (Non N-BPs, First generation), Alkyl-amino BPs (Second Generation) and Heterocyclic Nitrogen-containing BPs (Heterocyclic N-BPs, Third generation) (106).

1.3.3. Therapeutic activity of bisphosphonates

The therapeutic activity of BPs derives either from their physicochemical effect or their cellular effect. The physicochemical effects consist on the inhibition of calcium phosphate crystal formation and precipitation, and retard the transformation of amorphous into crystalline HA, even at very low concentrations, as well as their dissolution *in vitro*, preventing also the calcification both *in vitro* and *in vivo* (100,128,129).

Once incorporated into bone tissue, specifically at sites of active bone remodeling where bone matrix is exposed, and once they are released from the bone mineral presumably by proteolytic enzymes, BPs are internalized by osteoclasts, likely by fluid-phase endocytosis along with other resorption products, where they exert directly their cellular effect, although they can also be taken up again by the skeleton or can be released in the circulation (106,130). The mechanism by which the affect osteoclasts and consequently inhibit bone resorption is dependent on whether they contain or not nitrogen in the R_2 chain of the molecule (Figure 6) (100). Non-nitrogen containing BPs are metabolized to non-hydrolysable ATP analogues, preventing ATP-dependent mechanisms to take place. These analogues then accumulate in the osteoclast cell, causing its apoptosis (125). Nitrogen-containing BPs, after absorption by osteoclasts, inhibit farnesyl pyrophosphate synthase, a key enzyme from the mevalonate pathway, preventing the prenylation of small guanosine triphosphate (GTP)-binding proteins (GTP-ases), namely Ras, Rac, Rho and Rab, consequently preventing the formation of isoprenoid lipids like farnesylpyrophosphate and geranylgeranylpyrophosphate, which are essential to multiple pathways required for the cytoskeletal organization, and cell function and survival, consequently leading to apoptosis of the osteoclast and, thus, reducing osteoclastic bone resorption (131). A mild stimulation of osteoblasts has also been reported, as well as the release of an inhibitory factor by osteoblasts to osteoclasts after exposure to bisphosphonates occurring due to the indirect effect on the bone remodeling cycle from the suppression of bone resorption by osteoclasts (106,132–134). Very low concentrations of various BPs have been shown to protect osteocytes from apoptosis induced by glucocorticoids *in vitro*, which appears to be mediated by a different mechanism than the one that induces the apoptosis of osteoclasts, consisting on the opening of connexin 43 hemichannels and subsequent activation of extracellular signal-regulated kinases (135,136).

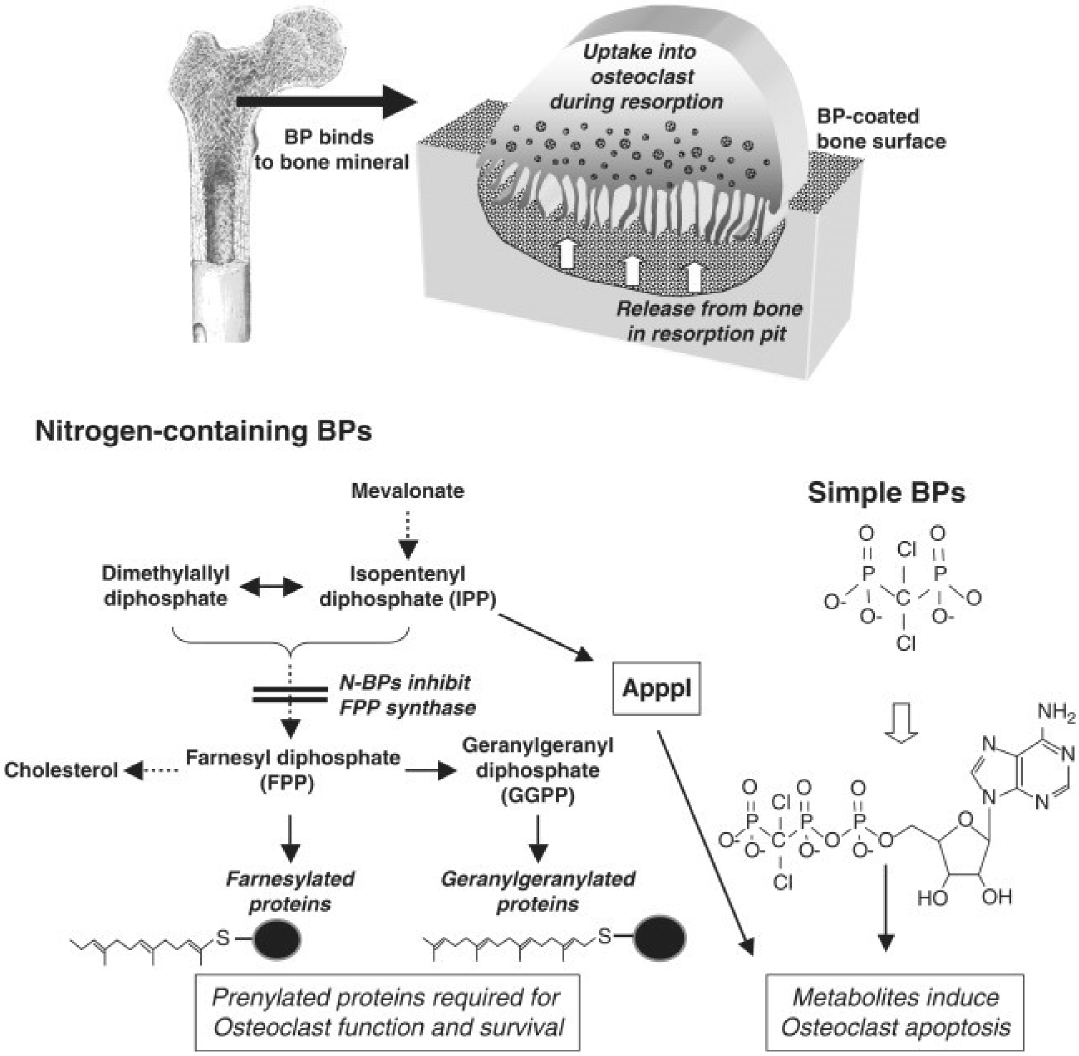

Figure 6 - Schematic representation of the mechanism of action of Nitrogen-containing BPs (left) and Non Nitrogen-Containing BPs (right) (137)

The inhibition of bone resorption leads to a reduction of the incidence of vertebral and non-vertebral fractures, being BPs the most effective antiresorptive drugs at present time, recommended to treat various types of osteoporosis, such as post-menopausal and glucocorticoid-induced osteoporosis, but also in senile osteoporosis in men.

BPs effects are dependent on the dose they are administered at, inhibiting mineralization at higher doses, used in the treatment of diseases like fibrodysplasia ossicans progressive, and inhibiting bone resorption at lower doses and consequently maintain or increase BMD, used in the treatment of osteoporosis and other diseases caused by excessive or dysregulated bone resorption (125).

1.4. CLINICAL TRIALS AND MARKET FORMULATIONS

1.4.1. Bisphosphonates clinical trials conducted around the world

BPs have been studied in clinical trials for the treatment and management of osteoporosis of at least 2 years with the primary end points assessed being the increase of BMD at relevant sites and the absence or risk reduction of fractures. For etidronate, alendronate, risedronate, zoledronic acid and minodronate there have also been extensions of the trials to evaluate their long-term effects.

Etidronate's intermittent administration at a 400 mg daily dose for 2 weeks, followed by a 13-week period in which no drug was given, repeating the cycle for 8 to 10 times, complemented by calcium and vitamin D supplementation, significantly increased BMD at the spine by 5.3% ($P<0.01$) in one study and approximately 4% in another, reducing also the serum levels of alkaline phosphatase ($P<0.01$), a bone turnover marker, after approximately 7 months, and reduced the incidence of vertebral fractures at 2 years (6 in etidronate treated patients vs. 54 fractures in placebo-treated patients per 100 patient-years; $P=0.023$ in one study and 29.5 in etidronate treated patients vs. 62.9 fractures in placebo-treated patients per 1000 patient-years; $P=0.043$) (107,138). The extension trial demonstrated that the bone mass gained at the spine in the first study was maintained and the fracture rate remained low when etidronate therapy continued for 1 more year. The BMD at proximal femur increased over the 3-year period (139). A meta-analysis found that etidronate increased BMD after 1 to 3 years of treatment, comparing to placebo by 4.06% at lumbar spine, by 2.35% at femoral neck and by 0.97% in total body, increasing for up to 4 years. It also reduced the incidence of vertebral fractures, though it had no effect on non-vertebral fractures (140). No significant adverse side effects were reported in either study, nor in the meta-analysis.

A randomized, blinded, placebo-controlled study evaluated the efficacy of alendronate in post-menopausal with low bone density with or without preexisting vertebral fractures, giving a daily dose of either 5 mg alendronate or placebo for 2 years, followed by 10 mg for the remaining time, complemented by 500 mg of calcium and 250 IU of cholecalciferol (vitamin D) in patients with calcium intake equal or below 1000 mg/day. In women with at least one prevalent vertebral fracture, alendronate significantly increased BMD at femoral neck, total hip and lumbar spine (4.1%, 4.7% and 6.2%, respectively), as well as the risk of new vertebral (8% *vs* 15%), wrist (2.2% *vs* 4.1%) and hip (1.1% *vs* 2.2%) fractures comparing to placebo. The loss of height was less pronounced with the alendronate treatment as well (6.1 mm *vs* 9.3 mm in placebo). Adverse events happened at similar percentages in both groups, including the ones occurring in the upper GI tract (112). In women with low bone density without preexisting vertebral fractures, the treatment with alendronate increased BMD at all sites studied (P<0.001), but the effect on all types of clinical fracture reduction was only significant in women with lower BMD, with only a small and non-significant reduction reported in women with higher BMD (141). The pooled analysis of the Fracture Intervention Trial (FIT) demonstrated that the reduction of the fracture risk happens 12 to 18 month after initiating treatment (142). The Long-term Extension trial of FIT (FLEX)compared continued therapy for 10 years with discontinuation of the treatment. The discontinuation caused declines in BMD at the total hip and spine of -2.4% and -3.7%, respectively, and higher serum bone turnover markers: 55.6% (P<.001) for C-telopeptide of type 1 collagen, 59.5% (P < .001) for serum n = pro-peptide of type 1 collagen, and 28.1% (P<.001) for bone-specific alkaline phosphatase, though BMD levels and serum bone turnover markers remained above pre-treatment levels. The cumulative risk of nonvertebral fractures and morphometric vertebral fractures was not significantly different between the groups who continued and who discontinued the therapy. However, the risk of clinically recognized vertebral fractures was lower with continued therapy (2.4% *vs* 5.3% with placebo) (143). The *post hoc* analysis of the FLEX trial indicated that continued treatment with alendronate significantly reduced non-vertebral fractures in postmenopausal women without vertebral fractures and with baseline femoral neck T-score ≤ -2.5 but not with -2 ≤ T-score < -2.5, and that the continuation for 10 years instead of only 5 reduces non-vertebral fractures in women without prevalent vertebral fracture whose femoral neck T-scores after the initial 5-year treatment were of T-score ≤ -2.5 but not in women with T-score > -2 (144).

Risedronate's efficacy was evaluated in a randomized, double-blind, placebo-controlled, 3-year long study in postmenopausal women with established osteoporosis (Figure 7) to whom 2.5 or 5 mg/day or placebo was given, complemented by calcium 1000 mg/day, and up to 500 IU/day vitamin D if baseline levels were low, though the 2.5 mg group was discontinued after two years as other data indicated that the 5 mg dose produced a more consistent effect in BMD increase while having a similar safety profile to the 2.5 mg dose. Risedronate (5 mg) significantly reduced the risk of new vertebral fractures by 61% over 1 year of treatment (P=0.001) and by 49% over 3 years (P<0.001). Nonvertebral fracture risk was 33% lower than the control over the 3-year period and a significant increase in BMD at the spine and hip was reported after 6 months. The rate of height loss was lower in the risedronate-treated group (5 mg) compared with control (-0.50 cm *vs* -0.68 cm in the overall population). The treatment was well tolerated and the adverse side effect occurring were similar to those reported in the control group, and most of them were of mild or moderate severity (108). The extension trial to 5 years continued with 265 women who participated in the first study, evaluating the effect of 5 mg of risendronate (n= 135) displayed results consistent with the first trial, with the risk of new vertebral fractures being significantly reduced in years 4 and 5 of treatment by 59% and maintaining or increasing the gains in BMD at lumbar spine and hip. Other fractures were less reported in the risedronate-treated group however their number was too small to show statistical significance. The reduced bone turnover markers were also maintained with the continuation of treatment. In the second extension trial analyzed the effect up to 7 years on 81 and 83 patients who had received placebo and risedronate for 5 years, respectively to whom 5 mg of risedronate was given. There was a decrease in the incidence of radiographic vertebral fracture in the placebo/risedronate group in years 6 to 7 (6.2%) compared with the first 5 years (7.6%–12.3%) and was maintained in the 7-year treatment group. There were significant increases in BMD and decreases in bone turnover within premenopausal levels. However, the sample in this trial was very small and may not represent the overall population of the initial study (145,146).

Ibandronate efficacy was evaluated in both oral and intravenous administration (Figure 7). The Monthly Oral Ibandronate in Ladies (MOBILE) trial was a 2-year long, randomized, double-blind trial that compared oral administration through either 2.5 mg daily, 50 + 50 mg once-monthly given in consecutive days, 100 mg once monthly or 150 mg once-monthly, complemented by daily calcium (500 mg) and vitamin D (400 IU) supplements, for the treatment of osteoporosis in postmenopausal women. After one year, the BMD at lumbar spine increased in all groups between 3.9% and 4.9%, with the highest increased being that of the 150 mg once monthly dose. At the hip, all treatment regimens increased BMD, with higher increases reported with the once monthly doses, and the greatest benefit achieved with the 150 mg dose. The decreases in serum levels of C-telopeptide, a bone turnover marker, were similar in all regimens. The treatment regimens were generally well tolerated, with the occurrence of GI adverse events reported in all groups and of influenza-like symptoms being reported, the latter mostly in the monthly regimens. After 2 years the increase in lumbar spine BMD was more pronounced, between 5.0% and 6.6%, and at other sites (proximal femur, total hip, femoral neck and trochanter), the highest increase being that of the 150 mg once-monthly dose ($P<0.001$), consistent with the previous results. The decrease in the serum bone turnover marker achieved in the first year was maintained, and the monthly regimens, especially the 150 mg dose, produced greater effect than the daily one (147,148). The extension trial evaluated the efficacy and tolerability of the daily, 100 mg once-monthly and 150 mg once-monthly regimens for 3 more years, resulting in increases in lumbar spine BMD of 8.2% with 100 mg and 8.4% with 150 mg. At the hip, femoral neck and trochanter, a plateau was reached between months 24 and 30 of the treatment, and the values achieved up until then were maintained for the rest of the study period. BMD mean increases were of 3% in the 100 mg group and 3.5% in the 150 mg group at the hip, 2.5% (100 mg) and 3.5% (150 mg) at the femoral neck and 5.5% (100 mg) and 6.3% (150 mg) at trochanter. The study also highlighted the tolerability of the treatment for the 5 year-period (149). The intravenous administration of ibandronate was evaluated in the Dosing IntraVenous Administration (DIVA) study, a randomized, double-blind, placebo-controlled trial, comparing the efficacy and tolerability of a 2 mg or 3 mg dose given once every 2 months or once every 3 months, respectively, plus daily oral placebo or 2.5 mg daily ibandronate plus intravenous placebo once every 2 months or once every 3 months, in postmenopausal osteoporotic women, complementing the treatment with supplemental vitamin D (400 IU) and calcium (500 mg). The 2- or 3-monthly ibandronate regimens lead to greater increases in lumbar spine BMD comparing to the daily regimen, increasing 6.4% for the once every 2-months, 6.3% for the once every 3 months dose, comparing to 4.8% in the daily regimen ($P<0.001$). The same was reported in proximal femur BMD. The reduction of serum concentration of the bone turnover marker was similarly reduced in all conditions. the treatment was well-tolerated, and the occurrence of adverse events was identical in all three conditions (150). The extension trial evaluated the same parameters for the 2 mg bimonthly and 3 mg quarterly regimens. The intravenous treatment showed consistent increases in lumbar spine BMD over the 5-year period, increasing 8.4% and 8.1% in the 2 mg bimonthly and 3 mg quarterly regimens, respectively. In total hip, femoral neck and trochanter, and similar to the trial analyzing oral administration, a plateau was reached between 24 and 36 months, with mean increases being generally maintained until the 5 years, and BMD gain between 2.8% and 3.0% at femoral neck, 3.0% and 3.4% at the hip, and 5.5% at the trochanter, with the higher gains achieved with the 2 mg bimonthly regimen. The decrease in the serum concentration of the bone turnover maker previously achieved was maintained, and the treatment remained well tolerated (151).

Few head-to-head studies have been made in order to compare the efficacy of bisphosphonates in comparison to each other. In the two head-to-head studies found in the literature, alendronate, at a once-weekly 70 mg dose, was shown to be more potent than risedronate, at a once-weekly 35 mg dose, in reduction of bone turnover markers (Fosamax Actonel Comparison Trial international study, FACTS) and had similar potency to ibandronate (Monthly Oral Therapy with Ibandronate for Osteoporosis INtervention trial, MOTION), give once-monthly at a 150 mg dose. The same was verified for the effect in BMD increase at various relevant sites(152,153).

The effects of the intravenous administration of various doses of zoledronic acid were evaluated in a one-year long, randomized, double-blind, placebo-controlled trial (Figure 7), administering doses of 0.25 mg, 0.5 mg, or 1 mg at three-month intervals, and one group received a total annual dose of 4 mg as a single dose, and another received two doses of 2 mg each, six months apart. The treatments produced similar increases in BMD at the spine and femoral neck of up to 5.1% and 3.5% higher than the placebo group, respectively ($P=0.001$). Distal radius BMD also significantly increased in all group except the four doses of 0.25 mg each ($P\leq0.05$ for all comparisons), and total-body BMD increased after 12 months to up to 1.3%, in all groups with the exception of the four doses of 0.5 mg each. Bone turnover markers were also significantly suppressed in all zoledronic acid-treated groups, with median decreases of 65% to 83%. Some adverse side effects were reported (154). The efficacy of a 5 mg dose of zoledronic acid (15-minute infusion) were evaluated in a double-blind, placebo-controlled trial lasting 3 years (Figure 7). The treatment reduced the risk of vertebral fractures in the 3-year period by 70%, in comparison to placebo, similar to the results after 1 and 2 years (60% and 71%, respectively), and the risk of hip fractures by 41%. Other nonvertebral fractures, clinical fractures, and clinical vertebral fractures were reduced by 25%, 33%, and 77%, respectively ($P<0.001$ for all comparisons). There was also less height loss comparing to the placebo group. ($P<0.001$). The treatment improved BMD at the total hip, lumbar spine, and femoral neck and reduced bone turnover markers after 6 months. Adverse side effects were similar in both groups, although serious atrial fibrillation was more frequent in the zoledronate-treated group (in 50 vs. 20 patients, $P<0.001$) (155). The extension trial evaluating the effect until 6 years showed that BMD at femoral neck remained constant with the continuous treatment and dropped slightly when zoledronic acid was discontinued, still remaining at values above pretreatment and the same occurred to BMD at other sites and also to bone turnover markers, except when zoledronic acid was discontinued where they rose slightly. New vertebral fractures were lower with the continued treatment, but other fractures did not differ between the two groups. The continuous treatment also lead to a transient increase in serum creatinine of less than 0.5 mg/dL but the increases of atrial fibrillation serious adverse events were nonsignificant (156). The second extension trial evaluated the effect of annual infusions for 9 years and did not provide evidence of a benefit from therapy beyond 6 years, though it ensured its safety as no progressive decrease in average bone turnover was reported (157). Hence, the prolonged treatment is only recommended for patients at high fracture risk.

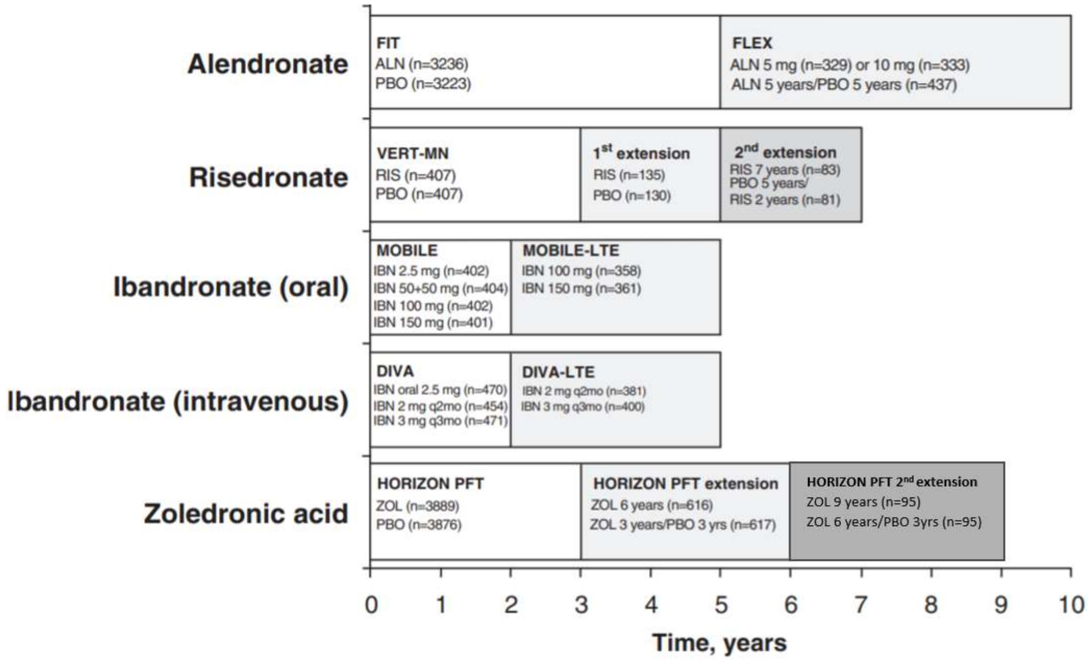

Figure 7 - Published long-term studies of the main bisphosphonates used for the treatment of osteoporosis. ALN, alendronate; DIVA, Dosing IntraVenous Administration; FIT, Fracture Intervention Trial; FLEX, Fracture intervention trial Long-term Extension; HORIZON PFT, Health Outcomes and Reduced Incidence with Zoledronic acid ONce yearly Pivotal Fracture Trial; IBN, ibandronate; LTE, long-term extension; MOBILE, Monthly Oral IBandronate in LadiEs; PBO, placebo; RIS, risedronate; VERT-MN, Vertebral Efficacy with Risedronate Therapy Multinational; ZOL, zoledronic acid. Adapted from (158).

Clodronate's efficacy in vertebral fracture incidence was analyzed in post-menopausal women and women with secondary osteoporosis in a 3- year double blind, placebo-controlled study. Patients received either an 800 mg daily, oral dose of clodronate or a similar placebo, alongside a calcium supplement of 500 mg daily. Clodronate significantly increased spine BMD over the 3-year period (percent change from baseline, 4.35 ± 6.34% versus 0.64 ± 6.02% in the placebo group, P<0.0001), maintaining hip BMD comparing to the placebo group, where a significant decrease was reported (percent change from baseline 0.70 ± 5.67% versus −3.03 ± 6.32%; P<0.0001), and similar results were obtained in hip and at the spine. A decrease in bone turnover markers, alkaline phosphatase and c-telopeptide of type I collagen was verified after 6 months of treatment. Clodronate also reduced vertebral fracture risk in women with or without prior vertebral fracture at baseline by the end of the first year of treatment, having a fracture incidence of 12.7% comparing to 23.3% in the placebo-group. Clodronate also significantly reduced height loss. The treatment proved to be safe, with no significant changes in adverse side effects, and no suggestion of upper GI intolerance was described (159). Similar results were obtained in a clinical trial using a larger sample of institutionalized elderly women, where the incidence of clinical fractures was reduced by 20% with clodronate treatment, alongside a 29% decrease in non-hip fractures, though its effect on hip fractures was not significant (160). The intravenous administration of 100 mg weekly or once every two weeks, complemented by oral calcium (1000 mg/day) and vitamin D (880 IU/day) also produced beneficial effects. A significant increase of BMD at vertebral and femoral sites in elderly osteoporotic women was reported and the therapy was well-tolerated with the exception of the occasional post-injection pain (161).

Neridronate's efficacy was evaluated in a randomized, open-label study of adults thalassemia-induced osteoporosis, with BMD T-score ≤ -2 at the level of the femoral neck or of the lumbar column. Patients were randomized approximately 1:1 to receive 500 mg calcium with 400 IU vitamin D daily or 500 mg calcium with 400 IU vitamin D daily plus 100 mg of neridronate intravenously every 90 days. The treatment with neridronate proved to be safe and produced a reduction in bone resorption and turnover, as indicated by the decrease in bone turnover markers in serum like bone alkaline phosphatase and C-telopeptide of collagen type-1 (P=0.04 and P<0.001, respectively) after 3 months of treatment, as well as significant increases in BMD at the lumbar spine and total hip (+3.1%; P<0.001 comparing to +0.5%; P = 0.002 in the calcium and vitamin D treated group) as early as 6 months of treatment at the same dose regimen currently approved in Italy for the treatment of osteogenesis imperfecta, with similar results obtained after 12 months of treatment (+3.6% *vs* +0.3%, P=0.001). The neridronate treatment also reduced backpain in these patients. The 3-monthly dosing schedule and the affordability of the drug were also helpful factors, as it did not overburden the patients and, consequently, allows for their adherence and persistence. Further studies are necessary to evaluate the long-term safety and efficacy of neridronate in these patients (162).

A randomized, double-blind, placebo-controlled 24-month long trial was conducted to examine the effect of daily oral 1 mg minodronate on vertebral fractures in post-menopausal women, along with daily calcium (600 mg) and vitamin D (200 IU) supplementation, given to both groups of patients. Minodronate suppressed bone turnover markers by approximately 50% after 6 months of treatment, which remained at the same levels from the on, and reduced the risk of vertebral fractures by 59%. When these fractures were eliminated in the first 6 months of the treatment, a 74% reduction of vertebral fractures was also reported and the treatment also significantly reduced height loss in the patients. The overall safety profile was similar in the minodronate and in the control group (163). The 1-year extension trial showed similar results, with a consistent increase in lumbar BMD in the third year of the study and stable, low levels of bone turnover markers. A decrease in vertebral fracture incidence on the placebo-treated patients of the first trial who initiated treatment with minodronate (164).

1.4.2. Bisphosphonates marketed formulations

The BPs currently available for the treatment of osteoporosis are Alendronate, Risedronate, Zoledronate and Ibandronate. Alendronate, commercially sold as alendronate sodium, under the name Fosamax, or in combination with Vitamin D (cholecalciferol), as Fosavance or Fosamax Plus, is the BP of choice as first-line treatment for most types of osteoporosis, due to its efficacy and affordability, being administered in an oral dose taken daily or once a week, depending on the dose. Risedronate, in the form of risedronate sodium, is administered orally either 2 days in a row once per month, once a week or daily depending on the dose, being available under the name Actonel, as well as in combination with calcium as Actonel plus calcium. It is also used in the treatment of Paget's disease. Alendronate and Risedronate are, at present time, the most prescribed BPs for the treatment of osteoporosis. Ibandronate, is sold in the form of ibandronate sodium, as Boniva, Bonviva or Bondronat, and is given through oral or intravenous administration, once a month or once every 3 months, respectively. Zoledronate is sold in the form of zoledronic acid, as Zometa, Reclast or Aclasta, is administered intravenously once a year. It is also used as treatment for Paget's disease, hypercalcemia of malignancy and myeloma (6,11,65,125,165).

Other BPs are prescribed for the treatment of other diseases of the skeletal system. Etidronate is sold under the commercial name Didronel, in the form of etidronate disodium, or when combined with calcium as Didronel-Kit, being administered orally or intravenously. When given orally, Etidronate is taken daily for two weeks followed by a daily dose of calcium. Etidronate is recommended for the treatment of Paget's disease and, in some cases, of hypercalcemia of malignancy. Pamidronate is sold as pamidronate disodium, under the commercial name Aredia, is administered intravenously in a single dose, 3 doses given in 3 days in a row or once every 3 to 4 weeks, being recommended for the treatment of bone lesions derived from breast cancer and myeloma, Paget's disease and also hypercalcemia of malignancy. Clodronate is indicated in the treatment of Paget's disease and in the management of osteolytic lesions, hypercalcaemia and bone pain associated with skeletal metastases in patients with carcinoma of the breast or multiple myeloma, being administered both orally and intravenously, and sold under the commercial names Bonefos and Ostac (100,125,165). Some of these BPs are also available in generic versions.

Tiludronate (Skelid) and Minodrate (Recalbon or Bonoteo), both administered orally, are also available for the treatment of Paget's disease and osteoporosis, respectively, as well as

Neridronate (Nerixia), administered through both oral and parenteral route, is recommended for osteogenesis imperfecta, Paget's disease and algodystrophy. These are, however, available only to a limited extent, being available in fewer countries (100,125,165–168).

1.5. ADMINISTRATION ROUTES, BIOAVAILABILITY AND SIDE EFFECTS

1.5.1. Restrictive and complicated dosage regimens

BPs are administered either orally or intravenously, the latter ones usually when a patient is intolerant to orally administrated BPs. As mentioned above, BPs administered exclusively through oral route are Alendronate, Risedronate, Tiludronate and Minodronate. Zoledronate and Pamidronate are administered intravenously only. Ibandronate, Etidronate, Clodronate and Neridronate can be administered through both routes.

When taken orally, BPs have complicated dosage regimens. They are taken daily, weekly or monthly, and must be taken only with full glass of water, to prevent the tablet from getting stuck in the esophagus, thus minimizing discomfort and adverse GI side effects, after an overnight fasting and followed by a 30 to 60-minute fasting, during which the patient must stand upright to prevent gastroesophageal reflux and, especially, calcium-rich food or beverages should be avoided in the first hours after taking the drug, as they interfere with the absorption of BPs (16). If these conditions are not followed correctly, the bioavailability of the drug decreases to ineffective amounts, for example decreasing up to 60% in the case of alendronate (169). The complexity and restrictiveness of the treatment regime often discourages patients from following it correctly, consequently reducing its efficacy in anti-fracture prevention. Fracture risk has been shown to rise 30% to 46%, in a meta-analysis, with non-adherence and non-persistence to the treatment (11,100,170,171). The treatment using intravenously-administered BPs, like Zoledronate, is an alternative that provides the delivery of a define dose, without the variation associated with oral BPs, being also less complex and restrictive, thus encouraging the commitment and adherence by patients to the treatment (154,155).

Other routes of administration have been investigated, such as administration of alendronate through nasal route has been reported which allows for a direct route for BPs to enter the blood stream, protecting them from enzymatic hydrolysis that happens with the oral administration after reaching the GI tract, therefore enhancing their bioavailability, as well as being more convenient, easier and painless in comparison to the oral and intravenous administration routes (172,173). However, this route is not available yet in the marketed formulations.

1.5.2. Pharmacokinetics and bioavailability

1.5.2.1. Absorption

With oral administration, they are quickly absorbed in the small intestine, through passive diffusion, likely by paracellular transport, with no transporters having been identified. However, though the absorption is quick, they are poorly absorbed in the intestine, presenting very low bioavailability, bellow 1% for most BPs, rarely achieving values above 5%. Absorption is slightly higher in Nitrogen-containing BPs (130,174). The poor absorption is probably due to the heavily negative charge of the molecule and its low lipophilicity, which hinders the transport across lipophilic cell membranes, as well as due to complexing with divalent cations like calcium and magnesium. The absorption can be affected by conditions such as celiac disease, gastro-jejunostomies and small bowel resection. However, the small amount that is absorbed, binds to the bone tissue, where it can remain for years, and has an impactful effect on bone resorption and turnover (100,174,175).

1.5.2.2. Distribution

BPs used for the treatment of osteoporosis have a short half-life in circulation, between 30 minutes to 2 hours in humans, being rapidly absorbed onto the bone mineral due to their remarkably high affinity for it, and only a negligible amount is distributed to soft tissues, and deposit in organs such as the stomach, liver, kidney and spleen, which appears to be in part due to formation of complexes or aggregates that takes place when a large dose is infused rapidly. About 50% of the administered dose through intravenous administration is taken up by the bone, in comparison to approximately 1% to 5% with oral BPs, and the uptake is higher at sites of active bone remodeling, thus, their distribution in bones is not homogenous. The uptake by the bone tissue varies depending on the age and gender of the patient, as well as the compound used (137,176). Once taken up by the bone tissue, BPs are retained there for long periods of time, being released when the site undergoes remodeling, to be internalized by osteoclasts, reabsorbed onto the bone or to the blood circulation and are later reabsorbed into the bone, explaining their long-time effect. It appears that no saturation of the total skeleton occurs when BPs are given at clinical amounts (137). The retention time and terminal half-lives of BPs in humans where estimated at up to 10 years, though it is possible that part of the administered dose can remain in the skeleton in inactive form for life (137,174,177,178).

1.5.2.3. Metabolism

There is no evidence that alendronate is metabolized in animals or humans, and no drug derivatives have been detected in urine (174,179).

1.5.2.4. Excretion

BPs that are not absorbed in the skeleton, approximately 30% to 70% of the dose administered intravenously, are quickly excreted from the organism unmetabolized in the urine, mostly within the first few hours after being administered. The renal excretion happens mainly via passive glomerular filtration, though active transportation in proximal tubular cells is also involved. Hence BPs are unsuited for patients with renal impairments. A very small percentage of the dose is excreted in the bile (130,174,180). Urinary excretion of BPs can be detected weeks or months after the discontinuation of the treatment due to their release from the skeleton onto the blood circulation (181,182).

1.5.3. Adverse/Secondary side effects

Overall, BPs are well tolerated, however some adverse secondary effects have been reported. The most common with oral BPs occur in the GI tract, such as esophageal irritation and inflammation, abdominal pain and nausea when administered. Dysphagia, esophagitis, gastric ulcers and esophageal cancer have been reported (9,183).

When administered through the intravenous route, BPs cause an acute phase reaction in over 30% of the patients after the first administration, characterized by fever, myalgia and lymphopenia, being less frequent and severe in the subsequent doses. This reaction happens due to the release of pro-inflammatory cytokines and some of the symptoms are fever, myalgia as well as lymphopenia and elevated C-reactive protein (CRP), that can be treated with acetaminophen to be taken from the date of the administration of the BPs until they pass, which is usually a few days. Headache and pain and stiffness in muscles, joints or bones have also been associated with intravenous BPs, as well as an increased risk of atrial fibrillation (9,184–186).

Rapid infusion of BPs through intravenous administration and the simultaneous treatment with other potentially nephrotoxic agents may induce acute renal failure, though the majority of cases reported have been reversible. Their removal by peritoneal dialysis is poor which must be taken into account particularly in patients with renal impairment or who are underhydrated (137,174,175,180,187).

Hypocalcemia due to use of BPs has also been reported, so correction of low calcium and vitamin D levels is required before starting treatment with a BPs (9).

Osteonecrosis of the jaw (ONJ) has been clearly associated with BPs therapy, especially the more potent Nitrogen-containing BPs administered intravenously for the treatment of skeletal complications of malignancy. ONJ consists on the exposure of necrotic bone in the oral cavity that does not heal for 6 to 8 weeks, in the absence of treatment with radiotherapy to the jaw. The mechanism that contributes to its development is not yet understood. Most cases are precipitated by trauma from dental procedures, such as tooth extraction or other dental surgery procedures. ONJ is one of the more severe side effects of BPs therapy, however, its incidence in osteoporotic patients treated with BPs is very low, approximately 1 cases per 100 000 person-years of exposure to oral BPs, being higher in the treatment of patients with cancer-related bone disturbances, with an incidence of 1% to 12%, and increasing with longer treatments (9,188,189).

Atypical femur fractures are subtrochanteric or femoral shaft fractures resultant from minimal trauma, that have been reported in patients of prolonged BPs therapy, presenting prodromal pain in the region of the pending fracture, typically tight or groin, and having characteristic radiographic findings which include cortical hypertrophy in the proximal femur, a site of high tensional stress, a straight transversal fracture line in completed atypical fractures and medial cortical spiking (9,175). Meta-analysis have shown an increase in the incidence of these fractures with prolonged BPs therapy, although that incidence is very low and no causal relationship has yet been identified, the main concern being that the long-term therapy with BPs can induce oversupression of bone turnover that may lead to increased fragility (190–192). Patients should be informed of this risk and notify their physicians if prodromal symptoms appear so that radiological evaluation can be done, and BP therapy is discontinued.

The adverse side effects, similarly to the complexity of the treatment regime, are one of the main factors that lead to poor adherence from the patients to the treatment, however, their overall benefits still outweigh their potential risks and adverse side effects, hence BPs are still the first-line and most commonly recommended treatment for osteoporosis.

1.6. NANOTECHNOLOGY AND BISPHOSPHONATES

1.6.1. How can drug delivery systems help?

Nanotechnology has been applied in the medicine field in the last decades, being denominated nanomedicine, with various purposes: in the diagnosis methods of multiple illnesses, particularly *in vitro* diagnosis, but also being investigated in new treatments and as a mean to improve existing drugs, aiming to overcome the drawbacks currently presented by them in their free form. Nanomaterials (materials with at least one of their dimensions in the nanoscale range) present unique physicochemical properties and biological characteristics that are not seen with their larger-scale counterparts, due to their small size and high surface-to-volume ratio, that often grants them higher reactivity (193–196). Nanocarriers and drug delivery systems, due to their small size, may cross biological barriers and are capable of bypassing the body's defense mechanisms, consequently allowing for the use of a lower required dose of the active compound as well as reducing the therapeutic toxicity and, thus, the side effects associated with them, as they can be designed to interact with cells and tissues at a molecular level with specificity, being deposited only in the morbid area, and may additionally change their pharmacokinetics and stability, and provide new, more efficient or convenient administration routes, which not only reduces the discomfort of patients but also the costs of production of the drug (195–198).

Various nanoparticle-based treatments have been introduced in the market in the last two decades to treat illnesses like cancer, pain and infectious diseases. The industry of nanomedicines had an estimated value of US$53 billion in 2009, and estimates point to a total market value increase to approximately US$334 billion by 2025. Anticancer therapies are the most numerous in the nanomedicine field, though a large number of nanotherapies have been studied in the last years for targeted drug delivery in a variety of diseases, including osteoporosis and other skeletal diseases, as well as new diagnostic methods (199–201).

1.6.2. Nanosystems used for bisphosphonates delivery

To overcome the drawbacks associated with the administration of free BPs for bone related purposes, whether through oral route or intravenously, and the adverse side effects they cause, novel nanocarriers and targeted drug delivery systems have been studied in the past decade, in order to increase the bioavailability of the drug as well as to lessen the side effects with them associated and, thus, increase the adherence and compliance of patients to the treatment. A resumed description of some nanosystems developed for BPs delivery is presented in Table 1. Besides usually being the main active compound in the nanosystems, BPs are also used as the bone targeting moiety of the nanoparticles to enable the targeted delivery of drugs that, otherwise, would not have affinity to the bone tissue.

Table 1 - Properties of different nanosystems used for the delivery of bisphosphonates.

Particle Type	**Bisphosphonate**	**Composition**	**Morphology**	**Size**	**Zeta Potential (mV)**	**Polydispersity Index**	**Entrapment Efficiency (%)**	**References**
Liposomes	Zoledronate; BPs derivative	PHPC, chol, DPPG, PEG, DSPE, HSPC; chol, DSPE, PEG	N/A; N/A	100 to 110 nm; 100 to 135 nm	0, -35.5 mV to -36.4 mV; -28 mV to -40 mV	N/A; >0.1	4-5%; non-applicable	(202–204)
Lipid Nanoparticles	Alendronate; Alendronate; thiolBPs derivative	Compritol, Tween 20, Poloxamer 407; Polyethyleneimine, Precitol, MCT, Poloxamer; DSPE, PEG	Spherical shaped; N/A; N/A	≈ 95 nm; 165 nm to 192 nm; 16 nm to 17 nm	-1.74 mV; -10.4 mV to 1.5 mV; N/A	>0.27; N/A; 0.288	75%; 87%; non-applicable	(205–207)
Polymeric Nanoparticles	Alendronate; Zoledronate	PEG, Zn^{2+}, DOPA, cisplatin; PLGA, DDAB Methotrexate	Round-shaped; spherical shaped	≈ 55 nm; 36 nm	N/A; -57.4 mV	N/A; 0.38	Non-applicable; non-applicable	(208,209)
Cyclodextrins Complexes	Alendronate; long-chained BPs	α-CD, PEG, polyrotaxane; α-CD, β-CD, 2-hydroxypropyl-β-CD	N/A; N/A	N/A; N/A	N/A; N/A	N/A; N/A	N/A; N/A	(210,211)
Dendrimers	Alendronate	PAMAM, PEG, methotrexate	N/A	66.9 nm	-15.6 mV	N/A	non-applicable	(212)
Hydrogels and Nanogels	Alendronate; Alendronate	Collagen, hydroxyapatite, genipin; PLGA, gellan gum	N/A; smooth spherical shape	N/A; 230 nm	N/A; -28 mV to -30 mV	N/A; 0.2	4.0 wt.% to 4.2 wt%; 5%	(213,214)
Bioceramics	Risedronate; Zoledronate	PEG, PLGA, HA; BMP-2, sucrose acetate isobutyrate, HA	Spherical shape; N/A	≈ 79 nm; N/A	-25 mV; N/A	N/A; N/A	93%; N/A	(215–217)
Gold Nanoparticles	Alendronate; Alendronate; Alendronate/Pamidronate	Gold nanoparticles	Spherical	10 nm to 15 nm; 20 nm to 30 nm; 18 nm	N/A; 0.262; 0.260	N/A; -41 mV; N/A	Non-applicable; non-applicable; non-applicable	(218–220)
Magnetic Nanoparticles	Medronate/etidronate; 1,5-dihydroxy-1,5,5-tris-phosphono-pentyl-phosphonic acid	^{99m}Tc, Fe_3O_4; γFe_2O_3.	Quasi-spherical;	45.6 nm to 51.9 nm; 36 nm	-47 mV to -50 mV; -54 mV	N/A; N/A	N/A; N/A	(221,222)
Carbon-based Nanoparticles	BPs; alendronate, pamidronate and neridronate	Fullerene; Multi-walled carbon nanotubes	Spherical	N/A; 80 nm to 100 nm (diameter)	N/A; N/A	N/A; N/A	N/A; N/A	(223,224)

N/A - data not available, PHPC - partially hydrogenated phosphatidyl-choline; chol – cholesterol; DPPG - dipalmitoylphosphatidylcholine; PEG – polyethylene glycol; DSPE - Distearoylphosphoethanolamine ; HSPC - Hydrogenated soybean phosphatidylcholine; MCT - medium chain triglycerides; PLGA - poly(lactic-co-glycolic acid); MTX – methotrexate; DOPA - Dioleoylphosphatidic acid; DDAB - Di-dodecyl dimethyl ammonium bromide; α-CD – α-cyclodextrin;

1.6.2.1. Liposomes

Liposomes (Figure 8) are spherical vesicles constituted by a single lipid bilayer or multiple concentric lipid bilayers with an aqueous vacuole inside, that are capable of encapsulating hydrophilic or hydrophobic compounds, inside the liposome or in the lipid bilayer respectively, protecting them during the circulation inside the organism. They are usually constituted by phospholipids, though other lipids can be used as long as these allow the formation of the bilayer and can be functionalized with molecules such as ligands to target specific cells and tissues. Liposomes were the first nanoparticles approved in the market for cancer treatment and have been extensively explored as drug nanocarriers, as they are biocompatible, versatile, physically stable, have low immunogenicity, can be cell specific and exhibit good entrapment efficiency. However, they can present disadvantages like poor scale up, short shelf life and, in some cases, toxicity, off target effect and fast elimination from blood and capture by the cells of the reticuloendothelial system, mainly in the liver. Liposomes can be coated with other compounds, such as inert and biocompatible polymers, like polyethylene glycol (PEG), in order to increase their circulation half-life (225–230). The conjugation of BPs to liposomes often uses BPs as the bone targeting moiety, encapsulating other drugs inside the liposome that will exert pharmacological activity.

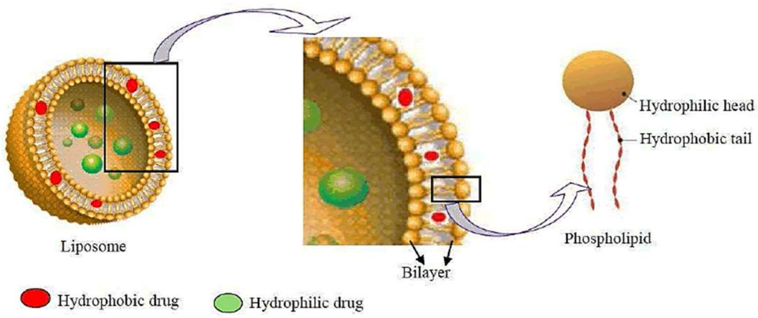

Figure 8 - Schematic representation of drug loading of hydrophobic and hydrophilic drugs in a liposome and a phospholipid detail (226).

Shmeeda *et al.* (202,203)encapsulated zoledronic acid in liposomes targeted to the folate receptor that is often over-expressed in tumor cells, where zoledronic acid would act as an anti-tumor agent. Particles measured 100 nm to 110 nm and were negatively charged (-35.5 mV to -36.4 mV), with the exception of PEG-containing nanoparticles which were neutral. Zoledronic acid recovery in encapsulated form determined through Bartlett phosphorus assay of Folch extracted samples was between 4% and 5%. Formulations were stable in storage and in the plasma, were it remained at high levels for a longer time than free zoledronate. The conjugation of folic acid to the BPs-encapsulating liposomes granted them with potent cytotoxic activity in folate-receptor expressing cells, being also efficient in non-folate-receptor upregulated cells. However, this liposomal encapsulation changes the tissue distribution of the drug *in vivo* and presents severe toxicity *in vivo*, therefore limiting its utility, though the same technique using less toxic BPs is under evaluation.

Hengst *et al.* (204) prepared a bone-targeted delivery system using liposomes as a drug reservoir and a cholesteryl-trisoxyethylene-bisphosphonic acid (CHOL-TOE-BP), a BPs derivative, as a bone target moiety for the treatment of bone diseases. Particles measured between 100 nm and 135 nm, being relatively monodisperse, with a polydispersity index below 0.1. The charge of the nanoparticles became increasingly negative when the cholesteryl-trisoxyethylene-bisphosphonic acid content increased. The conjugation of the liposome and the BPs derivative clearly increased the binding affinity to hydroxyapatite, with maximum binding achieved with a ratio of CHOL-TOE-BP-targeted liposomes to HAP of about 0.005 (25 mol% CHOL-TOE-BP), and this binding affinity was influenced by the density of CHOL-TOE-BP on the liposome surface, being higher with a higher CHOL-TOE-BP ligand density.

BPs-decorated liposomes can be loaded with, for example, anticancer drugs, such as doxorubicin, for the treatment of bone metastases, but also bone growth factors, like bone morphogenic protein 2 (BMP-2), as shown by Wang *et al.* (207) with a thiol-containing BP conjugated to distearoylphosphoethanolamine-polyethylene glycol-maleimide (DSPE-PEG-thiolBP), which were conjugated to liposomes prepared by lipid film hydration and reverse-phase evaporation vesicle methods, obtaining relatively monodisperse particles (PdI of about 0.124) measuring 98 nm to 105 nm, which displayed strong affinity to hydroxyapatite *in vitro* and in HA-impregnated collagen sponges that simulated *in vivo* conditions, with maximum binding at a concentration of only 1% to 5% of DSPE-PEG-thiolBP in the liposomes. The encapsulation efficiency of doxorubicin and a model protein lysozyme, which is similar to BMP-2, of about 65% to 34% and 13% to 30% was obtained, respectively.

1.6.2.2. Lipid Nanoparticles

Other than liposomes, solid lipid nanoparticles (SLN) (Figure 9) and nanostructured lipid carriers (NLC) are lipid-based nanoparticles nowadays commonly used as drug nanocarriers. Solid lipid nanoparticles are novel drug delivery systems being studied for controlled and targeted delivery, whose particles present submicron size (50–1000 nm), consisting of a biocompatible solid lipid matrix at room and body temperatures, stabilized by an amphiphilic surfactant outer shell, forming an aqueous colloid dispersion, that provide dispersion sites for both hydrophilic and hydrophobic compounds. By varying the drug distribution in the SLN it is possible to change the drug release behavior. This formulation is an attractive drug delivery system for their high drug payload, improving drug stability, high biocompatibility and biodegradability, for their capacity to incorporate lipophilic or hydrophilic drugs and for their easy to scale-up synthesis processes, and these nanosystems have been used as carrier in cancer therapy, vaccine, gene and targeted drug delivery. Nanostructured lipid carriers are novel solid lipid nanoparticles used in drug delivery produced by controlled mixing of solid lipids with spatially incompatible liquid lipids, which disrupts the crystal lattice of the solid lipids and forms a matrix containing imperfections where drugs can be loaded. These nanoparticles allow for greater controlled drug release and stability profile when compared to SLN, exhibiting also the same advantages as a nanocarrier system as those (231,232).

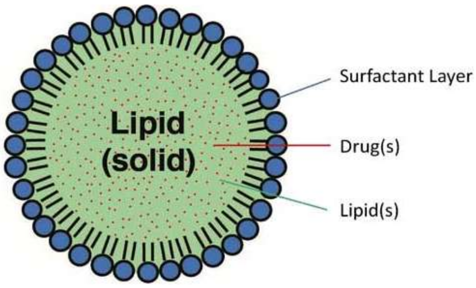

Figure 9 - Schematic representation of a drug-loaded lipid nanoparticle (233)

Alendronate was incorporated onto SLN using Compritol 888 ATO ®, as a novel delivery system through pulmonary administration for the treatment of the most common bone illnesses. The nanoparticles prepared were spherically shaped and presented sizes averaging 95 nm, with PdI below 0.27, thus indicating narrow size distribution, and were slightly negatively charged, with a zeta potential of -1.74 mV. Alendronate incorporation efficiency was of 70% to 85% and the formulation was shown to be physically stable and not cytotoxic (205).

Hamid *et al.* (206) conjugated alendronate to polyethyleneimine and incorporated this complex in NLC by a modified solvent injection, aiming to increase the oral bioavailability of alendronate. The encapsulation efficiency of the complex onto the carriers was 87%, a drastic improvement when comparing to 10% encapsulation efficiency of free alendronate. Particles measured between 165 nm and 192 nm and presented increasingly less negative charge with a higher drug/lipid ratio, the zeta potential values increasing from -10.4 mV to 1.5 mV. The drug release profile was shown to be pH dependent, being significantly reduced when compared to plasma-relevant conditions. The encapsulation of the complex increased the flux of alendronate across the intestinal barrier *in vitro* by up to 3-fold, without affecting the bioavailability of the cells at an alendronate concentration of 2.5 mM, hence representing a promising novel drug delivery system for the drug.

A conjugate of distearoylphosphoethanolamine-polyethylene glycol with 2-(3-mercaptopropylsulfanyl)-ethyl-1,1-bisphosphonic acid (DSPE-PEG-thiolBPs) was synthesized and incorporated into lipid micelles by Wang *et al.* (207) to encapsulate doxorubicin and model protein lysozyme that mimics BMP-2. The micelles measured 16 nm to 17 nm with a narrow size distribution, having a PdI of 0.288. The micelles exhibited high encapsulation efficiency of doxorubicin, varying between 38.5% and 45.7%, though the encapsulation of the model protein lysozyme presented much lower values, below 5%, indicating their unsuitability for that purpose. The conjugation with the DSPE-PEG-thiolBPs increased the binding affinity of the micelles for HA to 65%, with 20% of DSPE-PEG-thiolBPs in the micelles, and the nanoparticles had no or very low cytotoxicity.

1.6.2.3. Polymeric Nanoparticles

Polymers are materials consisting of long-chain like molecules of repeating units with identical structure, the monomers, presenting high molecular weight, of either natural, like collagen, chitosan and alginate, or synthetic origin, such as polyethylene glycol (PEG), polylactic acid (PLA), polyglycolic acid (PGA) and poly(lactic-co-glycolic acid) (PLGA). Some natural polymers however, present disadvantages such as being easily biodegraded due to the high prevalence of biodegradable bonds in their structure, and the limited number of functional groups suited for drug binding. The use of synthetic polymers has become more appealing as the structure of the polymer is easy to design and control which allows for a number of modifications without altering the properties of the bulk material and also can be used to mimic biomolecules and thus increase the efficacy of drug delivery (234,235).

Polymeric nanoparticles (Figure 10) are solid colloidal nanoparticles measuring between 10 nm and 1000 nm, that use biocompatible and biodegradable polymers for drug delivery purposes, by encapsulating the drug inside the carrier, chemically linking it onto the polymer surface or by physically adsorbing the drug onto the surface. Polymeric nanoparticles and polymer-drug conjugates are highly attractive as drug carriers as they present various advantages such as the small size, water solubility, biocompatibility and biodegradability, as well as their capacity to increase the shelf life and storage stability and reduce the immunogenicity of drugs and proteins, as is the case of PEG nanoparticles. They have also been found to be more stable in the GI tract than other nanocarrier, like liposomes, hence more effective at protecting the drug from degradation in the GI tract. Polymeric nanoparticles can be divided based on the structural organization of the nanoparticle into nanospheres, which consist on a matrix system where the bioactive molecule is physically and uniformly dispersed, or nanocapsules, where a polymer membrane surrounds the bioactive molecule, forming a vesicle around it (236,237).

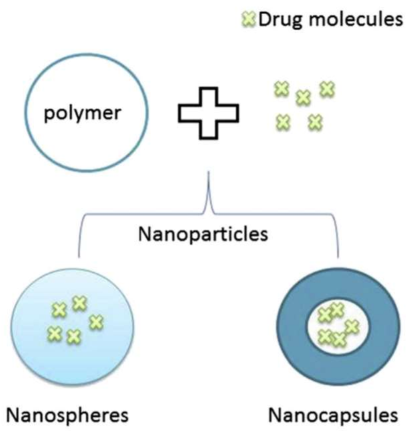

Figure 10 - Structure and classification of polymeric nanoparticles (236).

He *et al.* (208) developed PEG coated nanoparticles made of a Zn^{2+} coordination polymer that was linked with a bone targeting moiety, alendronate, to deliver cisplatin prodrug to the bone for the treatment of bone metastasis derived from breast cancer. The nanoparticles produced measured about 55 nm and round-shaped and displayed much higher affinity for HA *in vitro* and for the bone tissue *in vivo* than the non-alendronate containing counterparts, being stable at simulated physiological pH and significantly reduced cisplatin's toxicity, releasing the drug faster at the lower pH microenvironment of metastatic lesions. Consequently, the blood circulation time was significantly prolonged and the delivery of cisplatin after intravenous administration to bone metastatic lesions increased by 4-fold comparing to healthy bone, due to the uptake of bisphosphonates being 10 to 20-fold higher in metastatic bone lesions than in healthy bone and the nanoparticles were also capable of inhibiting the tumor growth as well as reducing the osteoclastic bone destruction.

Raichur *et al.* (209) prepare zoledronic acid-conjugated PLGA ultrasmall nanoparticles loaded with methotrexate for bone targeted delivery of this drug for the treatment of bone metastasis. The nanoparticles prepared were spherically shaped measuring 36 nm with PdI of 0.38 and were negatively charged, with a zeta potential of -57.4 mV. The conjugation of zoledronic acid drastically increased the binding affinity to HA in comparison to free methotrexate, binding specifically to this mineral over other calcium salts. The affinity for the bone tissue was also confirmed by *in vivo* biodistribution studies, where the conjugate mainly accumulated 1 hour after being injected in swiss albino mice, with accumulation in other organs such as heart, liver, spleen, kidney and brain.

1.6.2.4. Cyclodextrins Complexes

Cyclodextrins (CD, Figure 11) are water-soluble 1,4-linked cyclic oligosaccharides of D-glucopyranose obtained from the enzymatic degradation of starch. They form a hollow truncated cone shaped structure in space with a hydrophilic exterior and a hydrophobic interior, thus enabling the formation of inclusion complexes with hydrophobic compounds in their interior, by non-covalent interaction without complex chemical reactions, and present numerous advantages such as no toxicity, good water-solubility, ease of modification and high biological availability. The complexation of hydrophobic compounds in the interior cavity consequently allows for the modification of some of the properties of these drugs, increasing their solubility in water and conferring them greater stability, but also reducing the adverse side effects they may cause in the human organism. Hence, cyclodextrins complexes have been widely investigated and used not only for biomedical purposes, for example in drug delivery, but also in the food industry, agriculture, environmental engineering and others, being approved as pharmaceutical excipients for manufacturing pharmaceutical preparations (238,239).

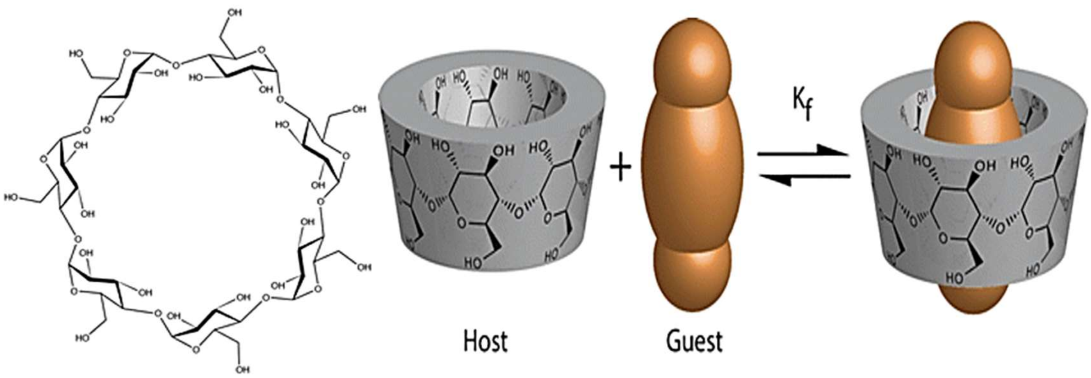

Figure 11 - Cyclodextrin molecule (left) and example of association of a guest drug to a cyclodextrin complex. Adapted from (238).

A novel multiblock osteotropic α-CD/PEG polyrotaxane was developed by Hein *et al.* (210) consisting on the conjugation of alendronate, the bone targeting moiety, to a cyclodextrin and subsequent threading onto a short PEG chain and copolymerized with sterically bulky monomers to prevent the dethreading of the complex, which can then be functionalized with imaging agents for diagnostics or therapeutic agents. The complex was shown to be quite versatile due to, not only the possibility to functionalize with imaging or therapeutic agents, but also because the binding affinity to bone can be adjusted by varying the concentration of alendronate in the complex, binding to bone *in vivo* extensively within 24 h post injection.

BPs with long alkyl chain were complexed to cyclodextrins as a possible new treatment for parasitic diseases, like Chagas disease. The complexes formed had a 1:1 BPs/cyclodextrin ratio, and the longer length of the BPs chain allowed for higher stability, being the only part involved in the inclusion and the BPs portion being either too bulky or hydrophobic to mobilize a second cyclodextrin for the complex. The complex displayed high values of formation which indicates that it could be a promising new formulation to improve oral bioavailability of BPs (211).

1.6.2.5. Dendrimers

Dendrimers (Figure 12) are synthetic, hyperbranched, three-dimensional polymeric structures, typically radially symmetrical, monodisperse and nanoscaled, with precisely-controlled architecture and specific functional surface groups, that were firstly developed in the 1980s (240,241). They are characterized by three components: a central core, consisting of an atom or molecule with at least two identical reactive groups, an interior dendritic structure denominated branches, originating from the core, of monomers bonded covalently to the core and to each other, repeating in an organized manner forming a series of concentric layers, called "generations", and, lastly an closely packed exterior surface with terminal functional groups (225). Examples include polyamidoamine (PAMAM) dendrimers, poly(propylene imine) dendrimers and phosphorous dendrimers.

Dendrimers have been extensively researched as drug carriers due to their molecular uniformity, versatility, multifunctional surface and presence of internal cavities, as well as high solubility and miscibility, which can be manipulated by varying the surface groups, and for high reactivity due to the presence of many chain-ends. Dendrimers like PAMAM present low toxicity, immunogenicity and antigenicity. Drugs can be incorporated into the dendrimer by encapsulation in the internal cavities or by complexation to the surface groups. In biomedicine, dendrimers are used as *in vitro* diagnosis techniques and in magnetic resonance imaging (MRI) conjugated to other molecules as contrasting agents, as vectors for gene transferring in gene therapy, as drug delivery systems and in regenerative medicine (225,228,229).

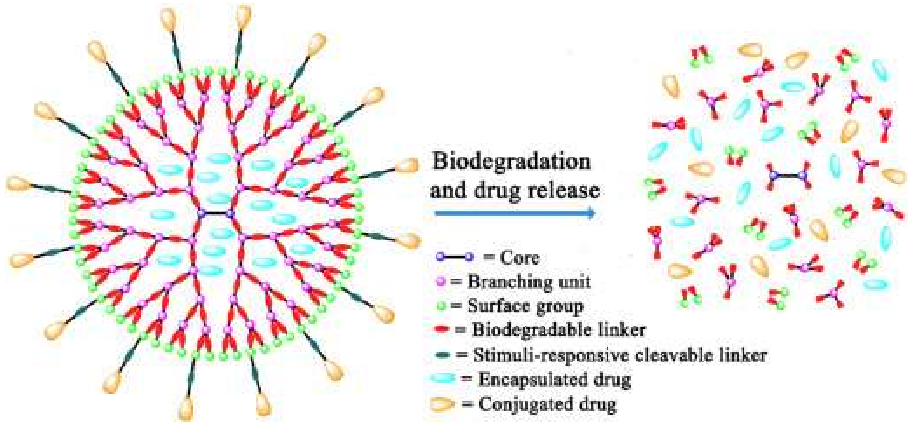

Figure 12 - Schematic representation of a biodegradable dendrimer as a drug carrier, with the drug loading occurring by complexation to the surface groups (242).

Alendronate, as a bone targeting moiety, was covalently bonded to a PEG-conjugated PAMAM dendrimer, for the targeted delivery of methotrexate to the bone tissue for the treatment of bone metastasis (212). The methotrexate-loaded dendrimers were negatively charged, with zeta potential of about -15.6 mV, measuring approximately 66.9 nm. They exhibited short circulation life and predominantly accumulated in bone 180 minutes after intravenous injection, due to the presence of alendronate and PEG, increasing the distribution of methotrexate to this by approximately 20-fold in comparison to the compound in its free form. The modified dendrimer was taken up by tumor cells in an adenosine triphosphate-mediated manner, through folic acid receptor-mediated endocytosis, then being cleaved inside the cell by peptidase, releasing the methotrexate which induces a cytotoxic reaction, thus being able to suppress the increase in number of tumor cells in the bone, consequently indicating a preventive effect against bone metastasis.

1.6.2.6. Hydrogels/Nanogels

Hydrogels (Figure 13) consist of hydrophilic crosslinked polymer networks, either water-based or swellable polymer chains, that are highly capable of retaining fluids, like water and other biological fluids, and swell, without dissolving in them, as they contain hydrophilic functional groups in the constituent molecule. Nanogels are considered a subcategory of hydrogels, as they differ only due to being nanosized, typically between 100 and 200 nm. They are mostly biocompatible and have a high loading capacity for compounds such as drugs due to their porous structure, protecting the drug from degradation and elimination in the organism. Their characteristics, for example size, shape, charge, porosity, biodegradability and mechanical characteristics can be adjusted for the intended purpose by varying the degree of cross linking of the gel matrix and by the addition of other compounds, and it is also possible to make them responsive to stimuli in the organism, such as temperature or pH, which can aid in the controlled and target-site specific release of the cargo, especially for nanogels which can respond quickly to the changes in the environment they are in because of their size and surface-to-volume ratio, facilitating the release (243–246). Therefore, hydrogels and nanogels are highly attractive for biomedical applications.

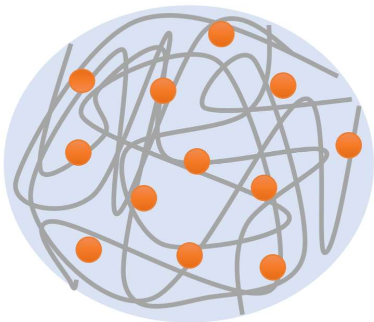

Figure 13 - Schematic representation drug-loaded nanogel, where the grey lines represent the polymer chains that constitute the nanogel and the orange circles represent the drug.

Ma *et al.* prepared biomimetic hybrid hydrogels composed of collagen, hydroxyapatite and alendronate, crosslinked using genipin. The hydroxyapatite/alendronate nanoparticles improved the individual components solubility in water, and the weight ratio of anchored alendronate on HA was estimated to be between 4.0 wt% and 4.2 wt.%. for the nanogel synthesis, the ratio of HA-alendronate conjugate to collagen was characterized using the molar ratio of alendronate/NH_2 which varied from 2.7/1 to 10.8/1. By varying the alendronate/NH_2 molar ratio of the nanogel and the genipin concentration used for the crosslinking, the nanogels' characteristics and swelling behaviour were easily modified and controlled, showing tunable degradation behaviors against collagenase, unlike collagen nanogels without the alendronate/hydroxyapatite nanoparticles. The nanogels were shown to be biocompatible and promoted the adhesion and growth of murine MC3T3-E1 osteoblastic cells, thus highlighting their potential as scaffolds for bone tissue engineering.

An injectable system for intra-bone delivery of alendronate consisting of alendronate-loaded PLGA nanoparticles suspended in a gellan gum hydrogel matrix was developed by Posadowska *et al* (214), to overcome the low bioavailability and high toxicity of the compound. The nanoparticles had an average hydrodynamic diameter of 230 nm and a narrow size distribution, with a PdI of 0.2, and were negatively charged, having zeta potential varying between -28 mV and -30 mV, and smooth, spherical shape. The solubilization and alendronate-loading efficiencies in the nanoparticles was of 70% and 5% respectively. The swelling of the hydrogel-nanoparticle system was lower than that of the gellan gum and encapsulated drug release rate was lower and more constant comparing to the PLGA-alendronate nanoparticles. The nanogel's nanoparticles were easily injectable and were able to reassemble their structure after extrusion. *In vitro* studies demonstrated that the hydrogel-nanoparticle system was able to inhibit RANKL-mediated osteoclast differentiation of RAW 264.7 cells without affecting osteoblast function of MG-63 cells.

1.6.2.7. Bioceramics

Bioceramics are non-metallic inorganic materials which can be crystalline or amorphous, and can be classified into bioinert, which are the materials that do not interact with the organism's environment with the exception of the initial "fibrous tissue" reaction, or bioactive, the materials that interact with the body forming a bond with living tissue and that are able to stimulate healing by tricking the system into responding as if it were a natural tissue. Bioceramics are biocompatible and can be biodegradable in physiological environments, hence being appealing as biomaterials. Examples include alumina, zirconia and calcium phosphates such as hydroxyapatite and β-tricalcium phosphate, that are especially suited for bone-related applications as this compound is the main non-organic constituent of the bone tissue, being frequently used in implants and replacements due to their high compression strength and wear resistance, or being used to coat bioinert implants in order to enhance their *in vivo* integration. For drug delivery, calcium phosphates and silica are the most frequently chosen (247,248).

Rawat *et al*. (215) prepared a HA based nanoconjugate of PEG, PLGA and risedronate for targeted delivery to bone tissue and effective treatment and management of osteoporosis. The nanoparticles obtained measured approximately 79 nm, presented spherical shape, were negatively charged, with a zeta potential of -25 mV, and the entrapment efficiency of risedronate in the nanoparticles was 93%. The nanoparticles produced a significant improvement in bone micro-architecture of Wistar rats with dexamethasone-induced osteoporosis when compared with other formulations tested, thanks to the presence of risedronate but also of HA in the formulation, which further induced osteogenesis and bone regeneration, and had a synergistic effect with risedronate.

Cheng *et al.* (216,217) developed an injectable system constituted by BMP-2 and sucrose acetate isobutyrate, acting as a carrier for BMP-2, to which zoledronic acid-adsorbed micro and nanoparticle sized HA was added for bone tissue engineering. The incorporation of sucrose acetate isobutyrate in the system resulted in robust bone nodule formation with lower doses of BMP-2 (2µg) than those required with other carriers, though the bone nodules formed in the mouse heterotropic ossification model were highly irregular likely affected by the forces they receive within the muscle, which will require a method to contain the injected sucrose acetate isobutyrate in order to form more regularly shaped nodules. Zoledronic acid displayed higher affinity for HA than β-tricalcium phosphate and bioglass tested, and the addition of 2% zoledronic acid and nano-HA particles to the BMP-2/sucrose acetate isobutyrate formulation produced an up to 10-fold increase in bone volume comparing to BMP-2/sucrose acetate isobutyrate alone, hence a lower dose of BMP-2 may be needed to induce bone formation. HA also conferred a protective effect against zoledronic acid's cytotoxicity and enhanced its efficacy in tissue engineering by sequestering them to the site of delivery.

1.6.2.8. Gold nanoparticles

Gold nanoparticles are small gold particles, measuring 1 nm to 100 nm that have been investigated for various biomedical applications, including diagnostic sensors, imaging contrast agents and as carriers for drug and gene delivery, as they are monodispersed and stable forming colloid solutions, biocompatible, present high X-ray attenuation and the binding with other molecules can alter their physicochemical properties like surface plasmon resonance, conductivity and redox behavior which leads to detectable signals in diagnostic techniques. These nanoparticles are easily functionalized with molecular groups such as thiols, phosphines and amines, which exhibit a high affinity for gold surface, and that can also be used to anchor other moieties like oligonucleotides, proteins, and antibodies, that can act as pharmacologically active drugs or targeting agents, making them extremely versatile and appealing as bioimaging agents and drug carriers (249–251).

Gold nanoparticles were functionalized with alendronate by Ross & Roeder (218,252) to be used as a targeted X-ray contrast agent for labeling microdamage in bone tissue. Nanoparticles measured 10 nm to 15 nm and the surface adsorption of the BPs occurred through the terminal amine group. The BP-functionalized nanoparticles presented higher binding affinity to HA and binding kinetics comparing to glutamic acid or phosphonic acid functionalized nanoparticles, thus enabling higher surface density of gold nanoparticles labelled damaged bone tissue. BPs-functionalized gold nanoparticles were also shown to exhibit targeted labeling of damaged bone tissue *in vitro*, as enable the colloidal stability in solution as well, and, consequently, produce greater contrast enhancement in X-ray tomography.

Lee *et al*. (219) conjugated alendronate to gold nanoparticles, between 20 nm to 30 nm in diameter, as a mean to improve bone tissue regeneration. Particles were relatively monodispersed, with a PdI of 0.262, and negatively charged, approximately -41 mV. These were able to suppress osteoclasts formation in a dose-dependent manner *in vitro* and produced higher bone density than the individual constituents in the treatment of ovariectomized mice, indicating that BPs-conjugated gold nanoparticles could be an efficient alternative for the treatment of osteoporosis.

Similar results were obtained by Conners *et al.* (220) who synthetized alendronate and pamidronate-conjugated gold nanoparticles, measuring about 18 nm (PdI of 0.260), that significantly reduced osteoclast viability at concentrations of approximately 1 µM and 0.3 µM, respectively, though a reduction of osteoblast viability also occurs at higher concentrations.

1.6.2.9. Magnetic nanoparticles

Magnetic nanoparticles (Figure 14) are small particles, measuring typically 5–500 nm, composed of either pure magnetic metals such as iron, nickel and cobalt, magnetic bimetallic alloy-like material or magnetic oxides, like iron oxides, that can be manipulated using external magnetic field gradient. They present various applications in biomedicine due to their biocompatibility with low toxicity, easy surface modification, and magnetic properties, namely for therapeutic applications, for example cancer therapy using the heat generated when placed in an external alternating magnetic field and the change in relaxation times of protons, as well as analytical applications, being particularly useful in Magnetic Resonance Imaging (MRI) which can be used in order to improve the therapeutic diagnostic for osteoporosis. It has been shown in *in vivo* studies that osteoporotic fractures could be better distinguished using parameters from bone architecture obtained by MRI than BDM. They have also been used for drug delivery, whether combine with an external magnetic field and/or magnetizable implants, or being functionalized with molecules for targeted drug delivery (253–256).

Mirković *et al.* (221) prepared water dispersible ^{99m}Tc–bisphosphonate–coated magnetic nanoparticles with a Fe_3O_4 core coated with two bisphosphonate ligands (Figure 14), medronic acid or etidronic acid, as diagnostic imaging agents and for therapeutic hyperthermia applications. At pH=7, the medronic acid and etidronic acid nanoparticles synthetized were quasi-spherical and exhibited hydrodynamic size of 45.6 nm and 51.9 nm, respectively, being highly negatively charged, with zeta potential between -47 mV and -50 mV. The presence of bisphosphonates induced greater biocompatibility, colloidal stability, inhibiting the aggregation of the nanoparticles, and both were radiolabelled with Technetium-99m in a high yield (<95%), being stable *in vitro* in saline solution and in human serum for over 24h. Results from *ex vivo* biodistribution and from scintigraphy technique after IV administration in Wistar rats indicated high liver and spleen accumulation immediately after injection and maximum bone uptake after 4 hours, thus noting the potential of the ^{99m}Tc -BP-coated nanoparticles for the proposed applications.

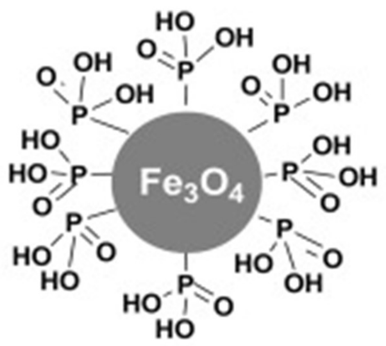

Figure 14 - Bisphosphonate-coated Fe_3O_4 nanoparticles. Adapted from (221)

Lalatonne *et al.* (222) synthetized superparamagnetic bifunctional bisphosphonate nanoparticles consisting of γFe_2O_3 nanoparticles conjugated to 1,5-dihydroxy-1,5,5-tris-phosphono-pentyl-phosphonic acid molecules with a bisphosphonate function at the outer of the nanoparticle surface for bone targeting, for potential diagnostic and therapy of osteoporosis. The prepared nanoparticles presented hydrodynamic diameter of 36 nm, highly negative zeta potential, -54 mV, and superparamagnetic behavior, generating good magnetic resonance contrast. The nanoparticles also displayed very high affinity for HA and no cytotoxicity, hence they may be used as diagnostic and therapeutic system.

1.6.2.10. Carbon-based nanoparticles

Carbon-based materials such as graphene, carbon nanotubes, either single or multi-walled, fullerenes (Figure 15), and carbon quantum dots, have become subject of interest in the last decades as they present various exceptional characteristics, such as remarkable mechanical strength, exceptional electrical and thermal conductivity, and also optical properties, derived from their unique macromolecular structure which consists of stacked layers of hexagonal arrays of sp^2 bonded carbon atoms. As they are constituted solely of carbon atoms, they have also been shown to not cause significant toxicity, presenting high stability and being environmentally friendly. Consequently, they have been extensively research for applications such as biosensing, imaging, diagnosis, tissue engineering and also for drug delivery (257,258).

A bone tissue-selective fullerene was synthetized by Gonzalez *et al.* (223) by conjugating a bisphosphonate to the structure, denominated $C_{60}(OH)_{16}$AMBP (Figure 15). The modified fullerene displayed significantly improved affinity for HA in comparison to the non-BP-containing fullerene, being also able to inhibit HA crystal growth (223).

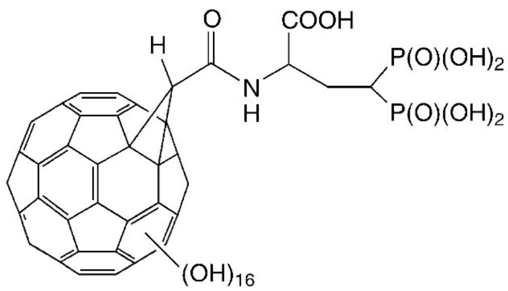

Figure 15 - C60(OH)16AMBP, the bone-vectored fullerene derivative prepared by Gonzalez *et al.* (223)

Multi-walled carbon nanotubes were conjugated to three BPs, alendronate, pamidronate and neridronate, by Dlamini *et al.* (224) for the treatment of bone metastasis. The nanotubes had a diameter between 80 nm and 100 nm, maintained structural integrity after conjugation to the BPs and were soluble when conjugated to glucosamine. The drug release profile for neridronate was pH dependent, being faster at lower pH values due to the protonation of the amine group. There was increased efficiency in anti-cancer activity in MCF-7 cells when alendronate was conjugated to the carbon nanotubes, with a 12.63% decrease in cell viability, probably due to enhance targeted release of the drug onto the cells, though the opposite occurred with the remaining BPs.

2. THESIS OBJECTIVES

Laponite®is a synthetic silica clay mineral constituted by nanosized disk-shaped crystals that produce clear, colloidal dispersion or thixotropic gels when mixed with water, depending on the experimental conditions, being used as a rheology modifier and as a film forming agent, presenting numerous industrial applications (259). It is also used for biomedical applications, specifically Laponite® XLG, due to the smaller amounts of heavy metals it contains and as it degrades in the physiological environment, releasing products like silica, sodium, magnesium and lithium ions into the cell medium, exhibiting no cytotoxicity bellow 1 mg/mL (259–261). Laponite®'s constituting disks interact strongly with numerous chemical compounds, which makes it easy to functionalize and attractive to use to protect drugs from degradation in the physiological environment by intercalating them within the crystal stacks (259,262). Laponite® has been shown to induce osteogenic differentiation, as well as one of its degradation products, orthosilicic acid ($Si(OH)_4$), enhancing Laponite®'s potential for applications in drug delivery, especially in bone-targeted drug delivery (261,263–266).

Therefore, the general objective of this thesis is the development of a new treatment for osteoporosis, consisting of a laponite-based nanogel to encapsulate a bisphosphonate, specifically alendronate (Figure 16). In this nanosystem, while laponite will induce the osteogenesis, alendronate will inhibit the action of osteoclasts, thus allowing for the treatment of the disease. Additionally, as alendronate is known to exhibit high affinity for the bone mineral hydroxyapatite, it may also act as a bone targeting moiety. The encapsulation of alendronate in the nanogel may also increase its bioavailability and decrease the side effects it has in the organism. Besides laponite, which acts as a biocompatible and osteoinductive silicate that will produce a more cohesive nanogel; and alendronate, an active compound whose antiresorptive properties were previously mentioned; nanogels are also constituted by alginate, an agent that increases the cohesion of the nanogels' constituents; calcium, that promotes the connection of laponite and the remaining components through electrostatic interactions and allows for the gelation of alginate by acting as a ionic crosslinking agent; and, lastly, PEG, that stabilizes the nanogels, increasing their shelf-life, and conceals the nanoparticles in the human organism preventing their detection by the immune system and elimination, consequently increasing their circulation time and the probability that alendronate reaches its target.

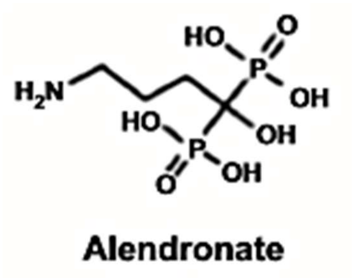

Figure 16 - Alendronate's structure (106)

In more detail, the present thesis aims at:

a) The synthesis of the aforementioned nanogels and their characterization by Dynamic Light Scattering (DLS), Electrophoretic Light Scattering (ELS) and Transmission Electron Microscopy (TEM); the alendronate entrapment efficiency was determined (using two different methodologies) and the effect of alendronate content on the nanogel's properties was evaluated.
b) The preparation of fluorescently labelled alendronate and its characterization by Nuclear Magnetic Resonance (^{1}H NMR) and Matrix-assisted laser desorption/ionization time-of-flight mass spectrometry (MALDI-TOF/TOF MS); additionally, fluorescent-labelled nanogels were prepared and characterized similarly to the non-fluorescent nanogels.
c) The study of the impact of freezing/thawing, as well as of lyophilization, on nanogels' properties in order to know the most suitable procedures for their handling and simultaneously assuring their stability along time.
d) The assessment of nanogels' swelling properties, biodegradation behavior and hemotoxicity.
e) The study of nanogels' kinetics of cell uptake and cellular internalization pathways using a relevant cell type (human Mesenchymal Stem Cells (hMSCs)).
f) The evaluation of the effect of the nanogels on the viability and osteogenic differentiation of hMSCs; the osteogenesis process *in vitro* was assessed using both quantitative (alkaline phosphatase (ALP) activity and osteocalcin expression measurements) and qualitative (ALP activity staining and calcium/phosphates staining) experiments.

3. MATERIALS AND METHODS

3.1. Nanogels Synthesis

The nanogels synthesis was done by firstly adding 1 mL of a calcium solution, with 0.0025 M calcium chloride (Sigma-Aldrich) and 0.0025 M calcium sulfate (Sigma-Aldrich), to 10 mL of distilled water, under magnetic stirring. 20 mg of Laponite® XLG (Rockwood) were then added to the solution, followed by 20 mg of Alginate (Alginic acid sodium salt from brown algae, Sigma), and then the alendronate (ALD, Sigma Aldrich) in the mass specific to each nanogel, from which their nomenclature was developed (0 mg for the Nanogel-0, 10 mg for the Nanogel-10 and 20 mg for the Nanogel-20). The solution was sonicated for 10 minutes at 25 kHz after each addition and the synthesis was performed under magnetic stirring. Lastly, 2 mL of a 6 kDa PEG (Fluka) solution (6 mg/mL) were added, without sonication and the stirring was maintained for 10 more minutes. The composition of each nanogel is summarized in Table 2 and the schematic representation of nanoparticles is in Figure 17.

Table 2 - Composition of the Nanogels.

Nanogel Code	Alendronate (mg)	Laponite (mg)	Alginate (mg)	Ca^{2+} solution (mL)*	PEG solution (mL)**
Nanogel-0	0	20	20	1	2
Nanogel-10	10	20	20	1	2
Nanogel-20	20	20	20	1	2

*$CaCl_2$/$CaSO_4$ solution at 2.5 mM; **PEG solution at 6 mg/mL.

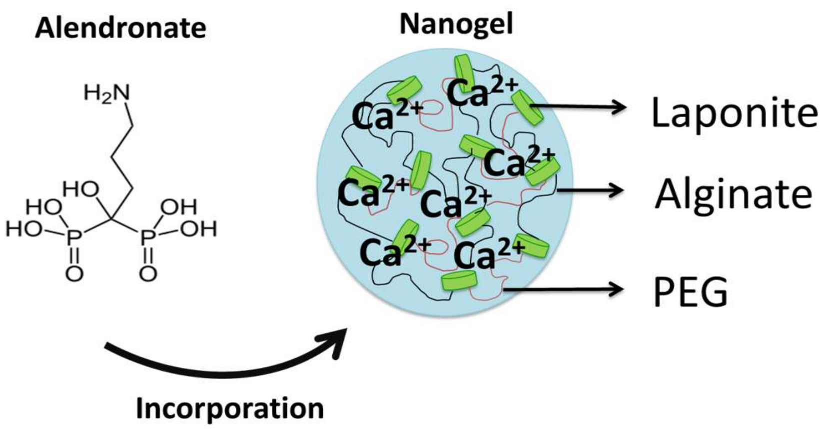

Figure 17 - Schematic representation of the nanoparticles that constitute the alendronate-loaded nanogel.

3.2. Synthesis and characterization of FITC-Alendronate conjugate

For the cellular uptake and the endocytosis assays, alendronate was conjugated to a fluorescent compound, fluorescein isothiocyanate (FITC, Sigma), in a protocol adapted from that described by *Thompson et al. 2006* (267).

FITC was dissolved in dimethyl sulfoxide (DMSO, Fisher Scientific) and mixed with alendronate in bicarbonate buffer (0.1 M, pH 9.5) in 3:2 mass ratio. The mix was incubated overnight under magnetic stirring and protected from light exposure. After that, the FITC-Alendronate conjugate was separated from the free components by silica column chromatography (Silica Gel for chromatography, 0.060-0.200 mm, 60A, Acros Organics), using a flash chromatography column, and using as eluent a mix of tetrahydrofuran (THF, Fisher Scientific):Methanol (Fisher Scientific) (1:10 volume ratio). To recover the conjugate, the colored portion of the silica was scraped and the conjugate resolubilized in water with manual agitation and with vortex, separating the silica by centrifugation at 2000 rpm for 5 minutes (Sigma 3K30 Centrifuge). This resolubilization was repeated 5 times, until the silica became white and the supernatant was clear. The solubilized conjugate was lyophilized and analyzed by ^{1}H NMR and MALDI-TOF/TOF MS.

NMR data was acquired with Bruker Avance II+ equipped with a 400 MHz magnet UltraShield ™ 400 Plus with an autosampler. ^{1}H NMR spectra were recorded using 64 scans. Chemical shifs (δ) were reported in parts per million (ppm) units and the spliting paterns were described as follows: s (singlet), d (duplet), q (quadruplet) and m (multiplet). Alendronate was dissolved in Deuterium oxide (D_2O), FITC in DMSO and the conjugates were dissolved in D_2O. The acquisition and analysis of all NMR data was performed on Topspin 3.5 software (Bruker)

For the Matrix-assisted laser desorption/ionization time-of-flight mass spectrometry (MALDI-TOF/TOF MS), the conjugate was dissolved in water at 1 mg/mL concentration and premixed with the matrix solution (1:1 volume ratio). For the matrix, α-cyano-hydroxy-cinnamic acid (CHCA) was dissolved at a concentration of 10 mg/mL in 50% acetonitrile (ACN)/water solution with 0.05% Trifluoroacetic acid (TFA). The small amount of TFA was added to increase concentration of protons and increase ionization of sample. MALDI-TOF/TOF MS spectra were acquired using Bruker Autoflex maX (Bruker, Bremen, Germany), that uses a Smartbeam™-II technology, with light emission at 355 nm and maximal frequency of 2 kHz. The spectrum was acquired in negative mode, using reflector detector (1970 V detector gain) and delayed extraction time (120 ns). Reflector mode and delayed extraction conditions improve the spectra resolution and mass precision. The method was calibrated by using internal standard from signals arising from CHCA. For each spectrum, 2000 individual laser “shots” at a frequency of 200 Hz were averaged.

The conjugate was later used to prepare fluorescent-labelled Nanogel-10 and Nanogel-20, according to the protocol previously described (2.1), denominated Fl-Nanogel-10 and Fl-Nanogel-20, respectively.

3.3. Dynamic Light Scattering and Electrophoretic Light Scattering

Nanogel-0, Nanogel-10, Nanogel-20 as well as Fl-Nanogel-10 and Fl-Nanogel-20 were characterized immediately after synthesis by Dynamic Light Scattering (DLS) at room temperature with a measurement angle of 173°, with a Zetasizer Nano ZS (Malvern Panalytical), determining their hydrodynamic size, polydispersity index (PdI) and zeta potential, this last one through Electrophoretic Light Scattering (ELS). The analysis was performed in triplicate with ten runs each.

3.4. Transmission Electron Microscopy

Firstly, Nanogels 0, 10 and 20 were diluted in H_2O (1:250). 10 µL of the samples were then mounted on Formvar/carbon film-coated mesh nickel grids (Electron Microscopy Sciences, Hatfield, PA, USA) and left standing for 2 minutes. The excess liquid was removed with filter paper and the grids were stained with 10 µL of uranyl acetate for 10 seconds. Visualization was performed on a JEOL JEM 1400 TEM at 120kV (Tokyo, Japan) and the images were digitally recorded using a CCD digital camera (Orious 1100W Tokyo, Japan at the HEMS / i3S of the University of Porto).

3.5. Ultracentrifugal filtration for nanoparticles separation from the supernatant

To calculate the entrapment efficiency of alendronate inside the nanogels, Nanogel-10 and Nanogel-20, as well as both fluorescently labelled nanogels, were diluted in water (1:250) and placed in Amicon® Ultra-4 Centrifugal Filter Devices (Millipore) with a MWCO of 3 kDa, being then filtrated through ultracentrifugal filtration at 4000 rpm for 50 minutes (ROTOFIX 32 A, Hettich). The supernatant was used to quantify the amount of free alendronate in Nanogel-10 and Nanogel-20. For non-fluorescent nanogels, two different methods were used to quantify the amount of free alendronate in the formulation: ^{31}P NMR due to the presence of phosphorus nuclei in the structure of alendronate; and alendronate derivatization to a chromophorus with absorbance at 405 nm. For the fluorescent-labelled nanogels, the free FITC-Alendronate conjugate was analyzed in a microplate reader using fluorescence detection at 485nm/535 nm ($\lambda_{exc}/\lambda_{em}$).

3.6. Quantification of Alendronate by Derivatization

As alendronate is not a chromophoric compound, its quantification was firstly done via a derivatization into a colored product, described by Walash et al. 2012 in “Method II”, using 2,4-Dinitrofluorobenzene (DNFB, Sigma) as the derivatizing agent and using borate buffer (0.2 M, pH 10.5) and HCl (6M) in the derivatization reaction (268). In this case, the filtrates obtained from the ultracentrifugal filtration previously described were then derivatized and analyzed at 405 nm in a microplate reader (Perkin Elmer VICTOR3TM), with borate buffer as a blank. A calibration curve was also created using standard alendronate solutions (Figure 45). The entrapment efficiency was calculated by the difference between the amount of alendronate initially added to the nanogels and the amount detected in the filtrate, as mentioned above.

3.7. Quantification of Alendronate by ^{31}P NMR

The quantification of free alendronate in the filtrate was also performed by ^{31}P NMR, as alendronate is the only molecule in the formulation containing phosphorus nuclei, making the method selective to the compound of interest.

Due to the fact that the NMR signal intensity is proportional to the number of nuclei, in precise and controlled conditions, this technique can also be used as a quantitative tool (269). Therefore, quantitative NMR (qNMR) gives the concentration of analytes directly determined via the integral value ratio. The results obtained by qNMR are considered accurate and precise when using internal standard methods. However, an external standard technique in qNMR has been also developed as an ERETIC tool (Electronic Reference to access in vivo Concentrations) by Bruker for the PULCON methodology (Pulse Length–based Concentration determination).

The alendronate concentration was measured by ^{31}P NMR using the ERETIC method without internal standards. All NMR spectra were acquired by a Bruker Avance II+ NMR spectrometer (^{31}P: 400 MHz) using standard NMR tubes, at room temperature and data acquisition and processing were performed with Topspin 3.5 software (Bruker). The acquisition parameters used for performance tests were the following: data acquisition time (AQ): 0.51 s; number of scans (NS): 24; loop count for TDO: 124; size of FID (TD): 64 K. Peak integration was manually selected, and the concentration of alendronate was quantified by using ERETIC tool in Topspin 3.5 software. Individual integral values, concentration and the number of protons in the signal used for quantitation in the reference were entered to ERETIC software and then the concentration of signal in sample was automatically calculated.

3.8. Entrapment efficiency

The entrapment efficiency (%EE) of alendronate or FITC-Alendronate conjugate inside the nanogels was calculated through the difference between the amount of alendronate or conjugate initially added to the formulation and the free compound still present in the filtrate, quantified by NMR and derivatization for Nanogel-10 and Nanogel-20, and by the analysis of the fluorescence for Fl-Nanogel-10 and Fl-Nanogel-20. The following formula was used, where C_i is the concentration of total alendronate in the initial solution and C_f the concentration of alendronate in the filtrate, corresponding to the non-entrapped compound still remaining outside the nanogels:

$$\%EE = \frac{C_i - C_f}{C_i} x\ 100$$

3.9. Freezing and Thawing

Nanogel-0 and Nanogel-20 were prepared in triplicate and immediately characterized through DLS at room temperature, determining their hydrodynamic size and polydispersity index. Following the characterization, the nanogels were frozen overnight at -20°C, -80°C or -196°C (in this last case using liquid nitrogen followed by overnight freezing at -80°C). Then, they were removed from the freezers and allow to thaw and warm up to room temperature for 1h, after which they were analyzed with DLS, evaluating the same parameters as before. They were analyzed again in 24h intervals until the hydrodynamic size returned to the initial values.

3.10. Lyophilization

Nanogel-0 and Nanogel-20 were synthetized, characterized and frozen as described in the previous topic. After overnight freezing they were lyophilized and, afterwards, resuspended in equal volume of water to the initial formulation, followed by homogenization through manual and vortex agitation, until all the lyophilizate was resuspended and the solution become clear. The solutions were left at room temperature and characterized with DLS, analyzing the same initial parameters, after 1h and then in 24h intervals until the hydrodynamic size returned to the initial values.

3.11. Swelling

Nanogels 0 and 20 were synthetized in triplicate and characterized using DLS, determining the hydrodynamic size and polydispersity index of the particles. They were then frozen at three temperatures: overnight freezing at -20°C, overnight freezing at -80°C and -196°C using liquid nitrogen followed by overnight freezing at -80°C. The nanogels were lyophilized and then resuspended in volume of H_2O equal to the initially added and characterized again with DLS immediately after the resuspension and for the following weeks until their stabilization, being stored at room temperature during the study. Swelling percentage was calculated using the formula bellow, where S_f is the size of the nanoparticle at the time of analysis and S_i is the initial size of the nanoparticle:

$$Swelling\ (\%) = \frac{S_f - S_i}{S_i} \times 100$$

3.12. Biodegradation

Nanogel-0 and Nanogel-20 were synthetized in duplicate and characterized using DLS at room temperature, analyzing their hydrodynamic size and polydispersity index, and then incubated with two lysozyme (Lysozyme from Chicken Egg White, Sigma) solutions (1000 U/mL and 10 000 U/mL) at 37°C. They were then characterized with DLS for the following weeks, until 31 days. The biodegradation percentage was determined through the variation of the size of the nanoparticles, using the following formula, with S_f being the size of the nanoparticle at the time of analysis and S_i is the size of the nanoparticle before incubation with the lysozyme solution:

$$Biodegradation\ (\%) = \frac{S_f - S_i}{S_i} \times 100$$

3.13. Hemotoxicity

The hemotoxicity of Nanogel-0 and Nanogel-20, as well as a free-alendronate solution of equivalent alendronate concentration to that of Nanogel-20, was determined in 5 concentrations each (10 µM, 50 µM, 100 µM, 500 µM and 1000 µM), with H_2O as a positive control and PBS as a negative control, using cyanmethemoglobin, in a method adapted from those of CLSI (The Clinical & Laboratory Standards Institute), ASTM (American Society for Testing and Materials) and ICSH (International Council for Standardization in Haemotology)(270–272).

Cyanmethemoglobin reagent (C reagent) was prepared by dissolving 50 mg of potassium ferricyanide, 12.5 mg potassium cyanide and 30 mg potassium dihydrogen phosphate in H_2O completing the volume to 250 mL and adding 250 µL of TritonX-100. Finally, the solution pH was adjusted to 7.4.

A standard curve of hemoglobin (Hg) concentration was plotted using a stock solution of hemoglobin (from bovine blood, Sigma) (Figure 46) and its purity was determined by reading the absorbance of hemoglobin solution in C reagent at 550 nm and 405 nm and calculating their ratio, which should be between 1.59 and 1.63.

$$Hg\ purity\ = \frac{A_{550}}{A_{405}}$$

To quantify the total concentration of hemoglobin in the blood used, a 250-fold dilution of blood in C reagent was prepared and its absorbance measured at 550 nm. The concentration of hemoglobin was calculated through the formula below, where A_{550} is the absorbance at 550 nm, D_f is the dilution factor (1:250) and F the slope of the equation of the standard Hg curve.

$$[Hg] = \frac{A_{550} \times D_f}{F}$$

A 10% blood solution in PBS was prepared and added to each compound solution as well as the controls in a 1:8 ratio. Total concentration of hemoglobin in test tubes was calculated according to the formula bellow, were D^f is the dilution factor (1:80).

$$T(g/L) = \ [Hg]/D_f$$

The solutions were incubated at 37°C for 3h, centrifuged at 3800 rpm and the supernatant was added to C reagent in a 1:5 proportion. The absorbance was then measured at 550 nm using C reagent as a blank, and the concentration of hemoglobin in the supernatants calculated through the following formula, where S is the total concentration of hemoglobin, A_{550} is the absorbance at 550 nm, D_f is the dilution factor (1:5) and F the slope of the equation of the standard Hg curve.

$$S = \frac{A_{550} \times D_f}{F}$$

The hemotoxicity of all compounds was determined by the formula bellow.

$$Hemolysis\ (\%) = \ (S \times T) \times 100$$

3.14. hMSCs isolation and culture

All cellular experiments were done using human Mesenchymal Stem Cells (hMSCs) as this cell line is capable of differentiating into osteoblasts *in vitro* (273). hMSCs were obtained from small fragments of trabecular bone rich in bone marrow from healthy adults during surgery interventions after trauma, that would have alternatively been discarded, with approval from the ethics committee of Hospital Dr. Nélio Mendonça. The cells were cultured with α-Minimum Essential Medium (α-MEM, Gibco) with 10% Fetal Bovine Serum (FBS, Gibco) and 1% of an antibiotic-antimycotic 100x solution (AA, Gibco with penicillin, streptomycin, and amphotericin B), in a 95% humidified atmosphere, 5% of CO_2 at 37°C.

3.15. Cytotoxicity

The cytotoxicity of Nanogel-0, Nanogel-10 and Nanogel-20 was determined by the Resazurin Reduction Assay. This test determines the cell viability in percentage, establishing a correlation between the cellular metabolic activity and the number of viable cells in culture, assuming that healthy cells are capable of reducing resazurin into its fluorescent product, resorufin, while non-viable cells cannot do it. Resazurin enters the cells, as it is membrane permeable, and is reduced to resorufin that is excreted and accumulates in the medium (274,275).

Cells were seeded in 24-well plates and exposed to the nanogels for 24 hours, followed by exposure to a resazurin solution (0.1 mg/mL) for 4 hours. The resorufin released from the cells was then quantified measuring the fluorescence of the supernatant (λ_{exc}= 530 nm; λ_{em}= 590 nm), in microplate reader. The cytotoxicity of fluorescent-labelled nanogels was also quantified using the same protocol.

3.16. Cellular Uptake in hMSCs

To determine the uptake of the fluorescent-labelled nanogels, cells from the 7th passage were used. Cells were seeded in 48-well plates, at a density of 50 000 cells/well, and in the following day exposed to Nanogel-20 with FITC-ALD conjugate, at a concentration of 1000 μM, at different times: 0, 0.5, 1, 2, 4, 6 and 24 hours, being incubated at 5% of CO_2 at 37°C. Then, cells were washed twice with PBS, detached using 0.25% trypsin-EDTA (1x, Gibco) and analyzed by flow cytometry (NovoCyte 3000, ACEA). The internalization profile of the nanoparticles indicates the efficiency of their delivery to the cells, and, therefore, the kinetics of cellular uptake were analyzed and curve-fitted to the Michaelis-Menten equation:

$$Y = \frac{V_{max} \times t}{k_m + t}$$

Where Y is the uptake in real time, t is the incubation time, V_{max} is the saturated cellular uptake and k_m is the time when the uptake is 50% of V_{max}. Thus, a smaller k_m implies a quicker cellular uptake.

3.17. Internalization pathways in hMSCs

With the purpose of determining the pathways involved in the internalization of the nanoparticles, Fl-Nanogel-20 formulation was used. Previously, cells from the 10th passage were seeded in 48-well plate at a density of 50 000 cells/well and preincubated with the following inhibitors: 3 µg/mL chloropromazine (Sigma-Aldrich), an inhibitor of clathrin-mediated endocytosis; 5 µg/mL cytochalasin D (Sigma), that inhibits micropinocytosis; 2 µg/mL nocozadole (Sigma), which inhibits phagocytosis; 4 µg/mL nigericin (Carbosynth), that acts as a lysosomotropic agent; and 1 µg/mL filipin III (Sigma), that inhibits caveolae-mediated endocytosis, at 5% of CO_2 at 37°C for 1 hour. Afterwards, they were washed twice with PBS and incubated with the Fl-Nanogel-20, at a concentration of 1000 µM, for 6 hours. Finally, they were washed again with PBS, detached with trypsin and analyzed with flow cytometry, as previously described. The results were compared with cells incubated without inhibitors.

3.18. Osteogenic differentiation of hMSCs

For the osteogenic differentiation and its evaluation assays, cells from the 5th passage were used. Cells were initially cultured in 24 well plates at a density of 5000 cells/cm^2 for 72 hours in α-MEM with 10% (v/v) FBS and 1% (v/v) AA. Then, they were incubated with the medium containing osteogenesis inducing agents, together with the samples to be tested (Nanogel-0, Nanogel-20 and Alendronate-20), for 24 hours. The nanogels solutions were at 10 µM alendronate concentration. The osteogenic agents were 1 nM of dexamethasone (Alfa Aesar), an inducer of osteogenic differentiation; 5 mM of ß-glycerophosphate (Sigma), a source of phosphate; and 250 µM of ascorbic acid, that increases the secretion of collagen (276,277). Cells were cultured for 18 days, changing the medium twice a week.

3.19. Evaluation of hMSCs osteogenic differentiation

3.19.1. Quantitative Assays

Alkaline Phosphatase Assay

The activity of Alkaline Phosphatase (ALP) was determined after 18 days, using a colorimetric test with p-nitrophenyl phosphate, that was reduced to p-nitrophenol by this enzyme, forming a complex with a yellow color and a inorganic phosphate. The cell lysis was performed by adding 50 µL of Triton X-100 1% (v/v) in PBS solution and incubating them at 4°C, for 30 minutes, under agitation, followed by sonication on ice for 2 minutes. 20 µL of each homogenized lysate were transferred to a 96-well plate and 200 µL of ALP substrate solution were added. The cell lysates were incubated with 2 mM p-nitrophenyl phosphate in sodium phosphate buffer (pH=10 with 15 mM $MgCl_2$), at 37°C for 1 hour protected from light exposure. Afterwards, 0.02 M NaOH was added to stop the reaction and develop the color. A calibration curve was also created with standard solutions of p-nitrophenol. The absorbance was read at 405 nm in a microplate reader.

Bicinchoninic Acid Assay

To calculate the specific percentage of ALP activity, the quantification of total protein was also performed through the bicinchoninic acid (BCA) assay, using bovine serum albumin as a standard to create a calibration curve.

Osteocalcin Assay

Osteocalcin is one of the main non-collagenous proteins in the extracellular matrix of the bone tissue expressed in the later stages of cells differentiation, the matrix mineralization, prior to the formation of calcium and phosphate deposits (278,279). The osteocalcin produced by cells after the 18-day differentiation was quantified using a Human Osteocalcin ELISA kit (Invitrogen).

3.19.2. Qualitative Assays

ALP Staining

For the ALP staining, cells were fixed with 1.5% (v/v) glutaraldehyde and a solution of Na-α-naphtyl phosphate (2 mg/mL) and fast blue RR salt (2 mg/mL) in 0.1 M Tris buffer (pH=10) was added. The solution was removed after 1 hour and the samples rinsed with water and analyzed. The presence of a yellow-brown color was indicative of ALP activity after 18 days of differentiation.

Besides the expression of proteins like osteocalcin, the later stages of osteogenic differentiation are also identified by the formation on calcium and phosphate deposits as the matrix is mineralized (280,281).

Alizarin Red Staining

To identify calcium deposits after 18 days of differentiation, the Alizarin Red staining was performed, which identifies these deposits by the development of a red stain. The cells were covered with a solution of 1% (w/v) S alizarin sodium sulfonate solution prepared in 0.028 % (v/v) NH_4OH (pH 6.4). After 2 minutes, cells were washed with water, acid ethanol (<15 s, ethanol containing 0.01% v/v in HCl) and again with water.

Von Kossa staining

Phosphate deposits were also detected with the Von Kossa staining after 18 days, that indicates their presence by developing a black coloration. Cells were fixed with 1.5% (v/v) glutaraldehyde, covered with a 2.5% (w/v) Silver Nitrate Solution and placed under UV light for 1 hour. The solution was removed, and the cells were rinsed with ultrapure water. A 5% sodium thiosulfate (w/v) solution was added for 2 minutes, rinsing the cells again with distilled water again and analyzing color developed.

All the staining assays were analyzed and photographed with Nikon Eclipse TE 2000E inverted microscope.

4. RESULTS AND DISCUSSION

The purpose of this thesis was to develop a nanosystem for the delivery of a bisphosphonate to the bone tissue for the treatment of osteoporosis. This nanosystem consisted on nanogels that were constituted by Laponite®, known for its osteogenic inducing properties, a varying amount of alendronate, with known antiresorptive properties, and from which the following nomenclature was developed: Nanogel-0 (with no alendronate), Nanogel-10 (with 10 mg of alendronate) and Nanogel-20 (with 20 mg of alendronate), as previously indicated in Table 2, and contained also alginate, which improves the biocompatibility and cohesion of the nanogel, calcium, that promotes the connection of laponite and the remaining constituents and also allows for the gelation of alginate, and, lastly, PEG, that increases the shelf-life of the nanogels and also their circulation time in the organism by concealing the nanoparticles and preventing their detection by the immune system. The nanogels' physicochemical properties were characterized, and they were also analyzed in multiple cellular assays. In order to evaluate the kinetics of cellular uptake as well as the internalization pathways through which the nanoparticles enter the cells, alendronate was conjugated to a fluorophore, FITC, characterized by two different techniques and that was then used to prepare fluorescent-labelled nanogels denominated Fl-Nanogel-10, with 10 mg of FITC-Alendronate conjugate, and Fl-Nanogel-20, with 20 mg of that conjugate, whose physicochemical properties were also characterized.

4.1. Synthesis and Characterization of FITC-Alendronate conjugate

After testing various eluents and eluent ratios using thin layer chromatography in silica plates (Figures 47-49), the conjugate was separated from the free components in the solution by silica column chromatography, using a flash chromatography column, as this allowed for a faster separation of the constituents of the mix. THF:Methanol (1:10 volume ratio) was used as a mobile phase as the polarity of this solution allowed the elution of FITC while the conjugate remained in the silica, being recovered afterwards (Figure 50).

To verify the formation of the FITC-Alendronate conjugate by ^{1}H NMR, both FITC and alendronate were characterized by the same technique to identify the signals arising from each component and their conjugation.

FITC (Figure 18) was dissolved in 100% DMSO-d6 and the chemical groups present in its structure produced the respective signals in the ^{1}H NMR spectrum that is present in the Figure 19. From right to left, the first two signals at δ = 2.50 ppm and δ = 3.35 ppm correspond to the solvent (DMSO). The following six signals appear between δ = 6.53 and δ = 8.05 ppm correspond to aromatic protons of FITC, identified with the numbers 1 to 6 in its structure (Figure 18), appearing further upfield in the spectrum the protons in the vicinity of the more electronegative groups, namely the protons at 5 and 6 in the structure. Lastly, a signal is detected at δ = 10.17 ppm, which corresponds to the protons of the OH groups, identified with number 7 in the structure, at furthest upfield in the spectrum as they are highly affected by the electronegativity of oxygen. The signals detected from the FITC molecule are in agreement with those found in the literature (282,283).

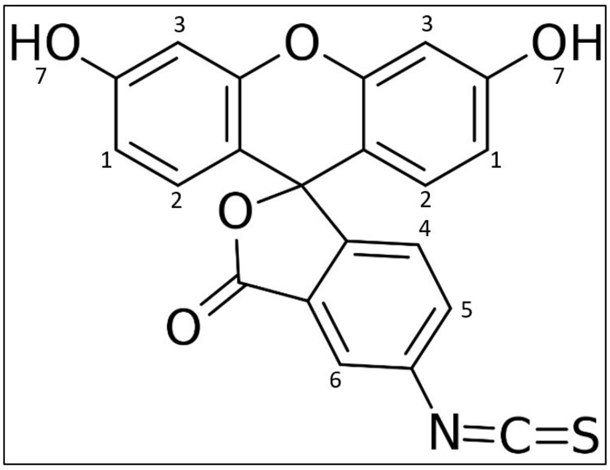

Figure 18 - FITC molecule with ^{1}H NMR signal identification.

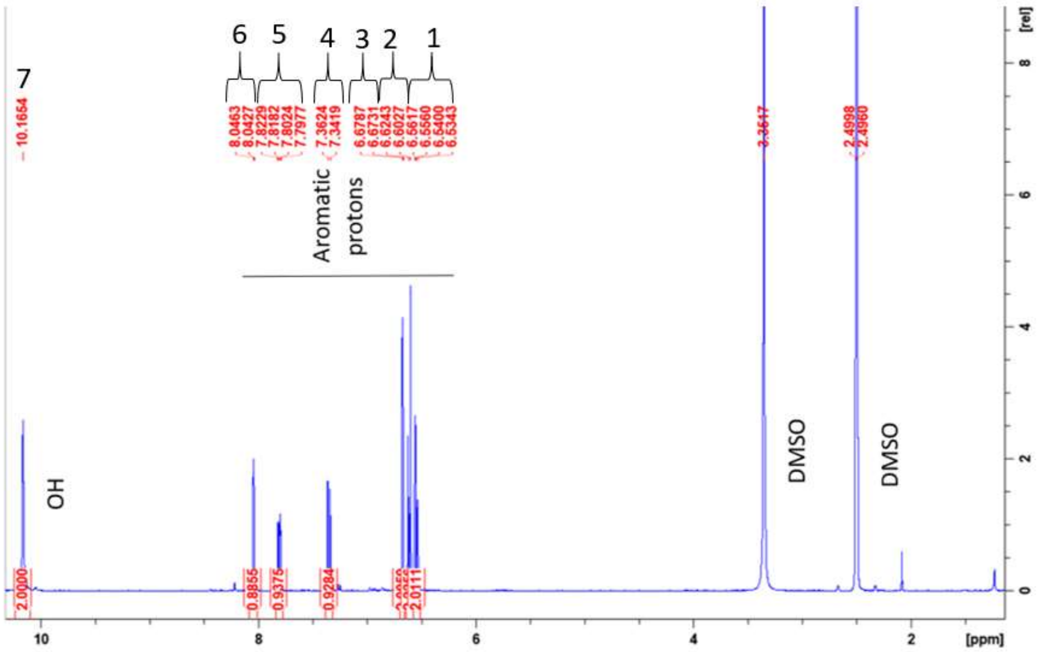

Figure 19 – ^{1}H NMR spectrum obtained for FITC in 100% DMSO with chemical shifts and proton quantification. Acquisition with 64 normal scans. ^{1}H NMR chemical shifts (in ppm): δ 2.50 (s, DMSO, solvent), δ 3.35 (s, DMSO), δ 6.53-6.56 (q, aromatic CH), δ 6.60-6.62 (d, aromatic CH), δ 6.67-6.68 (d, aromatic CH), δ 7.34-7.36 (d, aromatic CH), δ 7.79-7.82 (q, aromatic CH), δ 8.04-8.05 (d, aromatic CH), δ 10.17 (s, OH).

Alendronate was also analyzed through ^{1}H NMR spectroscopy, being dissolved in 100% deuterium oxide (D_2O). Its molecular structure with identified chemicals groups that produced signals in the NMR spectrum and the obtained spectrum are represented in Figure 20. Three signals corresponding to alendronate were identified in the spectrum. From right to left, the first signal detected, at δ = 1.97 ppm corresponds to the protons in the CH_2 groups of alendronate (Numbers 2 and 3 in the structure), followed by a signal at δ = 3.01 ppm corresponding to the protons in the CH_2 group connected to the NH_2 at the end of the molecule (Number 1 in the structure), both with shifts similar to those reported in the literature (284). Then, a signal corresponding to the solvent, D_2O, appears at δ = 4.80 ppm. Lastly, a small signal appears at δ = 7.60 ppm corresponding to the protons of NH_2, however it is hardly visible due to their exchange with the deuterium in the solvent.

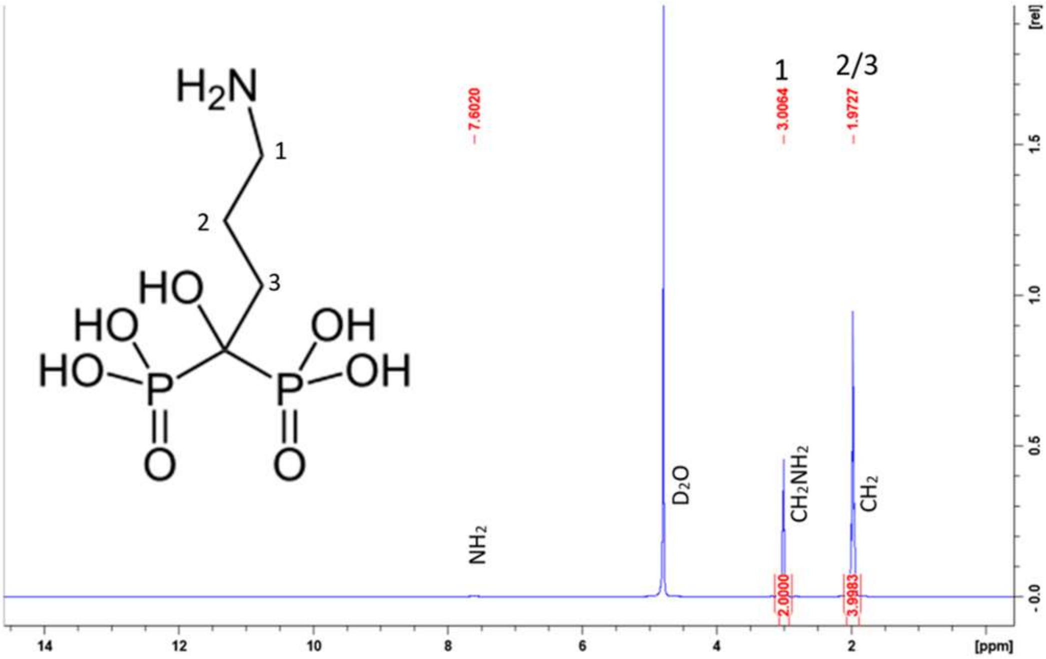

Figure 20 - Alendronate structure with ^{1}H NMR signal identification (left) and ^{1}H NMR spectrum obtained for Alendronate in 100% D_2O with chemical shifts and proton quantification. Acquisition with 64 normal scans (400MHz, D_2O).^{1}H NMR chemical shifts (in ppm): δ 1.97 (s, CH_2), δ 3.01 (s, CH_2NH_2), δ 4.80 (s, D_2O, Solvent), δ 7.60 (s, NH_2).

The FITC-Alendronate conjugate was dissolved in 100% D_2O for ^{1}H NMR analysis. The structure of the compound is represented in Figure 21, with the identification of the chemical groups that produced the signals in the NMR spectrum, while the obtained spectrum is shown in Figure 22. A total of 9 signals arising from the conjugate were identified. From right to left, the first signal identified corresponds to the protons of the CH_2 groups of alendronate, number 1, at δ = 1.96 ppm, followed by a signal at δ = 2.69 ppm corresponding to the protons of the CH_2NH group of alendronate, being shifted and more intense than in the free alendronate spectrum, since there is a new bond in the vicinity, the thiourea bond, that changes the chemical environment of this group where in the conjugate form. A signal appears at δ = 3.03 ppm that presumably also corresponds to the CH_2NH group, as there might still be some free alendronate that did not form conjugate and that presents a signal at this chemical shift. This is supported by the sum of the integration areas of the peaks at δ = 2.69 and δ = 3.03 ppm, which is approximately 50 and correspond to CH_2NH group of alendronate (number 2); while the integration of the peak at δ = 1.96 ppm, referring to the protons of the CH_2 groups (number 1) is approximately 100, meaning that this latter groups correspond to double the protons of those two peaks, as shown in the structure, with two CH_2 groups, totaling 4 protons, and one CH_2NH group, with only 2 protons. The conjugation of the two molecules is confirmed by the formation of the thiourea bond, identified with number 3 in the structure, whose signal is detected at δ =

3.62 ppm, corresponding to the aliphatic protons in the $CH_2NHC=S$ group, previously reported in the literature (282,283).

The signal from the protons of NH group of alendronate is not detected, likely being overlapped with the signals from the aromatic protons of FITC, which appear from δ = 6.61 to δ = 7.69 ppm, numbers 4 to 9 in the conjugate structure, appearing at higher shifts due to the change of the solvent. No signal from the OH group of FITC was detected in the conjugate spectrum, presumably due to the use of D_2O as the solvent, whose protons can exchange with the ones from the OH group.

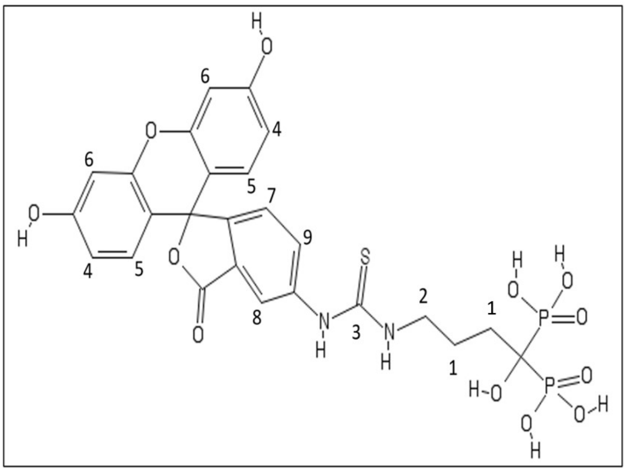

Figure 21 - FITC-Alendronate conjugate structure with ^1H NMR signals identification.

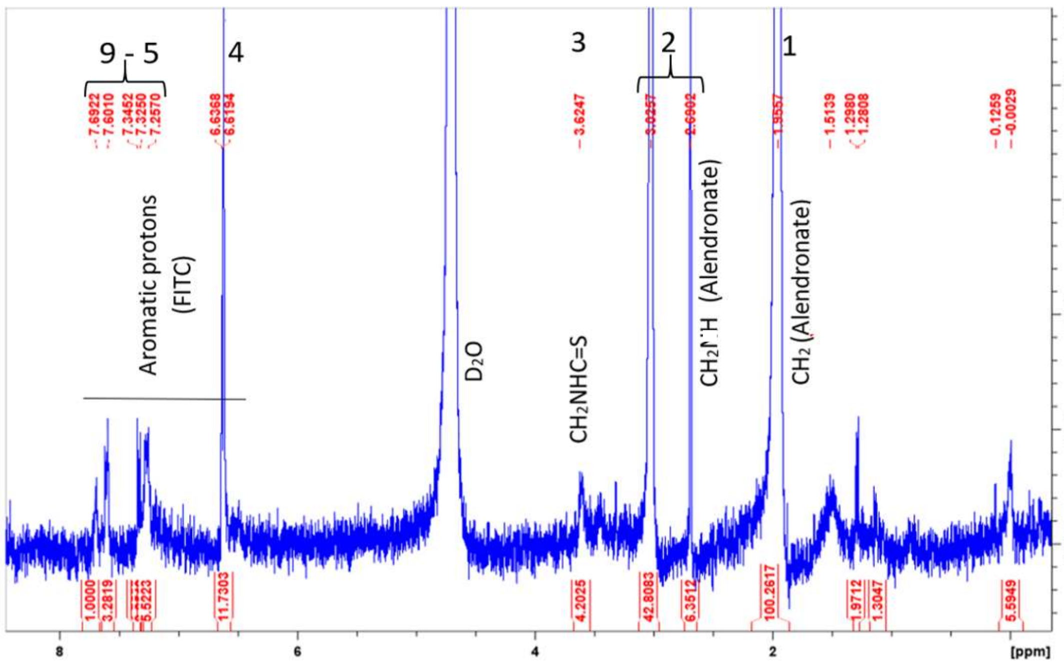

Figure 22- ^1H NMR spectrum obtained for FITC-Alendronate conjugate in 100% D_2O with chemical shifts and proton quantification. Acquisition with 64 normal scans.^1H NMR chemical shifts (in ppm): δ 1.96 (s, CH_2), δ 2.69 (s, CH_2NH), δ 3.03 (s, CH_2NH), δ 3.62 (s, $CH_2NHC=S$ bond), δ 4.80 (s, D_2O), δ 6.61-6.63 (d, aromatic CH), δ 7.26-7.69 (m, aromatic CH).

The formation of the FITC-Alendronate conjugate is also easily detected in the MALDI-TOF mass spectrum obtained (Figure 23).

Negative ion mode was used as the compounds used in the synthesis are very negatively charged, therefore being more readily detected as negative ions rather than positive ions in MALDI-TOF. The signals in negative ion mode are generated by subtraction of one proton to give a singly negatively charged ion and, consequently, detected ions are shifted towards lower values for 1. The values indicated in the spectrum are theoretical, presenting a deviation from experimental m/z positions of less than 0.02 m/z units.

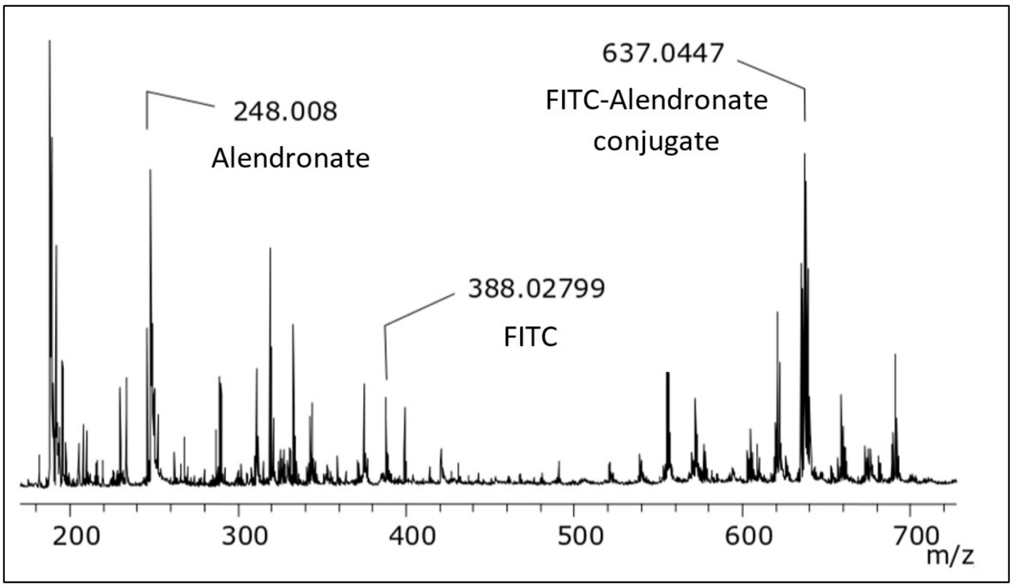

Figure 23 - Negative ion mode MALDI TOF mass spectrum of FITC-Alendronate conjugate acquired with CHCA matrix. Signals arising from the conjugate and individual components are indicated by their m/z ratio. Other signals arise from applied matrix. m/z = 248.008 (Alendronate), m/z = 388.02799 (FITC), and m/z = 637.0447 (FITC-Alendronate conjugate).

The expected mass calculated from the molecular structure of the FITC-Alendronate conjugate (Figure 21) is 638.48 g/mol and it is possible to identify in the spectrum an intense signal arising at m/z = 637.0447 from the conjugate, as well as a signal at m/z = 388.02799 arising from the FITC moiety of the molecule and a signal arising at m/z = 248.008 arising from the alendronate moiety, detected in fragmentation spectrum. It is, therefore, possible to conclude that the synthesis of the fluorescent-labelled alendronate was successful.

Apart from molecular ion derived signals, there are also signals arising from fragmentation products (not labelled in the spectra), with lower intensity compared to non-fragmented ions, and various signals arising from the matrix, CHCA, as this molecule yields numerous polymerization products, especially in negative ion mode.

4.2. Hydrodynamic Diameter, Polydispersity Index and Zeta Potential

The DLS analysis (Table 3) of the nanogels demonstrates that the addition of increasing amounts of alendronate does not affect de polydispersity index of the nanoparticles, that is approximately 0.400 in all nanogel formulations (Figure 24, left), a reasonable value that indicates an acceptable distribution of nanoparticle hydrodynamic diameter, without formation of large aggregates. However, there is a slight change in the particle hydrodynamic diameter (Figure 24, left), reducing it from 211 nm to roughly 180 nm. The superficial charge of the nanoparticles, zeta potential, became slightly less negative (Figure 23, right), remaining nonetheless highly negative, which allows the repulsion of the nanoparticles from each other and prevents the formation of aggregates, ensuring good stability of the nanogels solutions. The changes in the hydrodynamic diameter and superficial charge of the nanoparticles occurs due to the presence of the amino groups in alendronate. As they are positively charged, the overall charge of the nanoparticle becomes less negative with increasing alendronate concentrations and they become more compact due to the electrostatic interaction with the remaining compounds in the formulation that present opposite charge in the present conditions, specifically laponite and alginate that are negatively charged.

The hydrodynamic diameter of the nanoparticles obtained is adequate to the aimed purpose, as particles with sizes from 70 nm to 200 nm were shown to remain in the bloodstream for a longer time period without being eliminated, and are successfully delivered to the bone tissue (285–287).

Table 3 - Effect of increasing quantities of Alendronate and FITC-Alendronate in the nanogels (hydrodynamic diameter, polydispersity index and zeta potential). Note: All data represent the mean ± standard deviation (n = 3).

Nanogel Code	Alendronate (mg)	Hydrodynamic Diameter (nm)	Polydispersity Index	Zeta Potential (mV)
Nanogel-0	0	211 ± 25	0.38 ± 0.01	-59.5 ± 3.3
Nanogel-10	10	185 ± 10	0.38 ± 0.01	-52.0 ± 1.5
Nanogel-20	20	179 ± 14	0.40 ± 0.01	-51.2 ± 2.3
Fl-Nanogel-10	10	204 ± 11	0.60 ± 0.01	-37.1 ± 0.6
Fl-Nanogel-20	20	385 ± 17	0.55 ± 0.13	-36.7 ± 0.2

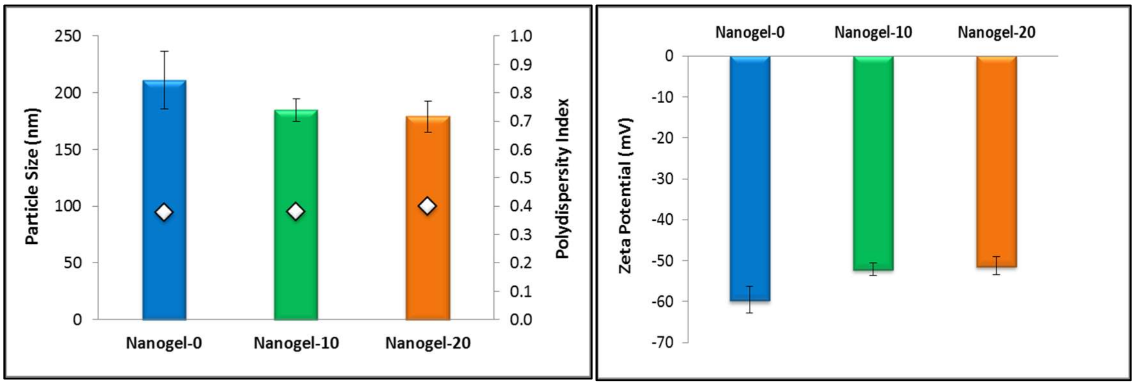

Figure 24 - Hydrodynamic diameter, PDI and zeta potential of nanogels with increasing alendronate concentrations. Note: All data represent the mean ± standard deviation (n = 3).

In the case of the fluorescent-labelled nanogels, the nanoparticle hydrodynamic diameter for Fl-Nanogel-10 (204 nm) is close to that of Nanogel-10 (185 nm), however that value nearly doubles for Fl-Nanogel-20 (384 nm). The PdI is similar in both nanogels containing FITC-Alendronate conjugate (0.55 to 0.60), with values higher than the non-fluorescent nanogels (Figure 25, left). As with non-fluorescent nanogels, the superficial charges of the fluorescent-labelled nanoparticles become slightly less negative with the addition of higher amounts of conjugate, from -37.1 to -36.7, (Figure 25, right).

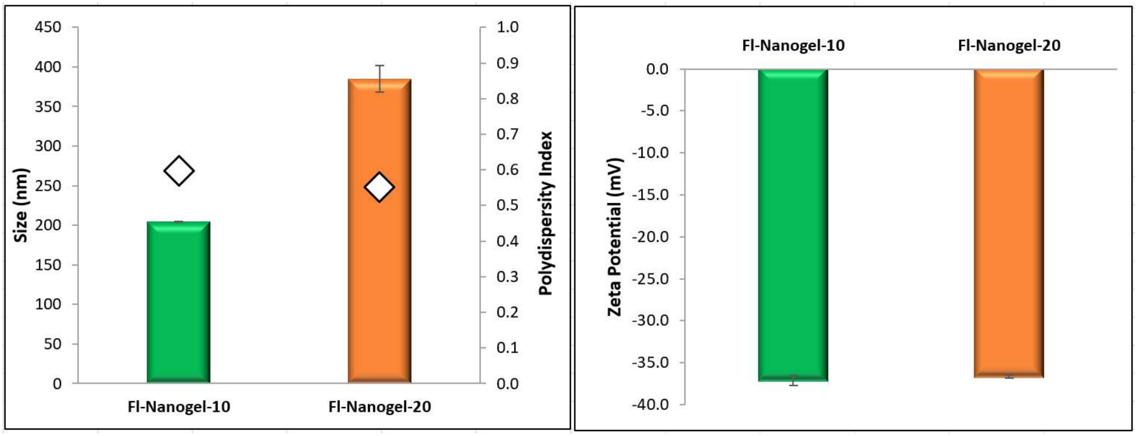

Figure 25 - Hydrodynamic diameter, PDI and zeta potential of fluorescent-labelled nanogels with increasing FITC-Alendronate conjugate concentrations. Note: All data represent the mean ± standard deviation (n = 3).

4.3. Transmission Electron Microscopy

In the micrograph obtained from TEM analysis, presented in Figure 26, it is possible to see that the nanoparticles from Nanogel-0 has a well-defined and structured round shape, having various white spots in its surface, appearing to be constituted by an agglomerate of filaments. However, the nanoparticles from the Nanogel-10 containing 10 mg of alendronate have a much more amorphous and less defined round shape with a uniformly darker surface. The nanoparticles of Nanogel-20 are also rounder and smaller than the ones of Nanogel-10, which is consistent with the results from DLS, again confirming the contraction of the nanoparticles, due to the electrostatic interactions of the amino groups in alendronate with the other constituents of the nanogel.

The size of the nanoparticles in the three nanogels is slightly smaller than the one determined by DLS, as DLS is a technique that measures the hydrodynamic diameter of the particles, i.e. the nanoparticles and their solvent layer, whereas TEM allows us to visualize the nanoparticle alone in a dry state.

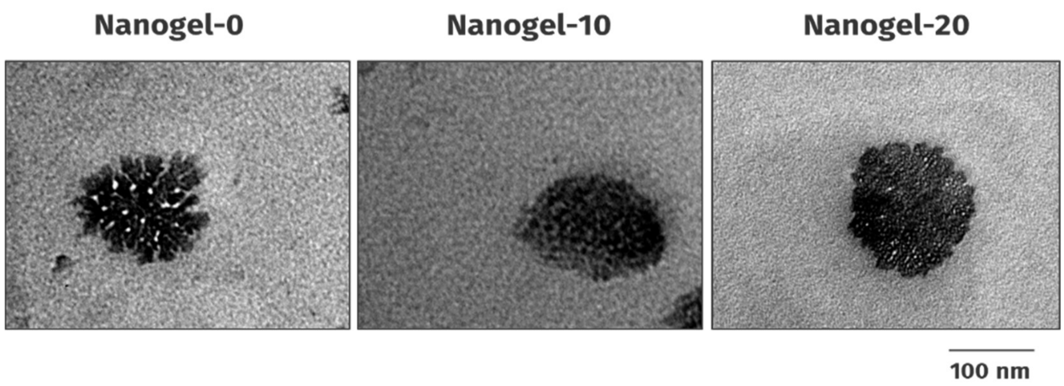

Figure 26 - TEM analysis of the nanogel particles (1:250 dilution in H_2O).

4.4. Ultracentrifugal filtration for nanoparticles separation from the supernatant

As the filtration of the nanogels was required for the quantification of the entrapment efficiency of alendronate inside the nanogels, the effect of the dilution and filtration on the nanoparticle size was evaluated. The dilution of the nanogels was necessary to prevent the clogging of the filters used.

The dilution of the nanogels in distilled water (250x) caused a decrease in the nanoparticle size (Figure 27), presumably because that dilution allows the particles to be more separated and, consequently, prevents their aggregation, decreasing their average size.

The filtration of nanogels through Amicon® Ultra-4 Centrifugal Filter Devices did not influence the size of the nanoparticles, which remained at about 150 nm before and after the process (Figure 26). This is important as it ensures the successful separation of nanoparticles from the supernatant with the purpose of using it later for quantifying the free alendronate that was not incorporated inside the nanogels.

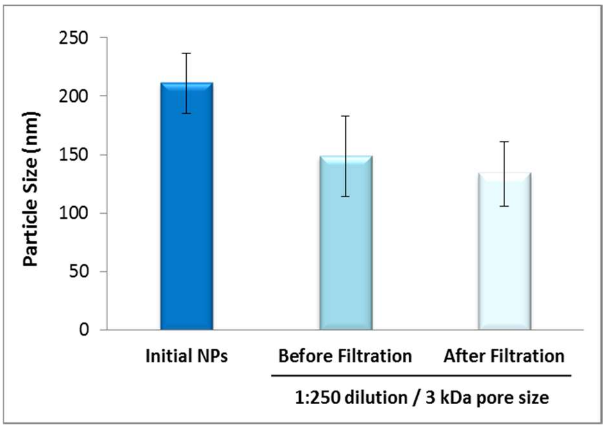

Figure 27 - Effect of ultracentrifugal filtration using Amicon® Ultra-4 Centrifugal Filter Devices with a 3kDa pore in a 1:250 diluted solution of Nanogel-0.

4.5. Entrapment efficiency

The entrapment efficiency of alendronate or FITC-Alendronate inside the nanogels was determined by quantifying the amount of alendronate in the filtrates resulting from the ultracentrifugal filtration and subtracting it to the amount initially added to the formulations.

For non-fluorescent nanogels, the quantification of alendronate was firstly performed through a derivatization into a colorimetric compound (λ = 405 nm) described by *Walash et al. 2012*, based on the reaction of the amino group with DNFB (268). Figure 28 displays the absorption spectrum of the derivatization product of the reaction between alendronate and DNFB, with the structure of the compound on the right. The absorbance was read at 405 nm.

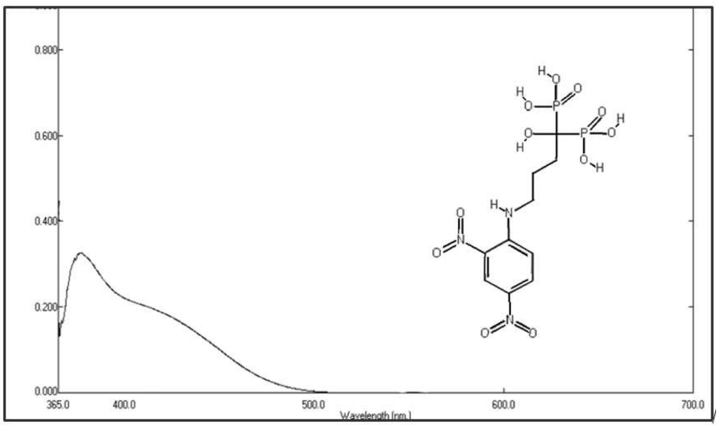

Figure 28 – Reaction product of the derivatization of alendronate and DNFB and its absorption spectrum. Adapted from: *Walash et al. 2012* (268).

A second method was also performed for the quantification of unlabelled-alendronate inside nanoparticles. Figure 29 (left) shows the ^{31}P NMR spectra of alendronate, with a peak detectable at approximately 17.7 ppm, and the increase of its area with higher concentration of alendronate, as expected. From peak integration, the concentration of alendronate can be obtained through the ERETIC tool of Bruker software. The calibration curve obtained is represented also in Figure 29 (right).

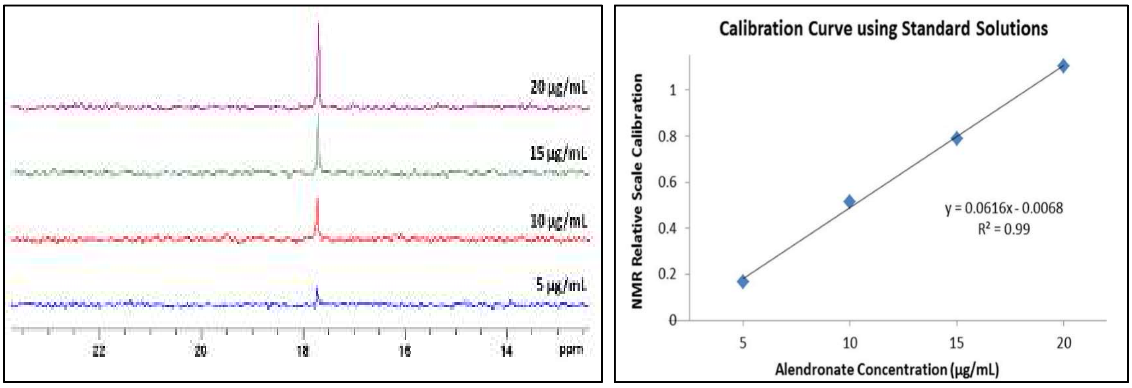

Figure 29 - ^{31}P NMR spectrum of the alendronate standard solutions (on the left) and the respective calibration curve with increasing alendronate concentration (on the right).

For the nanogels with unlabelled-alendronate, both ^{31}P NMR and spectrometric analysis of the derivatization compound gave similar results (Table 4), with both nanogels presenting high entrapment efficiencies, Nanogel-10 with 64-71% and Nanogel-20 with 75-80%, having Nanogel-20 slightly higher values than Nanogel-10 with either methods. The synthesis performed was, therefore, successful in the incorporation of alendronate, especially considering its simplicity.

Fluorescent-labelled nanogels also exhibited high entrapment efficiencies, above 60%, with Fl-Nanogel-20 having a higher value (88%) than Fl-Nanogel-10 (64%) (Table 4), ensuring that the synthesis of the nanogels with the conjugate produced nanogels of similar entrapment efficiencies to the ones containing unlabelled-alendronate. These fluorescent-labelled nanogels were later used to study the kinetics of cellular uptake and the internalization pathways of the nanoparticles in hMSC cells.

Table 4 - Alendronate and Fl-Alendronate entrapment efficiency in the nanogels. Note: All data represent the mean ± standard deviation (n = 3).

Supernatant Samples	Method	Entrapment Efficiency (%)
Nanogel-10	Spectrometric analysis of the derivatization compound of alendronate with DNFB in the filtrate	64.3±4.7
Nanogel-20	Spectrometric analysis of the derivatization compound of alendronate with DNFB in the filtrate	75.8±2.7
Nanogel-10	^{31}P qNMR of alendronate in the filtrate	71.1±3.0
Nanogel-20	^{31}P qNMR of alendronate in the filtrate	79.6±0.5
Fl-Nanogel-10	Fluorometric analysis of FITC-Alendronate conjugate in the filtrate	63.5±2.1
Fl-Nanogel-20	Fluorometric analysis of FITC-Alendronate conjugate in the filtrate	88.1±0.1

4.6. Freezing and Thawing

The analysis of the effect of freezing and thawing on the nanogels was performed to determine which freezing method is the best in terms of storage stability but also because the freezing of the nanogels was required for the swelling studies.

The freezing procedures did not cause notable changes in particle size in Nanogel-0, with only a slight enlargement verified, that was reversed after 24 hours of thawing (Figure 30, left). The PdI was also not largely affected, varying from 0.40 to 0.43, approximately (data not shown).

With Nanogel-20, a drastic increase of nanoparticle size occurred when the nanogel was frozen at -20°C, with the nanoparticle size increasing to about three times the original size (Figure 30, right) and the polydispersity index rising from 0.41 to 0.49 (data not shown). Both parameters returned to values close to their initial ones 48 hours after thawing. When frozen at -80°C, the nanoparticles became more compact after 24 hours of thawing, the same being verified for the freezing using liquid nitrogen followed by overnight freezing at -80°C, with the polydispersity index in both cases remaining approximately the same. This alteration is possibly due to a reorganization of the structure of the nanoparticle, presumably due to the interaction of alendronate with the remaining components in the solution, that takes place when the freezing is done at -20°C, as at this temperature the nanogel freezes at a slower rate, that also could allow the formation of agglomerates of nanoparticles. Freezing at -80°C or with liquid nitrogen/-80°C induces a quicker freezing of the nanogels which likely does not allow for the reorganization of the nanoparticles nor their agglomeration. However, the nanoparticles' size returns to values very close to the initial ones, in both nanogel solutions, indicating that the alteration of the nanoparticle size caused by the low temperatures is fully reversible. Possibly, this is due to electrostatic interactions between the components with opposite charges, that is, laponite and alginate that are negatively charged and alendronate which is positively charged in the present conditions. These changes are also visible in the appearance of the nanogels (Figure 31), with Nanogel-20 becoming whiter and more opaque after thawing, which is reversed after 24 hours, with the solution returning to its original clear state.

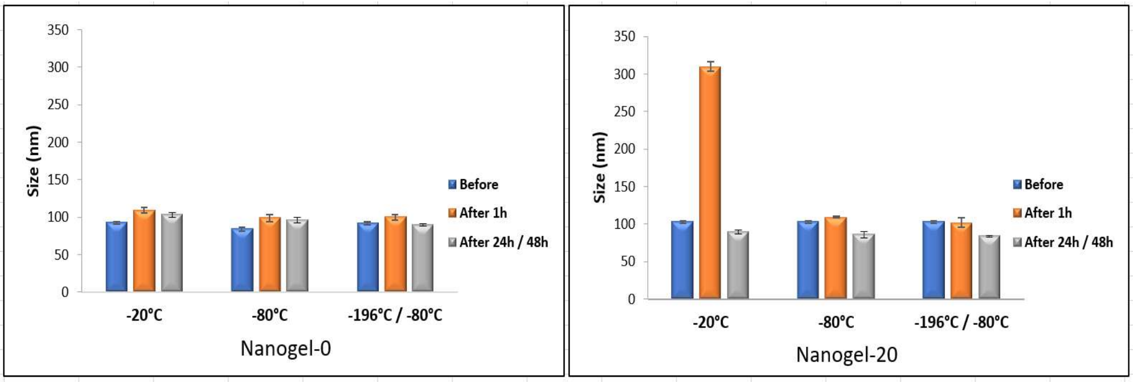

Figure 30 - Effect of one freezing-thawing cycle at different freezing temperatures on the size of the nanoparticles of Nanogel-0 and Nanogel-20. Samples were frozen overnight at -20°C, overnight at -80°C and with liquid nitrogen (-196°C) followed by overnight freezing at -80°C.

Figure 31 - Nanogel-0 (left) and Nanogel-20 (right) 1 hour after thawing. Note: The opacity of Nanogel-20 is reversed after 24 hours, with the solution returning to its original clear state.

Therefore, the freezing of the alendronate-loaded nanogels should be done at temperatures that promotes a quick freezing of the solution, either at overnight at -80°C or using liquid nitrogen for immediate freezing, in order to maintain the initial characteristics of the nanoparticles after thawing.

4.7. Lyophilization

After freezing and thawing studies, the effect of lyophilization of the nanogels was evaluated, again to determine the stability of the nanogels when subjected to this process and as it is a necessary step in the swelling studies.

The lyophilization process affected all nanogel formulations in all freezing temperatures, except for Nanogel-0 when frozen at -80°C, where the variation in the nanoparticle size was minimal (Figure 32).

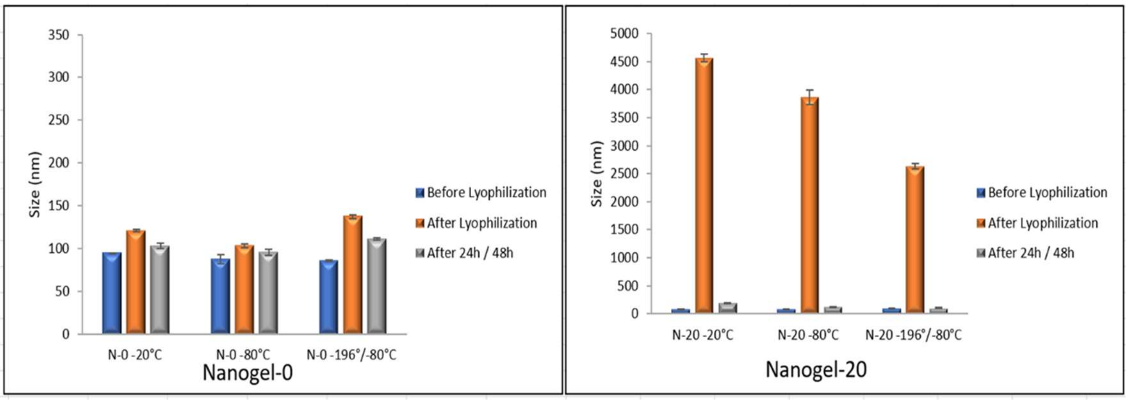

Figure 32 - Lyophilization studies of Nanogel-0 and Nanogel-20 at three different freezing conditions: overnight freezing at -20°C, overnight freezing at -80°C and freezing at -196°C with liquid nitrogen followed by overnight freezing at -80°C.

The effect on the nanoparticles of Nanogel-0 was overall less impactful, with particle size slightly increasing, and the nanogel being more affected by the freezing with liquid nitrogen followed by -80°C where nanoparticles changed from 90 to 150 nm, being almost reverted to their initial size (Figure 32). The PDI of the nanoparticles suffers a slight increase from 0.43 before the lyophilization to 0.45 after the resuspension, remaining stable even after particles return to their initial size (data not shown).

Nanogel-20 is greatly affected by this process, with nanoparticles becoming much bigger, although they return to a size approximate to their initial one 48 hours after the resuspension, noting their restructuring capacity (Figure 32). PdI is mildly affected, decreasing from approximately 0.47 to 0.32 after the lyophilization and resuspension, and again increasing to 0.48 once particles return to the initial size (data not shown), denoting that the overall solution recovers its initial characteristics and nanoparticles remain uniform afterwards. Like in the freezing and thawing studies, the Nanogel-20 solutions also became whiter and more opaque after the lyophilization and resolubilization, recovering its original appearance after 48 hours. It appears that the disorganization of the nanoparticle structure proposed in the process of freezing and thawing also happens when the nanogels are lyophilized and resolubilized, although it is intensified.

However, as in the freezing study, the nanoparticle size returns to values close to the initial ones in all nanogel samples and temperatures, except Nanogel-20 when frozen at -20°C, where particle size stabilizes at roughly 200 nm. This is probably justified by the interactions between the different constituents of the nanogel, due to their electrical charge, that allow their attraction and the reorganization of nanoparticles identical to those initially created. This also remarks the stability of both nanogels after being subjected to lyophilization, an important factor for their storage stability, except when frozen at -20°C.

Hence, for the lyophilization process of Nanogel-20, freezing the sample at -80°C or using liquid nitrogen followed by overnight freezing at -80°C are the best options, while for Nanogel-0 freezing overnight at -80°C is more suitable than the other alternatives.

4.8. Swelling

Swelling behavior and structural integrity are key design factors in developing hydrogels, being relevant not only for their storage stability but also to understand their behavior in the organism. Swelling of Nanogel-0 and Nanogel-20 was studied in the function of time after the resuspension in distilled water of the lyophilized nanogel, determined by their water absorption capacity (Figure 33).

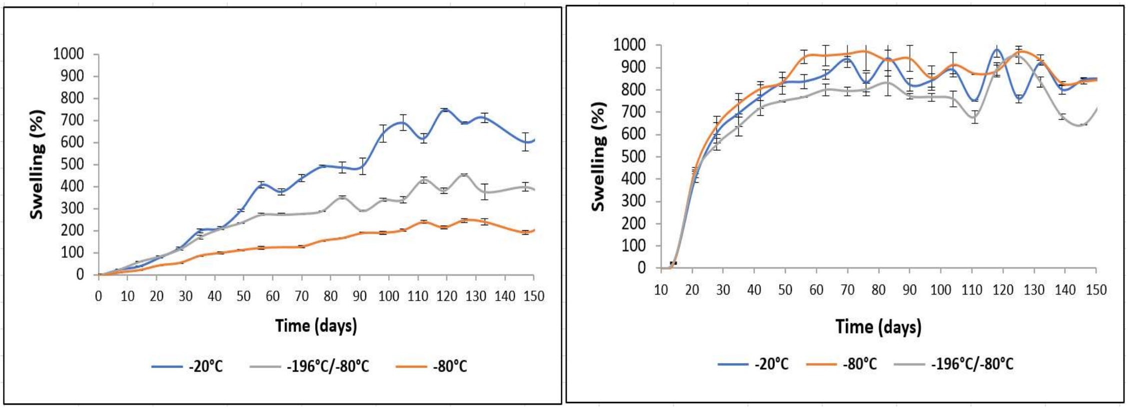

Figure 33 - Swelling studies of Nanogel-0 (left) and Nanogel-20 (right).

Nanogel-20 displayed a much quicker and drastic swelling, compared to Nanogel-0, although it stabilized earlier, at approximately 60 days (Figure 33, right), with the particle size increasing to over 1 µm. One can also verify that there is less variations induced by the freezing temperature. Nanogel-0 presented a more gradual and less intense swelling, only stabilizing after about 120 days (Figure 33, left), at a particle size of 772 nm when frozen at -20°C, and a less severe swelling verified when frozen at lower temperatures and particle size reaching between 330 nm and 460 nm (Figure 33). The PdI of Nanogel-20 nanoparticles increased from around 0.44 to 0.66 when frozen at -20°C, 0.73 when frozen at -80°C and 0.71 when frozen with liquid nitrogen followed by overnight freezing at -80°C, indicating a broad distribution of particle size (data not shown). There could also be the formation of agglomerates of particles taking place throughout the process. With Nanogel-0, the PdI of the nanoparticles remained relatively stable throughout the study, with the largest increase verified when the nanogel is frozen with liquid nitrogen/overnight freezing at -80°C, going from 0.42 to 0.48 (data not shown). As previously mentioned, nanogels are capable of absorbing large amounts of water, thus the swelling behavior of Nanogel-0 is expected, but one can verify that the incorporation of alendronate in the nanogels, and the interactions it has with the remaining components, which are mostly hydrophilic, exacerbates that capacity, causing nanoparticles size to increase, although in a heterogenous manner, as indicated by the PdI (288).

Similarly to the previous studies, the alendronate-loaded nanogels became whiter, more opaque and a slight increase of their viscosity was noted immediately after their resuspension, and these changes were reversed after 48 hours (Figure 34). However, as time passed, the nanogels containing alendronate developed the whiter and more opaque coloration again, although less intense, and retained that aspect until the end of the studies.

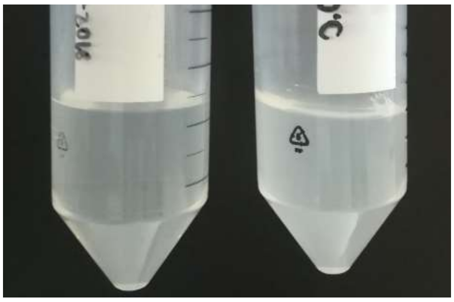

Figure 34 – Nanogel-0 5 weeks after the resuspension (left) and Nanogel-20, 21 days after the resuspension.

When it comes to the freezing procedure that is overall best suited for each nanogel, one can conclude that overnight freezing at -80°C is more adequate in the case of Nanogel-0 and that in Nanogel-20, although all freezing temperatures caused a similar swelling pattern, using liquid nitrogen (-196°C) followed by overnight freezing at -80°C leads to smaller swelling percentages, thus being more appropriate, consistent with what was verified with the freezing and thawing and the lyophilization studies. In the future, it would be recommended to study the swelling of the nanogels in response to stimuli such as pH and temperature, factors that will likely affect the behavior of the nanogels in the organism.

4.9. Biodegradation

The biodegradation of a material intended for biomedical applications is a very important parameter, as non-biodegradable materials could lead to accumulation in the body, inducing a toxic response. However, it is also important that the degradation products of the material do not present toxicity.

The degradation of this nanogel is also significant for the release of the active compound, alendronate, and its diffusion in the system until it reaches the target site, but also the remaining components that will also assist in the regeneration of the bone tissue, namely laponite and calcium.

The nanogels were incubated with a lysozyme solution, an enzyme that has been found in various human fluids, at varying concentrations, like serum, where its concentration varies from 4 to 13 mg/L, catalyzing the hydrolysis of ß(1-4) glycosidic bonds in certain polysaccharides, playing an important role in the defense of the organism against gram-positive bacteria. It is widely used to evaluate the *in vitro* degradation of polymers, like chitosan, and hydrogels

(289,290). The biodegradation rate was calculated based on the variation in the size of the nanoparticles in comparison to their initial size.

The incorporation of alendronate in the nanogel drastically increased its degradation rate (Figure 35). Nanogel-20 achieves 90% biodegradation much quicker than Nanogel-0, at 10 days compared to 31 days of Nanogel-0. This could possibly be due to the different structure of the nanoparticle which, as seen with the TEM micrograph, in Nanogel-0 is of a particle more organized and more defined, that would likely be harder to degrade by the enzyme, while in Nanogel-20 nanoparticles are more amorphous and not as structured as Nanogel-0, being easier to degrade. The changes are also visible in the appearance of the solution. In both nanogels, after 1 hour of incubation with the lysozyme solution, a small, white agglomerate is formed (Figure 36) that slowly dissolves throughout the duration of the study, and that does not form in the lysozyme solution alone (data not shown).

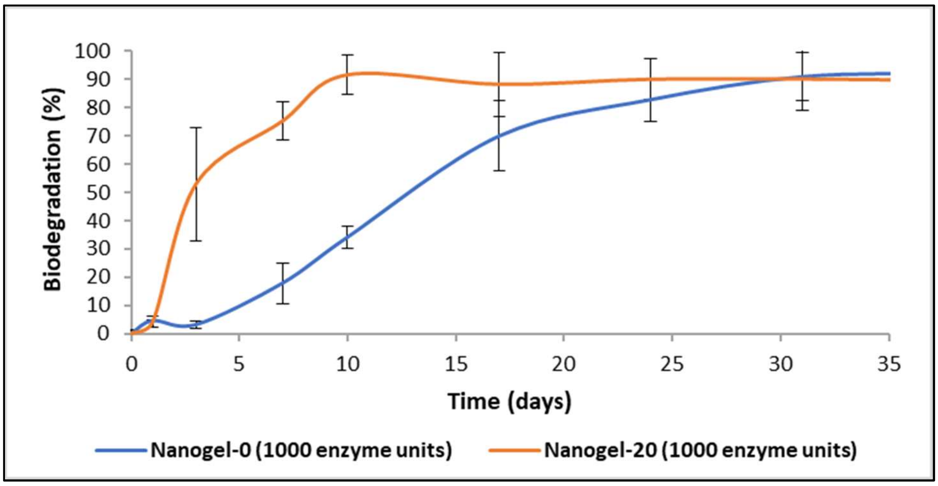

Figure 35 – Biodegradation studies of Nanogel-0 and Nanogel-20 using a lysozyme solution (1000 enzyme units).

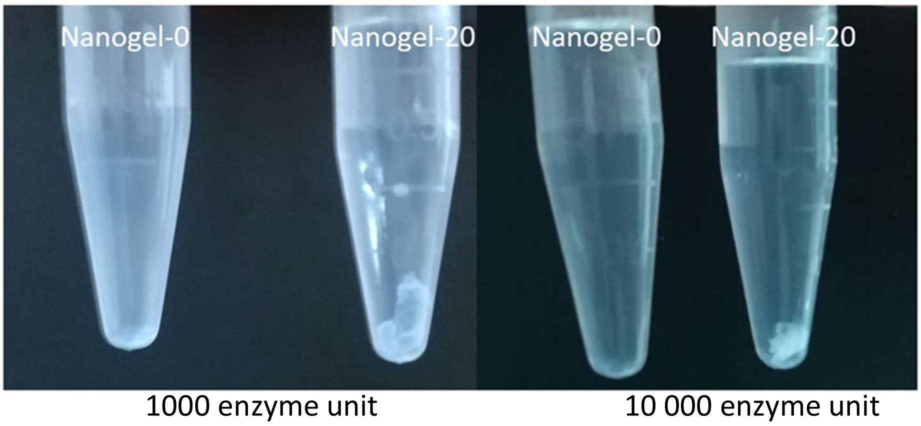

Figure 36 – Nanogel-0 and Nanogel-20 after 1 hour of incubation with a 1000 enzyme unit lysozyme solution (left) and a 10 000 enzyme unit lysozyme solution (right), with a translucent, white agglomerate visible that is larger and more noticeable in the nanogels incubated with the 10 000 enzyme unit lysozyme solution.

It would be recommended to study the biodegradation of the nanogel through different techniques, for example TEM, and when exposed to stimuli like varying temperature and pH that would mimic or resemble these conditions in the organism.

4.10. Hemotoxicity

The evaluation of the hemotoxicity or the hemocompatibility of biomaterials consists of analyzing the interactions between that compound and the different blood constituents, to detect any adverse effects that may arise from it and that are a key concern for their application in tissue engineering. This parameter can be evaluated through various assays, such as the erythrocyte composure, whether through their hemolysis or hemagglutination, thrombogenicity and complement system activation (291).

The determination of the hemotoxicity of the samples was done by analyzing their effect on erythrocyte hemolysis, through a colorimetric assay, consisting in, after the incubation with the nanoparticles, the addition of a hemolysis reagent, Triton X-100, to erythrocytes to release hemoglobin (Fe^{2+}) that is converted to methemoglobin (Fe^{3+}) by adding an oxidation reagent, potassium ferricyanide, to which a cyanisation reagent, potassium cyanide, is added to produce cyanide hemoglobin, in pH 7.4, maintained by potassium dihydrogen phosphate, allowing for a faster reaction (292). Cyanide hemoglobin has a broad absorption peak (530-550 nm), with a maximum at 540 nm, where the color intensity detected is proportional to the total hemoglobin concentration. By this method, the reagents are combined into one solution, C Reagent or Drabkin's reagent, and all forms of hemoglobin are converted to cyanmethemoglobin, except sulfemoglobin, that is present in blood only in minimal concentrations (293). The absorbance was measured at 550 nm as it was not possible to measure at 540 nm due to the filters available in the multilabel plate reader.

Neither the nanogels nor the free-alendronate solution caused hemolysis of red blood cells (Figure 37), therefore exhibiting no hemotoxic effect, even at higher concentrations, presenting hemolysis values below 5%, similar to that of the negative control (PBS). There is also not a gradual increase of the hemotoxicity with the increase of the concentration of each solution, nor with increasing the concentration of alendronate. These results ensure that both the nanogels and alendronate by itself are hemocompatible and will not induce a toxic response of the erythrocytes once they reach and circulate in the bloodstream.

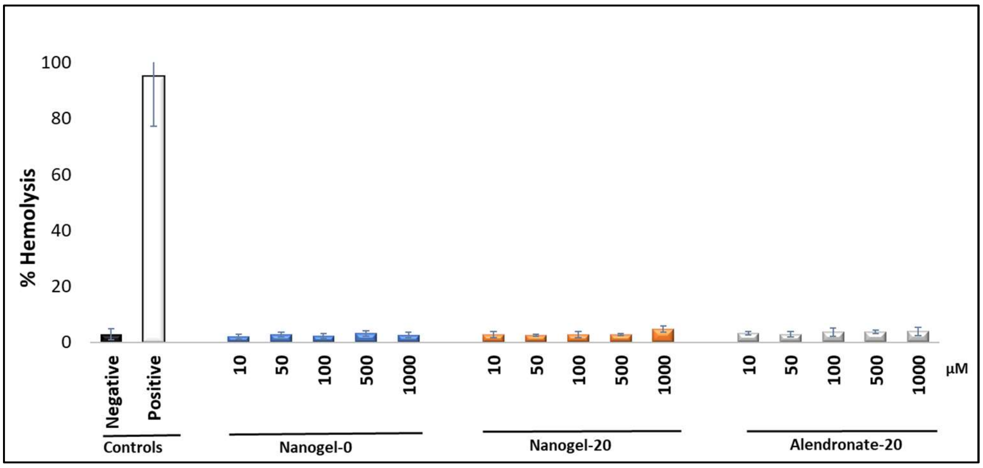

Figure 37 - Hemotoxicity studies of Nanogel-0, Nanogel-20 and a free alendronate solution of equivalent concentration to the nanogel. All data represent the mean ± standard deviation (n=4).

4.11. Cytotoxicity

Cytotoxicity is an important parameter to assess when nanomaterials are aimed at biomedical applications and can be evaluated, for example, by alterations in the integrity of the cell membrane or in their metabolic activity.

The cytotoxicity of the nanogels were evaluated after 24 hours of exposure to hMSC cells through the resazurin reduction assay that measures the metabolic activity of cells (Figure 38). The results showed that alendronate cytotoxicity is considerably lower when it is incorporated inside both nanogels (Nanogel-10 and Nanogel-20), especially at higher concentrations (1000 µM). While in its free form, alendronate caused a 60% decrease in cell viability, that reduction was of only 20% in both nanogels. Nanogel-0 also lead to a small reduction, with viability percentages similar to alendronate-loaded nanogels. This demonstrates the protecting effect conferred by the nanogels, which would minimize the side effects of the compound in the organism.

As both nanogels produced similar effects in terms of cytotoxicity and as Nanogel-20 contained more alendronate, it was chosen for the following osteogenic differentiation and its evaluation assays.

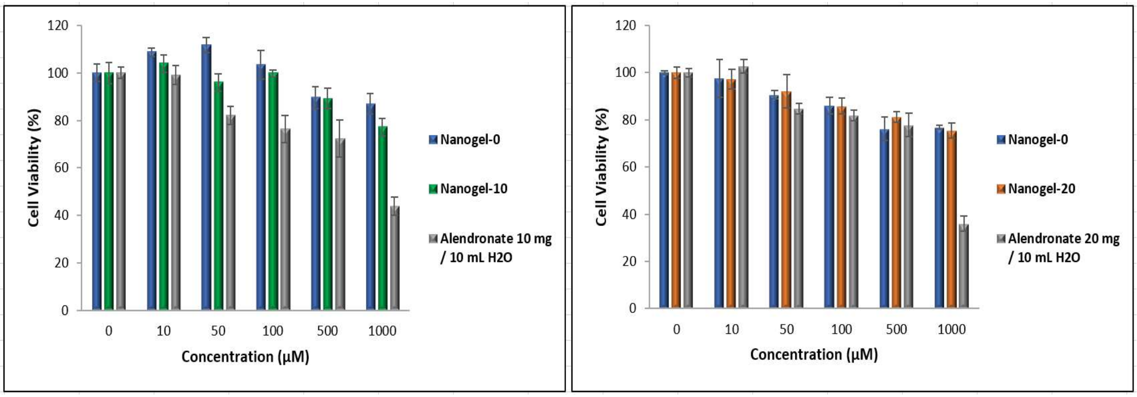

Figure 38 - Cell viability (%) of hMSC calculated from the metabolic activity through the resazurin reduction assay, after exposure to Nanogel-0 (with no alendronate), Nanogel-10 and Alendronate-10 (both with 10 mg of alendronate) on the left side; and Nanogel-0 (with no alendronate), Nanogel-20 and Alendronate-20 (both with 20 mg of alendronate) on the right side. Note: All data represent the mean ± standard deviation (n = 3).

The cytotoxicity of the fluorescent-labelled nanogels, analyzed in the same manner as the unlabelled nanogels, showed that none of the samples presented cytotoxicity, with all samples resulting in a decrease in viability of less than 30% (Figure 39). The FITC-Alendronate conjugate also caused low cytotoxicity, with viability percentages close to those of the nanogels.

As before, both nanogels displayed similar cytotoxicity effects, being therefore selected the Fl-Nanogel-20 for the following cellular tests, as it contains double the amount of alendronate.

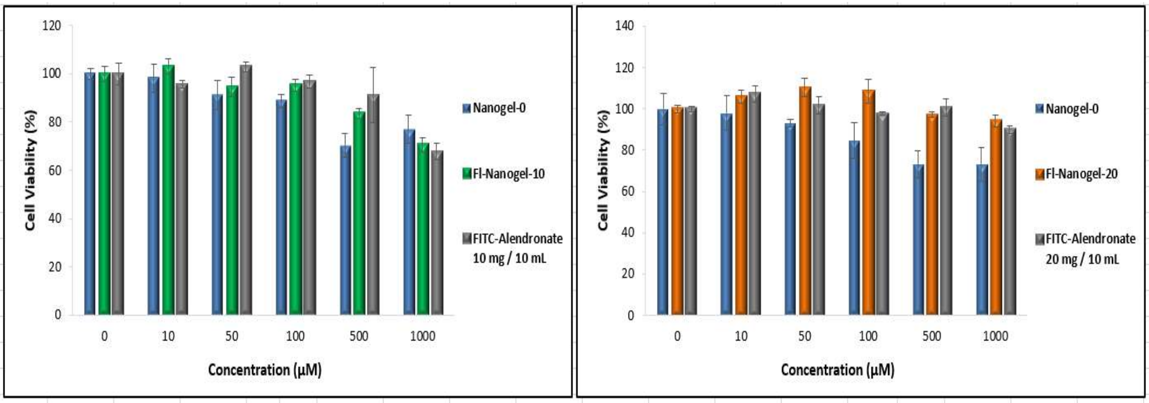

Figure 39 - Cell viability (%) of hMSC calculated from the metabolic activity through the resazurin reduction assay after exposure to Nanogel-0 (with no Fl-Alendronate), Fl-Nanogel-10 and Fl-Alendronate-10 (both with 10 mg of alendronate) on the left side; and Nanogel-0 (with no Fl-Alendronate), Fl-Nanogel-20 and Fl-Alendronate-20 (both with 20 mg of Fl-Alendronate), on the right side. Note: All data represent the mean ± standard deviation (n = 3).

4.12. Kinetics of cellular uptake

The cell membrane is the responsible for the protection of its intracellular constituents from the extracellular environment, maintain the cell homeostasis and ion concentration gradients, the entry and exit of various molecules and nutrients, but also provides structural support to the cell (294–296). As most nanomaterials are designed to exert their effects inside the cells, often targeting specific organelles and subcellular compartments, it is necessary to understand the cellular uptake mechanisms and the factors that influence it, therefore allowing us to design and modify the nanoparticles to improve their therapeutic action and their biocompatibility. Even before the nanoparticles enter the cell, they suffer changes, as they circulate in biological fluids, particularly the adsorption of biomolecules like proteins in the surface, known as the protein corona, that affects their interaction with the cell membranes and, consequently, their uptake and intracellular localization. Shape, size and superficial charge and composition are some of the characteristics of a nanoparticle that will affect their entry in the cell (297).

The analysis of the cellular uptake kinetics of the nanoparticles in hMSC cells through flow cytometry showed a time-dependent accumulation in the cells, where the cellular uptake follows the Michaelis-Menten kinetics (Figure 40). The saturated cellular uptake (V_{max}) obtained was of approximately 119,000 RFU after 24 hours, half of it (k_m) being achieved after approximately 5 hours of incubation. However, it is also possible to see that a plateau is not reached, indicating that the maximum cellular uptake is not yet achieved in those 24 hours of incubation and that it must take place only after a longer incubation time. Therefore, the kinetics of cell uptake of the nanogel will be repeated in the future, not only to confirm these results, but also to determine the maximum uptake and the time at which it occurs.

It is possible to verify in Figure 39 that a considerable uptake is reached at 6 hours. Consequently, this was the time selected for the incubation of the nanoparticles to evaluate the internalization pathways by which they enter the cell.

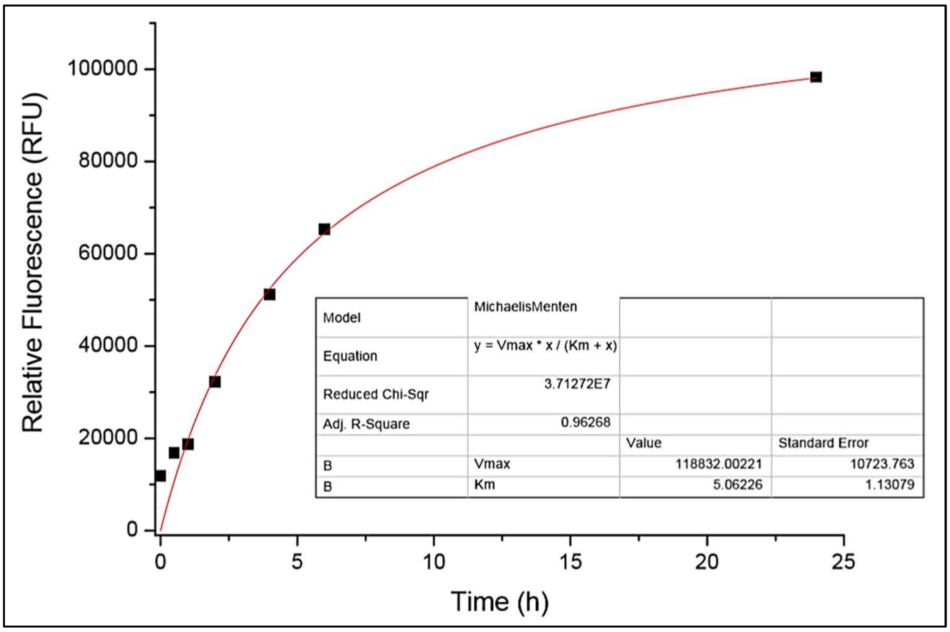

Figure 40 - Cellular uptake kinetic profile of Nanogel-20 in hMSCs, obtained by flow cytometry. Cells were exposed to Fl-Nanogel-20 for different times (0, 0.5, 1, 2, 4, 6 and 24 hours). Fluorescence intensity is presented as relative fluorescence units (RFU). Note: All data represent the mean ± standard deviation (n = 3)

4.13. Internalization pathways

The internalization pathways by which particles enter cells are commonly divided into passive transport and active transport, also known as endocytosis, which can be further divided into phagocytosis, mainly occurring in professional phagocytes, and pinocytosis, that includes clathrin-mediated endocytosis, caveolae-mediated endocytosis, clathrin- and caveolin-independent endocytosis and macropinocytosis (220,297). As with the cellular uptake kinetics, this dependents on factors such as nanoparticles size, shape, surface charge, hydrophobicity and surface functionality, as well as the cell type where the same nanoparticles can be up taken through different pathways in different cell lines (237,297).

Different endocytic pathway inhibitors were used in order to identify which internalization pathways were involved in the cellular uptake of the nanoparticles of Fl-Nanogel-20 on hMSC cells. Figure 41 displays the effect of each inhibitor on the uptake of the nanoparticles. The fluorescence of cells incubated without inhibitors was considered to be 100% of cellular uptake and the fluorescence after the incubation with each inhibitor was expressed as a relative percentage compared to the fluorescence of cells without inhibitors.

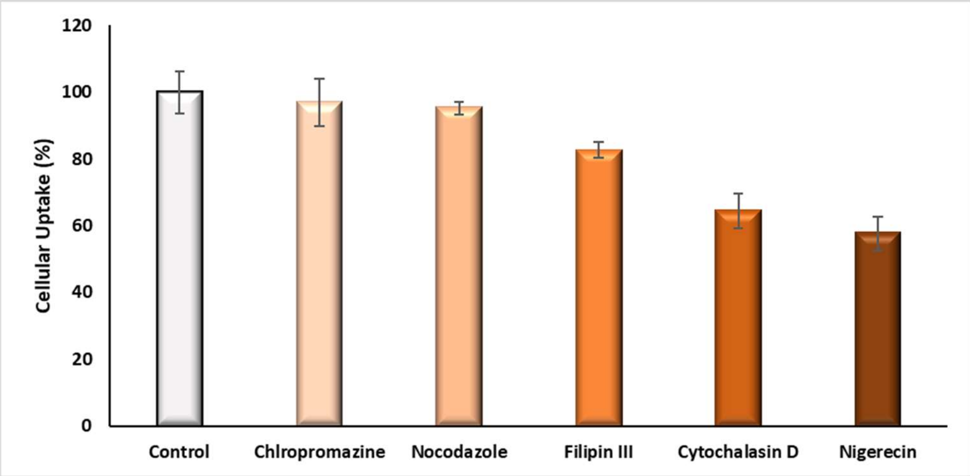

Figure 41 - Effect of different inhibitors on hMSC cells internalization pathways of Nanogel-20 after 6h of incubation at 37°C. Chlorpromazine inhibits clathrin-mediated endocytosis, nocozadole inhibits phagocytosis, filipin III inhibits caveolae-mediated endocytosis, cytochalasin D inhibits macropinocytosis and nigericin is a lysosomotropic agent. Note: Flow cytometry values were normalized against the cells with no inhibitor. The results were analyzed and compared with the cells with no inhibitor and all data represent the mean ± standard deviation (n = 3).

Chlorpromazine was used to evaluate the role of clathrin-mediated endocytosis as it disrupts the formation of the clathrin-coated vesicles, nocodazole inhibits phagocytosis through the depolymerization of the microtubules needed for this pathway, and Filipin III inhibits caveolae-mediated endocytosis by disrupting cholesterol domains required for the formation of caveolae (298–302). The inhibition of clathrin-mediated endocytosis and phagocytosis had no effect on the internalization of the nanoparticles, suggesting no involvement of these pathways on their uptake. With the exposure to filipin III, a 17% reduction is verified, indicating a small involvement of caveolae in the uptake. However, considering the size of the nanoparticles, which is around 380 nm, and the size of caveosomes, known to measure 50 nm to 80 nm, it seems unlikely that the internalization would occur through this pathway (303). Macropinocytosis was inhibited using cytochalasin D, which depolymerizes the actin filaments needed in this pathway (304). It is possible to notice that the use of cytochalasin D negatively affected the uptake of the nanoparticles, with a decrease of 36%, indicating that this is the preferred pathway for their cellular uptake. Macropinosomes are known to measure between 0.2 µm to 5 µm, and entrap a large portion of the extracellular fluid, allowing for the non-selective uptake of nanoparticles and other compounds dissolved in it (305,306). As the nanoparticles that constitute Fl-Nanogel-20 measure roughly 380 nm, and with this factor being the most impactful on the defining the endocytic uptake pathway of nanoparticles, it is plausible that their uptake takes places through this mechanism (307). Nigericin is an ionophore, that specifically acts as K^+/H^+ antiporter, raising the pH of acidic compartments in the cells, and has been shown to reduce protein degradation by lysosomes due to their alkalization (308–310).

Here, it was used to evaluate the involvement of lysosomal compartments in the intracellular trafficking of the nanoparticles. The notorious decrease cause by its use suggests that the nanoparticles likely follow lysosomal trafficking inside the cells. This is important for drug delivery purposes as particles that follow the endosomal pathway without fusion with lysosomes may cross the cell without being degraded, being released in the cytoplasm or in other intracellular compartments, and particles that follow the lysosomal pathway will, most likely, suffer degradation and release its contents in the cell (237,297). To confirm these preliminary results, the investigation of the internalization pathways of the nanoparticles that constitute Fl-Nanogel-20 will be reinvestigated in the future. In particular, it will be important to evaluate the impact of the functionalization of the nanoparticles with FI since, as could be seen, it strongly affects nanoparticle's hydrodynamic diameter thus possibly affecting nanoparticle's mechanisms of cell internalization too.

4.14. Evaluation of osteogenic differentiation of hMSC cells

4.14.1. Quantitative assays

ALP Activity

Alkaline phosphatase is a membrane enzyme whose maximal expression is achieved during maturation of the extracellular matrix and that acts as a nucleation agent, being associated with the development of the bone cell phenotype, with its expression declining once the mineralization of the matrix occurs. Therefore, it is used as an earlier marker of osteogenic differentiation. It can be evaluated through its mRNA and protein expression, although assays to determine the enzyme activity are most commonly performed (278,311,312).

After 18 days of differentiation, the Nanogel-0 had a positive impact on ALP activity (Figure 41), being the improvements a consequence of the presence of laponite in the formulation. Indeed, it is well reported that, in the physiological environment, laponite is degraded and releases orthosilicic acid ($Si(OH)_4$), which has been shown to increase the gene expression of ALP in human osteosarcoma cells (MG-63), thus promoting the osteoblastic differentiation (260,313).

In the presence of alendronate, Nanogel-20 induced a notable increase in the activity of the enzyme, probably due to the alendronate osteogenic inducing properties together with Laponite®-based nanoparticles, presumably because the nanoparticles were capable of encapsulating alendronate, increasing its delivery into the cells, and consequently allowing it to reach its target in the cell while promoting hMSC cells differentiation into osteoblasts. This effect was not evident when the cells were exposed to the free compound, possibly due to its incapacity to solely target the cells and also due to some cytotoxic effect of the unprotected compound in the cell culture medium.

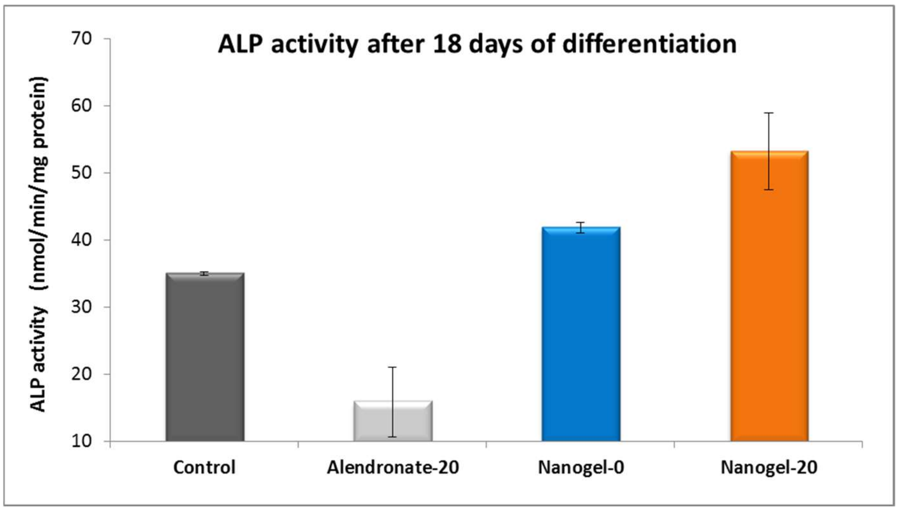

Figure 42 - Alkaline phosphatase activity (nmol/min/mg protein) after 18 days of differentiation. Note: All data represent the mean ± standard deviation (n = 3). Alendronate-20 and Nanogel-20 were previously diluted to 10 μM alendronate concentration to minimize cytotoxicity on hMSC cells. Nanogel-0 was also diluted accordingly. Control sample contains 1 nM dexamethasone, 5 mM β-glycerophosphate and 250 μM ascorbic acid.

Osteocalcin Expression

Osteocalcin is the most abundant non-collagenous protein in the extracellular matrix of bone tissue, where it acts as a regulator of bone mineralization and bone turnover, having higher expression in the later stages of the osteoblastic differentiation, thus being used as a later marker of osteogenic differentiation (280,314,315).

Analyzing the expression of this protein after the 18-day of differentiation, one can verify that all solutions tested had a beneficial effect in its expression in comparison to the control (Figure 42), with the biggest enhancements being those of the free alendronate solution and the alendronate-containing nanogel (Nanogel-20), though Nanogel-0 also lead to a noticeable improvement.

This indicates that alendronate is the most stimulating component in the formulation for the expression of osteocalcin, drastically improving it in the remaining healthy cells. However, based on the increased expression caused by Nanogel-0, this also validates the osteogenic inducting properties of laponite and highlights those of the overall nanogel formulation.

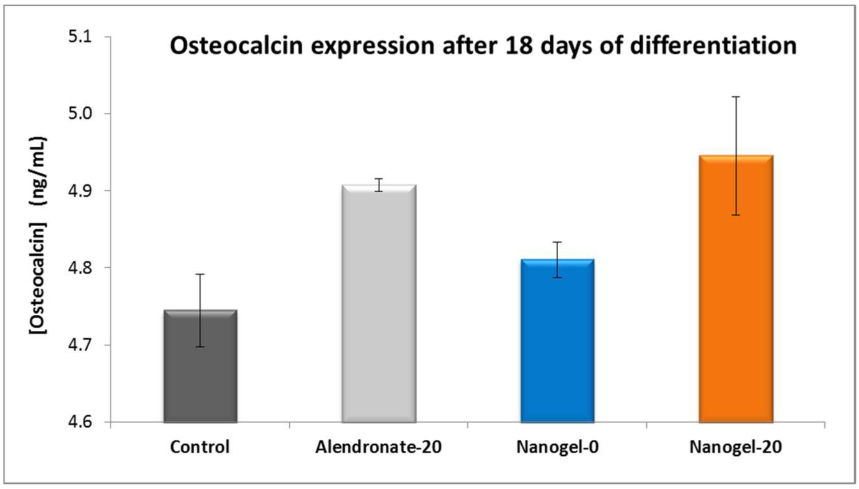

Figure 43 - Osteocalcin expression (ng/mL) after 18 days of differentiation into osteoblasts. Note: All data represent the mean ± standard deviation (n = 3). Alendronate-20 and Nanogel-20 were previously diluted to 10 µM alendronate concentration to minimize cytotoxicity on hMSC cells. Nanogel-0 was also diluted accordingly. Control sample contains 1 nM dexamethasone, 5 mM β-glycerophosphate and 250 µM ascorbic acid.

4.14.2. Qualitative assays

ALP Staining

Alkaline phosphatase staining is a qualitative colorimetric assay that detects the activity of this enzyme by the presence of brownish-yellow spots. The results from this staining (Figure 43) were consistent with the ones of the ALP activity assay. One can note the various sparse spots in the image that indicate the decrease in ALP activity, when cells were exposed to the free alendronate solution, while both nanogels enhanced it, with more yellow and dark spots visible, being the presence of dark spotsdue to multilayer cell growth. This highlights not only the protection of alendronate and enhancement of its osteogenic inducting properties, but also the same properties verified, to a smaller degree, in Nanogel-0, due to the presence of laponite.

Alizarin Red and von Kossa Stainings

The final stage of the *in vitro* osteoblastic differentiation is considered the mineralization of the extracellular matrix, that occurs once osteoblasts are terminally differentiated, and that consists on the formation of calcium and phosphate deposits that will later mature into bone apatite (316,317). The Alizarin red staining is used to detect calcium and the von Kossa staining is used to visualize phosphate in the mineralized deposits.

In both of these stainings, the results obtained are in agreement with the results of the ALP staining (Figure 43). A drastic reduction of the mineralization occurs when free alendronate solution is used, as noted by the absence of calcium deposits in the Alizarin red staining and the few phosphate deposits detected in the von Kossa staining.

The nanogels, on the contrary lead to improvements in the mineralization, particularly with the use of the alendronate-loaded nanogel, that induced the formation of far more deposits in both staining assays, again demonstrating the osteogenic inducting properties of both nanogels, and the protection against alendronate's cytotoxic effects.

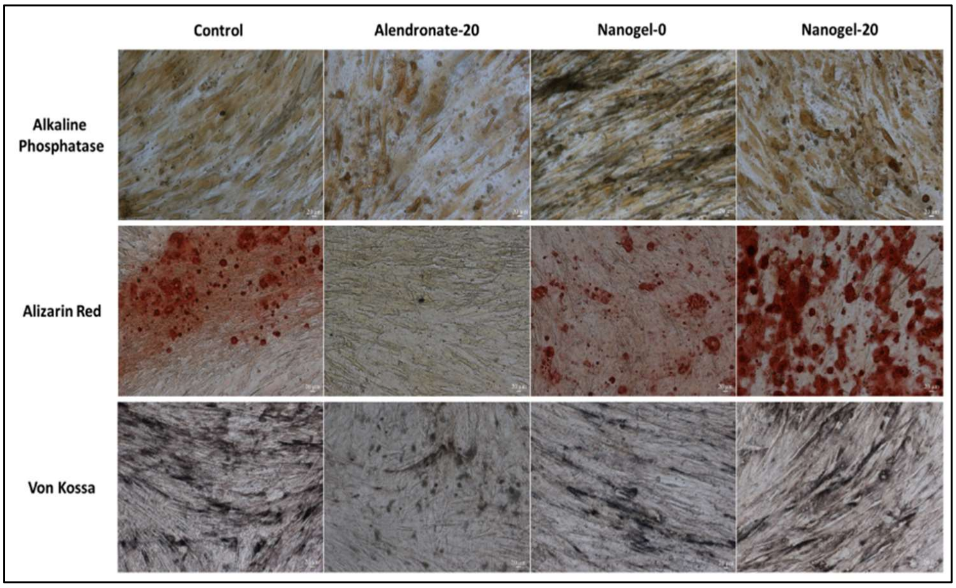

Figure 44 - Alkaline phosphatase activity, Alizarin Red and Von Kossa stainings on hMSC cells after 18 days of differentiation into osteoblasts. Note: Alendronate-20 and Nanogel-20 were previously diluted to 10 µM alendronate concentration to minimize cytotoxicity on hMSC cells. Nanogel-0 was also diluted accordingly. Control sample contains 1 nM dexamethasone, 5 mM β-glycerophosphate and 250 µM ascorbic acid.

5. CONCLUSIONS AND FUTURE WORK

Nanotechnology, nanomaterials and tissue engineering have become valuable tools in the field of medicine, in the diagnosis, management and treatment of various illnesses and health conditions, with research aiming to develop new therapies that are more cost-effective and biocompatible, and that present fewer side effects than the ones currently available, as well as drugs that present new properties such as response to different stimuli in the organism. The number of nano-based therapies available in the marked is increasing significantly and the industry is predicted to dramatically rise its market value in the next years.

Osteoporosis is the most common disease of the skeletal system, being a leading cause of morbidity in the elder population and its incidence is predicted to rise in the next years as the population ages. The use of nanotechnology for its treatment has been widely studied in the last decades as a mean to overcome the drawbacks associated with the most prescribed treatments for the illness, bisphosphonates. Many nanosystems have been developed and research for bisphosphonates delivery is ongoing in order to protect the drugs in the organism, minimizing their adverse side effects and increasing their bioavailability and efficiency.

In this thesis, laponite-based nanogels loaded with alendronate were prepared, physico-chemically characterized and in vitro biologically assayed as a possible new targeted drug delivery system for the treatment for osteoporosis. Nanosystems like the ones described in this thesis have never been reported in the literature.

The synthesis of the nanogels was successful, as well as their loading with alendronate at two different concentrations. Both nanogels, Nanogel-10 and Nanogel-20, exhibited high entrapment efficiencies and resulted in nanoparticles with a hydrodynamic diameter of approximately 180 nm. Moreover, the zeta potential of the nanogels became 8 - 9mV less negative upon alendronate loading.

The labelling of alendronate with a fluorescent compound, FITC, was accomplished in order to later prepare labelled-nanogels to use in the biological experiments. The synthesis proved to be successful, leading to the formation of a conjugate which was confirmed by the thiourea bond detected in the ^{1}H NMR spectrum, as well as by MALDI-TOF mass analysis. The nanogels prepared with FITC-labelled alendronate showed, however, higher hydrodynamic diameter values and much less negative zeta potentials than the correspondent non-labelled nanogels.

Importantly, storage seems not to be a problem regarding the prepared nanogels as the study of the impact of freezing/thawing, as well as of lyophilization, on nanogels' hydrodynamic diameter revealed that this parameter, although affected by those processes, returned to values close to the original ones after 24/48h. Moreover, the nanogels are capable of absorbing a high quantity of water and are biodegradable (releasing their active content) in conditions that simulate the physiological environment. Also, the nanogels proved to be efficient in their purpose, effectively encapsulating and protecting alendronate, causing a noticeable reduction in its cytotoxicity. They also showed no hemotoxicity, thus ensuring that no adverse effects will occur to the erythrocytes once the nanogel's nanoparticles reach the bloodstream and while they are in circulation.

The kinetic studies of cell uptake also demonstrated that the developed nanogels can be readily internalized by hMSCs and the analysis of the internalization pathways, using various inhibitors, showed that the macropinocytosis was the preferred mechanism for their uptake by cells. However, here, one should have in mind a possible interference on the results of the change in nanogel's properties (namely hydrodynamic diameter and zeta potential) caused by FITC labelling.

Finally, the nanogels enhanced the osteogenic induction properties of alendronate, as verified by the qualitative and quantitative assays done to assess osteogenesis. Globally, results point out that there was a synergistic effect when Laponite® is simultaneously being used with alendronate in the same nanosystem.

In the near future, and before proceeding to other studies, considering that the present work is of preliminary nature, part of the experiments will be repeated and improved in order to further validate the exposed data. Additionally, further studies using these nanogels are envisaged, namely for determining their porosity and response to different stimuli, such as calcium concentration, light, temperature and pH.

At a long term, studies will be also needed to ensure that the nanogel can safely surpass the harsh conditions of the gastrointestinal tract. Then, *in vivo* distribution and bioavailability of the nanogels after oral administration should also be assessed using animal model systems. Their bone-healing and regeneration properties will need to be evaluated too, for example through the use of the rat tibial bone defect model system (radiographic images and histological analysis should be performed following a treatment with the formulations).

6. BIBLIOGRAPHY

1. Cooper C, Ferrari S. IOF Compendium of Osteoporosis About IOF. 2017.
2. NIH Consensus Development Panel on Osteoporosis Prevention, Diagnosis and T. Osteoporosis Prevention, Diagnosis, and Therapy. JAMA - J Am Med Assoc. 2001;285:785–95.
3. Liu H-Y, Wu ATH, Tsai C-Y, Chou K-R, Zeng R, Wang M-F, et al. The balance between adipogenesis and osteogenesis in bone regeneration by platelet-rich plasma for age-related osteoporosis. Biomaterials. 2011;32:6773–80.
4. Feldstein A, Elmer PJ, Orwoll E, Herson M, Hillier T. Bone Mineral Density Measurement and Treatment for Osteoporosis in Older Individuals With Fractures. Arch Intern Med. 2003;163:2165.
5. What is Osteoporosis? | International Osteoporosis Foundation [Internet].
6. WHO. Prevention and management of osteoporosis. World Health Organ Tech Rep Ser. 2003;921:1–164.
7. Riggs BL, Wahner HW, Seeman E, Offord KP, Dunn WL, Mazess RB, et al. Changes in Bone Mineral Density of the Proximal Femur and Spine with Aging. J Clin Invest. 1982;70:716–23.
8. Emkey GR, Epstein S. Secondary Osteoporosis. Encycl Endocr Dis. 2014;28:911–35.
9. Daroszewska A. Prevention and treatment of osteoporosis in women: an update. Obstet Gynaecol Reprod Med. 2012;22:162–9.
10. Who are candidates for prevention and treatment for osteoporosis? In: Osteoporosis International. 1997. p. 1–6.
11. Hernlund E, Svedbom A, Ivergård M, Compston J, Cooper C, Stenmark J, et al. Osteoporosis in the European Union: medical management, epidemiology and economic burden. Arch Osteoporos. 2013;8:136.
12. Wright NC, Looker AC, Saag KG, Curtis JR, Delzell ES, Randall S, et al. The recent prevalence of osteoporosis and low bone mass in the United States based on bone mineral density at the femoral neck or lumbar spine. J Bone Miner Res. 2014;29:2520–6.
13. Cummings R, Kelsey J, Nevitt M, O'Dowd K. Epidemiology of osteoporosis and osteoporotic fractures. Epidemiol Rev. 1985;7:178–208.
14. Center JR, Nguyen T V., Schneider D, Sambrook PN, Eisman JA. Mortality after all major types of osteoporotic fracture in men and women: An observational study. Lancet. 1999;353:878–82.
15. Bliuc D, Nguyen ND, Milch VE, Nguyen T V., Eisman JA, Center JR. Mortality risk associated with low-trauma osteoporotic fracture and subsequent fracture in men and women. JAMA - J Am Med Assoc. 2009;301:513–21.
16. Melton LJ, Atkinson EJ, O'Connor MK, O'Fallon WM, Riggs BL. Bone density and fracture risk in men. J Bone Miner Res. 1998;13:1915–23.
17. Melton LJ, Chrischilles EA, Cooper C, Lane AW, Riggs BL. Perspective how many women

have osteoporosis? J Bone Miner Res. 1992;7:1005–10.

18. Kanis JA, Johnell O, Oden A, Sernbo I, Redlund-Johnell I, Dawson A, et al. Long-term risk of osteoporotic fracture in Malmo. Osteoporos Int. 2000;11:669–74.

19. Johnell O, Kanis JA. An estimate of the worldwide prevalence and disability associated with osteoporotic fractures. Osteoporos Int. 2006;17:1726–33.

20. Henríquez S, de Tejada Romero MJG. Osteoporosis. Med - Programa Form Médica Contin Acreditado. 2018;12:3499–505.

21. Bickerstaff DR, Kanis JA. Algodystrophy: An under-recognized complication of minor trauma. Rheumatology. 1994;33:240–8.

22. Silman AJ. The patient with fracture: the risk of subsequent fractures. Am J Med. 1995;98:12S-16S.

23. Keene GS, Parker MJ, Pryor GA. Mortality and Morbidity after Hip Fractures. BMJ. 1993;307:746–7.

24. Poor G, Atkinson EJ, O'Fallon WM, Melton LJ. Determinants of reduced survival following hip fractures in men. Clin Orthop Relat Res. 1995;260–5.

25. Osnes EK, Lofthus ACM, Meyer AHE, Falch AJA, Nordsletten L, Cappelen AI, et al. Consequences of hip fracture on activities of daily life and residential needs. Osteoporos Int. 2004;15:567–74.

26. Dhanwal DK, Dennison EM, Harvey NC, Cooper C. Epidemiology of hip fracture: Worldwide geographic variation. Indian J Orthop. 2011;45:15–22.

27. WHO. Publication of "The Burden of Musculoskeletal Conditions at the Start of the New Millennium." Vol. 52, Morbidity and Mortality Weekly Report. 2003. p. 1081.

28. Holroyd C, Cooper C, Dennison E. Epidemiology of osteoporosis. Best Pract Res Clin Endocrinol Metab. 2008;22:671–85.

29. Peasgood T, Herrmann K, Kanis JA, Brazier JE. An updated systematic review of health state utility values for osteoporosis related conditions. Osteoporos Int. 2009;20:853–68.

30. Kanis JA, Cooper C, Rizzoli R, Reginster JY. Executive summary of the European guidance for the diagnosis and management of osteoporosis in postmenopausal women. Calcif Tissue Int. 2019;104:235–8.

31. Johnell O, Kanis JA, Odén A, Sernbo I, Redlund-Johnell I, Petterson C, et al. Fracture risk following an osteoporotic fracture. Osteoporos Int. 2004;15:175–9.

32. Klotzbuecher CM, Ross PD, Landsman PB, Abbott TA, Berger M. Patients with Prior Fractures Have an Increased Risk of Future Fractures: A Summary of the Literature and Statistical Synthesis. J Bone Miner Res. 2010;15:721–39.

33. Tatangelo G, Watts J, Lim K, Connaughton C, Abimanyi-Ochom J, Borgström F, et al. The Cost of Osteoporosis, Osteopenia, and Associated Fractures in Australia in 2017. J Bone Miner Res. 2019;34:616–25.

34. Hopkins RB, Burke N, Von Keyserlingk C, Leslie WD, Morin SN, Adachi JD, et al. The current economic burden of illness of osteoporosis in Canada. Osteoporos Int. 2016;27:3023–32.

35. Si L, Winzenberg TM, Jiang Q, Chen M, Palmer AJ. Projection of osteoporosis-related fractures and costs in China: 2010–2050. Osteoporos Int. 2015;26:1929–37.

36. Japan Ministry of Health L and W. National Medical Expenditure Survey. In: Japan Ministry of Health Labour and Welfare (ed). Tokyo, Japan; 2016.

37. Rachner TD, Khosla S, Hofbauer LC. Osteoporosis: now and the future. Lancet. 2011;377:1276–87.

38. Ukon Y, Makino T, Kodama J, Tsukazaki H, Tateiwa D, Yoshikawa H, et al. Molecular-Based Treatment Strategies for Osteoporosis: A Literature Review. Int J Mol Sci. 2019;20:2557.

39. Brincat M, Gambin J, Brincat M, Calleja-Agius J. The role of vitamin D in osteoporosis. Maturitas. 2015;80:329–32.

40. Ross C, Taylor CL, Yaktine AL, Valle HB Del, editors. Institute of Medicine (US) Committee to Review Dietary Reference Intakes for Calcium and Vitamin D [Internet]. Dietary Reference Intakes for Calcium and Vitamin D. Washington (DC): National Academies Press (US); 2011.

41. Shea B, Wells G, Cranney A, Zytaruk N, Robinson V, Griffith L, et al. VII. Meta-Analysis of Calcium Supplementation for the Prevention of Postmenopausal Osteoporosis. Endocr Rev. 2002;23:552–9.

42. Reid IR, Mason B, Horne A, Ames R, Reid HE, Bava U, et al. Randomized Controlled Trial of Calcium in Healthy Older Women. Am J Med. 2006;119:777–85.

43. Bolland MJ, Leung W, Tai V, Bastin S, Gamble GD, Grey A, et al. Calcium intake and risk of fracture: systematic review. BMJ. 2015;351:4580.

44. Gallagher JC, Rapuri PB, Haynatzki G, Detter JR. Effect of Discontinuation of Estrogen, Calcitriol, and the Combination of Both on Bone Density and Bone Markers. J Clin Endocrinol Metab. 2002;87:4914–23.

45. Bolland MJ, Grey A, Reid IR. Should we prescribe calcium or vitamin D supplements to treat or prevent osteoporosis? Climacteric. 2015;18:22–31.

46. O'Donnell S, Moher D, Thomas K, Hanley DA, Cranney A. Systematic review of the benefits and harms of calcitriol and alfacalcidol for fractures and falls. J Bone Miner Metab. 2008;26:531–42.

47. Weaver CM, Alexander DD, Boushey CJ, Dawson-Hughes B, Lappe JM, LeBoff MS, et al. Calcium plus vitamin D supplementation and risk of fractures: an updated meta-analysis from the National Osteoporosis Foundation. Osteoporos Int. 2016;27:367–76.

48. Kahwati LC, Weber RP, Pan H, Gourlay M, LeBlanc E, Coker-Schwimmer M, et al. Vitamin D, Calcium, or Combined Supplementation for the Primary Prevention of Fractures in Community-Dwelling Adults. JAMA. 2018;319:1600–12.

49. Lewis JR, Calver J, Zhu K, Flicker L, Prince RL. Calcium supplementation and the risks of atherosclerotic vascular disease in older women: Results of a 5-year RCT and a 4.5-year follow-up. J Bone Miner Res. 2011;26:35–41.

50. Bolland MJ, Grey A, Reid IR. Calcium supplements and cardiovascular risk: 5 years on. Ther Adv drug Saf. 2013;4:199–210.

51. Rodrigues AM, Canhão H, Marques A, Ambrósio C, Borges J, Coelho P, et al. Portuguese recommendations for the prevention, diagnosis and management of primary osteoporosis - 2018 update. Acta Reumatol Port. 2018;2018:123–44.

52. Silva BC, Bilezikian JP. Parathyroid hormone: anabolic and catabolic actions on the

skeleton. Curr Opin Pharmacol. 2015;22:41–50.

53. Lim S-J, Yeo I, Yoon P-W, Yoo JJ, Rhyu K-H, Han S-B, et al. Incidence, risk factors, and fracture healing of atypical femoral fractures: a multicenter case-control study. Osteoporos Int. 2018;29:2427–35.

54. Langdahl BL, Silverman S, Fujiwara S, Saag K, Napoli N, Soen S, et al. Real-world effectiveness of teriparatide on fracture reduction in patients with osteoporosis and comorbidities or risk factors for fractures: Integrated analysis of 4 prospective observational studies. Bone. 2018;116:58–66.

55. Haas A V, LeBoff MS. Osteoanabolic Agents for Osteoporosis. J Endocr Soc. 2018;2:922–32.

56. Wysolmerski JJ. Parathyroid hormone-related protein: an update. J Clin Endocrinol Metab. 2012;97:2947–56.

57. Tella SH, Kommalapati A, Correa R. Profile of Abaloparatide and Its Potential in the Treatment of Postmenopausal Osteoporosis. Cureus. 2017;9:e1300.

58. Nakamura T, Sugimoto T, Nakano T, Kishimoto H, Ito M, Fukunaga M, et al. Randomized Teriparatide [Human Parathyroid Hormone (PTH) 1–34] Once-Weekly Efficacy Research (TOWER) Trial for Examining the Reduction in New Vertebral Fractures in Subjects with Primary Osteoporosis and High Fracture Risk. J Clin Endocrinol Metab. 2012;97:3097–106.

59. Tu KN, Lie JD, Wan CKV, Cameron M, Austel AG, Nguyen JK, et al. Osteoporosis: A Review of Treatment Options. P T. 2018;43:92–104.

60. Poole KES, van Bezooijen RL, Loveridge N, Hamersma H, Papapoulos SE, Löwik CW, et al. Sclerostin is a delayed secreted product of osteocytes that inhibits bone formation. FASEB J. 2005;19:1842–4.

61. Krause C, Korchynskyi O, Rooij K de, Weidauer SE, Gorter DJJ de, Bezooijen RL van, et al. Distinct Modes of Inhibition by Sclerostin on Bone Morphogenetic Protein and Wnt Signaling Pathways. J Biol Chem. 2010;285:41614–26.

62. McClung MR, Grauer A, Boonen S, Bolognese MA, Brown JP, Diez-Perez A, et al. Romosozumab in Postmenopausal Women with Low Bone Mineral Density. N Engl J Med. 2014;370:412–20.

63. Markham A. Romosozumab: First Global Approval. Drugs. 2019;79:471–6.

64. FDA Approves EVENITY romosozumabaqqg For The Treatment Of Osteoporosis In Postmenopausal Women At High Risk For Fracture [Internet]. 2019.

65. Chen LR, Ko NY, Chen KH. Medical treatment for osteoporosis: From molecular to clinical opinions. Int J Mol Sci. 2019;20.

66. Rossouw JE, Anderson GL, Prentice RL, LaCroix AZ, Kooperberg C, Stefanick ML, et al. Risks and benefits of estrogen plus progestin in healthy postmenopausal women: Principal results from the women's health initiative randomized controlled trial. J Am Med Assoc. 2002;288:321–33.

67. Torgerson DJ, Bell-Syer SEM. Hormone Replacement Therapy and Prevention of Nonvertebral Fractures. JAMA. 2001;285:2891–7.

68. Yates J, Barrett-Connor E, Barlas S, Chen YT, Miller PD, Siris ES. Rapid loss of hip fracture

protection after estrogen cessation: Evidence from the National Osteoporosis Risk Assessment. Obstet Gynecol. 2004;103:440–6.

69. Beral V, Chlebowski R, Hendrix S, Langer R, Banks E, Reeves G. Breast cancer and hormone-replacement therapy in the Million Women Study. Lancet (London, England). 2003;362:419–27.

70. Chlebowski RT, Hendrix SL, Langer RD, Stefanick ML, Gass M, Lane D, et al. Influence of Estrogen Plus Progestin on Breast Cancer and Mammography in Healthy Postmenopausal Women: The Women's Health Initiative Randomized Trial. J Am Med Assoc. 2003;289:3243–53.

71. de Villiers T, Gass M, Haines C, Hall J, Lobo R, Pierroz D, et al. Global consensus statement on menopausal hormone therapy. Climacteric. 2015;16:203–4.

72. Laurent M, Gielen E, Claessens F, Boonen S, Vanderschueren D. Osteoporosis in older men: Recent advances in pathophysiology and treatment. Best Pract Res Clin Endocrinol Metab. 2013;27:527–39.

73. Katznelson L, Finkelstein JS, Schoenfeld DA, Rosenthal DI, Anderson EJ, Klibanski A. Increase in bone density and lean body mass during testosterone administration in men with acquired hypogonadism. J Clin Endocrinol Metab. 1996;81:4358–65.

74. Golds G, Houdek D, Arnason T. Male Hypogonadism and Osteoporosis: The Effects, Clinical Consequences, and Treatment of Testosterone Deficiency in Bone Health. Int J Endocrinol. 2017;2017.

75. Ettinger B, Black DM, Mitlak BH, Knickerbocker RK, Nickelsen T, Genant HK, et al. Reduction of vertebral fracture risk in postmenopausal women with osteoporosis treated with raloxifene: Results from a 3-year randomized clinical trial. J Am Med Assoc. 1999;282:637–45.

76. Barrett-Connor E, Mosca L, Collins P, Geiger MJ, Grady D, Kornitzer M, et al. Effects of raloxifene on cardiovascular events and breast cancer in postmenopausal women. N Engl J Med. 2006;355:125–37.

77. Delmas PD, Ensrud KE, Adachi JD, Harper KD, Sarkar S, Gennari C, et al. Efficacy of raloxifene on vertebral fracture risk reduction in postmenopausal women with osteoporosis: Four-year results from a randomized clinical trial. J Clin Endocrinol Metab. 2002;87:3609–17.

78. Salari SP, Abdollahi M, Larijani B. Current, new and future treatments of osteoporosis. Rheumatol Int. 2011;31:289–300.

79. Silverman SL, Christiansen C, Genant HK, Vukicevic S, Zanchetta JR, De Villiers TJ, et al. Efficacy of bazedoxifene in reducing new vertebral fracture risk in postmenopausal women with osteoporosis: Results from a 3-year, randomized, placebo-, and active-controlled clinical trial. J Bone Miner Res. 2008;23:1923–34.

80. Miller PD, Chines AA, Christiansen C, Hoeck HC, Kendler DL, Lewiecki EM, et al. Effects of bazedoxifene on BMD and bone turnover in postmenopausal women: 2-Yr results of a randomized, double-blind, placebo-, and active-controlled study. J Bone Miner Res. 2008;23:525–35.

81. Tabatabaei-Malazy O, Salari P, Khashayar P, Larijani B. New horizons in treatment of osteoporosis. DARU, J Pharm Sci. 2017;25:1–16.

82. Pinkerton J V., Thomas S. Use of SERMs for treatment in postmenopausal women. J Steroid Biochem Mol Biol. 2014;142:142–54.

83. Meunier PJ, Roux C, Seeman E, Ortolani S, Badurski JE, Spector TD, et al. The Effects of Strontium Ranelate on the Risk of Vertebral Fracture in Women with Postmenopausal Osteoporosis. N Engl J Med. 2004;350:459–68.

84. Recommendation to restrict the use of Protelos / Osseor (strontium ranelate) | European Medicines Agency [Internet]. 2013.

85. Cummings SR, Martin JS, McClung MR, Siris ES, Eastell R, Reid IR, et al. Denosumab for prevention of fractures in postmenopausal women with osteoporosis. N Engl J Med. 2009;361:756–65.

86. Kearns AE, Khosla S, Kostenuik PJ. Receptor activator of nuclear factor κB ligand and osteoprotegerin regulation of bone remodeling in health and disease. Endocr Rev. 2008;29:155–92.

87. McClung MR, Michael Lewiecki E, Cohen SB, Bolognese MA, Woodson GC, Moffett AH, et al. Denosumab in postmenopausal women with low bone mineral density. N Engl J Med. 2006;354:821–31.

88. Lewiecki EM, Miller PD, McClung MR, Cohen SB, Bolognese MA, Liu Y, et al. Two-Year Treatment With Denosumab (AMG 162) in a Randomized Phase 2 Study of Postmenopausal Women With Low BMD. J Bone Miner Res. 2007;22:1832–41.

89. Bone HG, Bolognese MA, Yuen CK, Kendler DL, Miller PD, Yang YC, et al. Effects of denosumab treatment and discontinuation on bone mineral density and bone turnover markers in postmenopausal women with low bone mass. J Clin Endocrinol Metab. 2011;96:972–80.

90. Lin T, Wang C, Cai XZ, Zhao X, Shi MM, Ying ZM, et al. Comparison of clinical efficacy and safety between denosumab and alendronate in postmenopausal women with osteoporosis: A meta-analysis. Int J Clin Pract. 2012;66:399–408.

91. Nakamura T, Matsumoto T, Sugimoto T, Hosoi T, Miki T, Gorai I, et al. Clinical trials express: Fracture risk reduction with denosumab in Japanese postmenopausal women and men with osteoporosis: Denosumab Fracture Intervention Randomized Placebo Controlled Trial (DIRECT). J Clin Endocrinol Metab. 2014;99:2599–607.

92. Cernes R, Barnea Z, Biro A, Zandman-Goddard G, Katzir Z. Severe Hypocalcemia Following a Single Denosumab Injection. Isr Med Assoc J. 2017;19:719–21.

93. Yoshimura H, Ohba S, Yoshida H, Saito K, Inui K, Yasui R, et al. Denosumab-related osteonecrosis of the jaw in a patient with bone metastases of prostate cancer: A case report and literature review. Oncol Lett. 2017;14:127–36.

94. McClung MR. Denosumab for the treatment of osteoporosis. Osteoporos Sarcopenia. 2017;3:8–17.

95. Austin LA, Heath H. Calcitonin: Physiology and Pathophysiology. N Engl J Med. 1981;304:269–78.

96. Chesnut CH, Silverman S, Andriano K, Genant H, Gimona A, Harris S, et al. A randomized trial of nasal spray salmon calcitonin in postmenopausal women with established osteoporosis: The prevent recurrence of osteoporotic fractures study. Am J Med. 2000;109:267–76.

97. Henriksen K, Byrjalsen I, Andersen JR, Bihlet AR, Russo LA, Alexandersen P, et al. A randomized, double-blind, multicenter, placebo-controlled study to evaluate the efficacy and safety of oral salmon calcitonin in the treatment of osteoporosis in postmenopausal women taking calcium and vitamin D. Bone. 2016;91:122–9.

98. Rosen HN. Calcitonin in the prevention and treatment of osteoporosis - UpToDate [Internet]. 2018.

99. Menschutkin N. Ueber die Einwirkung des Chloracetyls auf phosphorige Säure. Ann der Chemie und Pharm. 1865;133:317–20.

100. Russell RGG. Bisphosphonates: the first 40 years. Bone. 2011;49:2–19.

101. Francis MD, Valent DJ. Historical perspectives on the clinical development of bisphosphonates in the treatment of bone diseases [Internet]. 2007.

102. Fleisch H, Russell RG, Francis MD. Diphosphonates inhibit hydroxyapatite dissolution in vitro and bone resorption in tissue culture and in vivo. Science. 1969;165:1262–4.

103. Francis MD, Russell RG, Fleisch H. Diphosphonates inhibit formation of calcium phosphate crystals in vitro and pathological calcification in vivo. Science. 1969;165:1264–6.

104. Minaire P, Depassio J, Berard E, Meunier PJ, Edouard C, Pilonchery G, et al. Effects of clodronate on immobilization bone loss. Bone. 1987;8:S63-8.

105. Francis MD, Gray JA, Griebstein WJ. The formation and influence of surface phases on calcium phosphate solids. Adv Oral Biol. 1968;3:83–120.

106. Russell RGG, Watts NB, Ebetino FH, Rogers MJ. Mechanisms of action of bisphosphonates: similarities and differences and their potential influence on clinical efficacy. Osteoporos Int. 2008;19:733–59.

107. Watts NB, Harris ST, Genant HK, Wasnich RD, Miller PD, Jackson RD, et al. Intermittent cyclical etidronate treatment of postmenopausal osteoporosis. N Engl J Med. 1990;323:73–9.

108. Reginster J, Minne HW, Sorensen OH, Hooper M, Roux C, Brandi ML, et al. Randomized trial of the effects of risedronate on vertebral fractures in women with established postmenopausal osteoporosis. Vertebral Efficacy with Risedronate Therapy (VERT) Study Group. Osteoporos Int. 2000;11:83–91.

109. Liberman UA, Weiss SR, Bröll J, Minne HW, Quan H, Bell NH, et al. Effect of oral alendronate on bone mineral density and the incidence of fractures in postmenopausal osteoporosis. N Engl J Med. 1995;333:1437–44.

110. Bone HG, Hosking D, Devogelaer JP, Tucci JR, Emkey RD, Tonino RP, et al. Ten Years' Experience with Alendronate for Osteoporosis in Postmenopausal Women. N Engl J Med. 2004;350:1189–99.

111. Harris ST, Watts NB, Genant HK, McKeever CD, Hangartner T, Keller M, et al. Effects of risedronate treatment on vertebral and nonvertebral fractures in women with postmenopausal osteoporosis: A randomized controlled trial. J Am Med Assoc. 1999;282:1344–52.

112. Black DM, Cummings SR, Karpf DB, Cauley JA, Thompson DE, Nevitt MC, et al. Randomised trial of effect of alendronate on risk of fracture in women with existing

vertebral fractures. Lancet. 1996;348:1535–41.

113. Boonen S, Laan RF, Barton IP, Watts NB. Effect of osteoporosis treatments on risk of non-vertebral fractures: Review and meta-analysis of intention-to-treat studies. Osteoporos Int. 2005;16:1291–8.

114. Van Staa TP, Abenhaim L, Cooper C. Use of cyclical etidronate and prevention of non-vertebral fractures. Br J Rheumatol. 1998;37:87–94.

115. McClung MR, Geusens P, Miller PD, Zippel H, Bensen WG, Roux C, et al. Effect of risedronate on the risk of hip fracture in elderly women. N Engl J Med. 2001;344:333–40.

116. Kyle RA. The Role of Bisphosphonates in Multiple Myeloma. Ann Intern Med. 2000;132:734.

117. Ibrahim A, Scher N, Williams G, Sridhara R, Li N, Chen G, et al. Approval summary for zoledronic acid for treatment of multiple myeloma and cancer bone metastases. Clin Cancer Res. 2003;9:2394–9.

118. Coleman RE, McCloskey E V. Bisphosphonates in oncology. Bone. 2011;49:71–6.

119. Clézardin P, Benzaïd I, Croucher PI. Bisphosphonates in preclinical bone oncology. Bone. 2011;49:66–70.

120. Rodan GA, Fleisch HA. Bisphosphonates: Mechanisms of Action. J Clin Invest. 1996;97:2692–6.

121. Schibler D, Russell RG, Fleisch H. Inhibition by pyrophosphate and polyphosphate of aortic calcification induced by vitamin D3 in rats. Clin Sci. 1968;35:363–72.

122. Favus MJ. Bisphosphonates for osteoporosis. N Engl J Med. 2010;363:2027–35.

123. Naidu A, Dechow PC, Spears R, Wright JM, Kessler HP, Opperman LA. The effects of bisphosphonates on osteoblasts in vitro. Oral Surgery, Oral Med Oral Pathol Oral Radiol Endodontology. 2008;106:5–13.

124. Ebrahimpour A, Francis M. No Bisphosphonate therapy in acute and chronic bone loss: Physical chemical considerations in bisphosphonate-related therapies. In: Bijvoet O, Fleisch H, Canfield R, Russell R, editors. Bisphosphonate on Bones. Amsterdam: Elsevier Science B. V.; 1995.

125. Russell RGG. Bisphosphonates: From Bench to Bedside. Ann N Y Acad Sci. 2006;1068:367–401.

126. Dunford JE, Thompson K, Coxon FP, Luckman SP, Hahn FM, Poulter CD, et al. Structure-activity relationships for inhibition of farnesyl diphosphate synthase in vitro and inhibition of bone resorption in vivo by nitrogen-containing bisphosphonates. J Pharmacol Exp Ther. 2001;296:235–42.

127. Ebetino FH, Bayless A V., Amburgey J, Ibbotson KJ, Dansereau S, Ebrahimpour A. Elucidation of a pharmacophore for the bisphosphonate mechanism of bone antiresorptive activity. Phosphorus, Sulfur Silicon Relat Elem. 1996;109:217–20.

128. Russell RGG, Mühlbauer RC, Bisaz S, Williams DA, Fleisch H. The influence of pyrophosphate, condensed phosphates, phosphonates and other phosphate compounds on the dissolution of hydroxyapatite in vitro and on bone resorption induced by parathyroid hormone in tissue culture and in thyroparathyroidectomised rats. Calcif Tissue Res. 1970;6:183–96.

129. Fleisch HA, Russell RGG, Bisaz S, Mühlbauer RC, Williams DA. The Inhibitory Effect of Phosphonates on the Formation of Calcium Phosphate Crystals in vitro and on Aortic and Kidney Calcification in vivo. Eur J Clin Invest. 1970;1:12–8.

130. Baroncelli GI, Bertelloni S. The use of bisphosphonates in pediatrics. Horm Res Paediatr. 2014;82:290–302.

131. Rodan G, Reszka A. Bisphosphonate Mechanism of Action. Curr Mol Med. 2005;2:571–7.

132. Luhmann T, Germershaus O, Groll J, Meinel L. Bone targeting for the treatment of osteoporosis. J Control Release. 2012;161:198–213.

133. Sahni M, Guenther HL, Fleisch H, Collin P, Martin TJ. Bisphosphonates act on rat bone resorption through the mediation of osteoblasts. J Clin Invest. 1993;91:2004–11.

134. Rogers M. New Insights Into the Molecular Mechanisms of Action of Bisphosphonates. Curr Pharm Des. 2005;9:2643–58.

135. Plotkin LI, Weinstein RS, Parfitt AM, Roberson PK, Manolagas SC, Bellido T. Prevention of osteocyte and osteoblast apoptosis by bisphosphonates and calcitonin. J Clin Invest. 1999;104:1363–74.

136. Plotkin LI, Manolagas SC, Bellido T. Dissociation of the pro-apoptotic effects of bisphosphonates on osteoclasts from their anti-apoptotic effects on osteoblasts/osteocytes with novel analogs. Bone. 2006;39:443–52.

137. Roelofs AJ, Ebetino FH, Reszka AA, Russell RGG, Rogers MJ. Bisphosphonates: Mechanisms of Action. In: Principles of Bone Biology, Two-Volume Set. Elsevier Inc.; 2008. p. 1737–67.

138. Storm T, Thamsborg G, Steiniche T, Genant HK, Sorensen OH. Effect of Intermittent Cyclical Etidronate Therapy on Bone Mass and Fracture Rate in Women with Postmenopausal Osteoporosis. N Engl J Med. 1990;322:1265–71.

139. Harris ST, Watts NB, Jackson RD, Genant HK, Wasnich RD, Ross P, et al. Four-year study of intermittent cyclic etidronate treatment of postmenopausal osteoporosis: three years of blinded therapy followed by one year of open therapy. Am J Med. 1993;95:557–67.

140. Cranney A, Guyatt G, Krolicki N, Welch V, Griffith L, Adachi JD, et al. A meta-analysis of etidronate for the treatment of postmenopausal osteoporosis. Osteoporos Int. 2001;12:140–51.

141. Cummings SR, Black DM, Thompson DE, Applegate WB, Barrett-Connor E, Musliner TA, et al. Effect of alendronate on risk of fracture in women with low bone density but without vertebral fractures. Results from the fracture intervention trial. J Am Med Assoc. 1998;280:2077–82.

142. Black DM, Thompson DE, Bauer DC, Ensrud K, Musliner T, Hochberg MC, et al. Fracture risk reduction with alendronate in women with osteoporosis: The fractureintervention trial. J Clin Endocrinol Metab. 2000;85:4118–24.

143. Black DM, Schwartz A V., Ensrud KE, Cauley JA, Levis S, Quandt SA, et al. Effects of continuing or stopping alendronate after 5 years of treatment: The Fracture Intervention Trial long-term extension (FLEX): A randomized trial. J Am Med Assoc. 2006;296:2927–38.

144. Schwartz A V., Bauer DC, Cummings SR, Cauley JA, Ensrud KE, Palermo L, et al. Efficacy of

continued alendronate for fractures in women with and without prevalent vertebral fracture: The FLEX trial. J Bone Miner Res. 2010;25:976–82.

145. Sorensen OH, Crawford GM, Mulder H, Hosking DJ, Gennari C, Mellstrom D, et al. Long-term efficacy of risedronate: a 5-year placebo-controlled clinical experience. Bone. 2003;32:120–6.

146. Mellström DD, Sörensen OH, Goemaere S, Roux C, Johnson TD, Chines AA. Seven years of treatment with risedronate in women with postmenopausal osteoporosis. Calcif Tissue Int. 2004;75:462–8.

147. Miller PD, Mcclung MR, Macovei L, Stakkestad JA, Luckey M, Bonvoisin B, et al. Monthly Oral Ibandronate Therapy in Postmenopausal Osteoporosis: 1-Year Results From the MOBILE Study. J Bone Miner Res. 2005;20:1315–22.

148. Reginster JY, Adami S, Lakatos P, Greenwald M, Stepan JJ, Silverman SL, et al. Efficacy and tolerability of once-monthly oral ibandronate in postmenopausal osteoporosis: 2 Year results from the MOBILE study. Ann Rheum Dis. 2006;65:654–61.

149. Miller PD, Recker RR, Reginster JY, Riis BJ, Czerwinski E, Masanauskaite D, et al. Efficacy of monthly oral ibandronate is sustained over 5 years: The MOBILE long-term extension study. Osteoporos Int. 2012;23:1747–56.

150. Eisman JA, Civitelli R, Adami S, Czerwinski E, Recknor C, Prince R, et al. Efficacy and tolerability of intravenous ibandronate injections in postmenopausal osteoporosis: 2-year results from the DIVA study. J Rheumatol. 2008;35:488–97.

151. Bianchi G, Czerwinski E, Kenwright A, Burdeska A, Recker RR, Felsenberg D. Long-term administration of quarterly IV ibandronate is effective and well tolerated in postmenopausal osteoporosis: 5-year data from the DIVA study long-term extension. Osteoporos Int. 2012;23:1769–78.

152. Rosen CJ, Hochberg MC, Bonnick SL, McClung M, Miller P, Broy S, et al. Treatment with once-weekly alendronate 70 mg compared with once-weekly risedronate 35 mg in women with postmenopausal osteoporosis: a randomized double-blind study. J Bone Miner Res. 2005;20:141–51.

153. Miller PD, Epstein S, Sedarati F, Reginster J-Y. Once-monthly oral ibandronate compared with weekly oral alendronate in postmenopausal osteoporosis: results from the head-to-head MOTION study. Curr Med Res Opin. 2008;24:207–13.

154. Reid IR, Brown JP, Burckhardt P, Horowitz Z, Richardson P, Trechsel U, et al. Intravenous zoledronic acid in postmenopausal women with low bone mineral density. N Engl J Med. 2002;346:653–61.

155. Black DM, Delmas PD, Eastell R, Reid IR, Boonen S, Cauley JA, et al. Once-yearly zoledronic acid for treatment of postmenopausal osteoporosis. N Engl J Med. 2007;356:1809–22.

156. Black DM, Reid IR, Boonen S, Bucci-Rechtweg C, Cauley JA, Cosman F, et al. The effect of 3 versus 6 years of Zoledronic acid treatment of osteoporosis: A randomized extension to the HORIZON-Pivotal Fracture Trial (PFT). J Bone Miner Res. 2012;27:243–54.

157. Black DM, Reid IR, Cauley JA, Cosman F, Leung PC, Lakatos P, et al. The effect of 6 versus 9 years of zoledronic acid treatment in osteoporosis: A randomized second extension to the HORIZON-pivotal fracture trial (PFT). J Bone Miner Res. 2015;30:934–44.

158. Eriksen EF, Díez-Pérez A, Boonen S. Update on long-term treatment with

bisphosphonates for postmenopausal osteoporosis: A systematic review. Bone. 2014;58:126–35.

159. McCloskey E, Selby P, Davies M, Robinson J, Francis RM, Adams J, et al. Clodronate reduces vertebral fracture risk in women with postmenopausal or secondary osteoporosis: Results of a double-blind, placebo-controlled 3-year study. J Bone Miner Res. 2004;19:728–36.

160. McCloskey E V, Beneton M, Charlesworth D, Kayan K, de Takats D, Dey A, et al. Clodronate Reduces the Incidence of Fractures in Community-Dwelling Elderly Women Unselected for Osteoporosis: Results of a Double-Blind, Placebo-Controlled Randomized Study. J Bone Miner Res. 2007;22:135–41.

161. Dominguez LJ, Galioto A, Ferlisi A, Alessi MA, Belvedere M, Putignano E, et al. Intermittent intramuscular clodronate therapy: A valuable option for older osteoporotic women [1]. Age Ageing. 2005;34:633–6.

162. Forni GL, Perrotta S, Giusti A, Quarta G, Pitrolo L, Cappellini MD, et al. Neridronate improves bone mineral density and reduces back pain in β-thalassaemia patients with osteoporosis: results from a phase 2, randomized, parallel-arm, open-label study. Br J Haematol. 2012;158:274–82.

163. Matsumoto T, Hagino H, Shiraki M, Fukunaga M, Nakano T, Takaoka K, et al. Effect of daily oral minodronate on vertebral fractures in Japanese postmenopausal women with established osteoporosis: A randomized placebo-controlled double-blind study. Osteoporos Int. 2009;20:1429–37.

164. Hagino H, Shiraki M, Fukunaga M, Nakano T, Takaoka K, Ohashi Y, et al. Three years of treatment with minodronate in patients with postmenopausal osteoporosis. J Bone Miner Metab. 2012;30:439–46.

165. Bartl R, Frisch B, von Tresckow E, Bartl C. Bisphosphonates from A-Z. Bisphosphonates in Medical Practice. Springer Berlin Heidelberg; 2007. 221–228 p.

166. Hegde S, Schmidt M. To Market, To Market - 2008. Annu Rep Med Chem. 2009;44:577–632.

167. Ohishi T, Matsuyama Y. Minodronate for the treatment of osteoporosis. Ther Clin Risk Manag. 2018;14:729–39.

168. Gatti D, Viapiana O, Idolazzi L, Fracassi E, Adami S. Neridronic acid for the treatment of bone metabolic diseases. Expert Opin Drug Metab Toxicol. 2009;5:1305–11.

169. Parker LRW, Preuss C V. Alendronate - StatPearls - NCBI Bookshelf [Internet]. 2019.

170. Ross S, Samuels E, Gairy K, Iqbal S, Badamgarav E, Siris E. A meta-analysis of osteoporotic fracture risk with medication nonadherence. Value Heal. 2011;14:571–81.

171. Imaz I, Zegarra P, González-Enríquez J, Rubio B, Alcazar R, Amate JM. Poor bisphosphonate adherence for treatment of osteoporosis increases fracture risk: Systematic review and meta-analysis. Osteoporos Int. 2010;21:1943–51.

172. Cruz L, Fattal E, Tasso L, Freitas GC, Carregaro AB, Guterres SS, et al. Formulation and in vivo evaluation of sodium alendronate spray-dried microparticles intended for lung delivery. J Control Release. 2011;152:370–5.

173. Sutton SC, Engle K, Fix JA. Intranasal delivery of the bisphosphonate alendronate in the

rat and dog. Pharm Res. 1993;10:924–6.

174. Cremers SCLM, Pillai G (Colin), Papapoulos SE. Pharmacokinetics/Pharmacodynamics of Bisphosphonates. Clin Pharmacokinet. 2005;44:551–70.

175. Diab DL, Watts NB, Miller PD. Bisphosphonates: Pharmacology and Use in the Treatment of Osteoporosis. In: Osteoporosis: Fourth Edition. Elsevier Inc.; 2013. p. 1859–72.

176. Weiss HM, Pfaar U, Schweitzer A, Wiegand H, Skerjanec A, Schran H. Biodistribution and plasma protein binding of zoledronic acid. Drug Metab Dispos. 2008;36:2043–9.

177. Kasting GB, Francis MD. Retention of etidronate in human, dog, and rat. J Bone Miner Res. 1992;7:513–22.

178. Lin JH. Bisphosphonates: A review of their pharmacokinetic properties. Bone. 1996;18:75–85.

179. Baron R, Ferrari S, Russell RGG. Denosumab and bisphosphonates: Different mechanisms of action and effects. Bone. 2011;48:677–92.

180. P. D. Miller. The kidney and bisphosphonates. Bone. 2011;49:77–81.

181. Cremers S, Sparidans R, Den Hartigh J, Hamdy N, Vermeij P, Papapoulos S. A pharmacokinetic and pharmacodynamic model for intravenous bisphosphonate (pamidronate) in osteoporosis. Eur J Clin Pharmacol. 2002;57:883–90.

182. Khan SA, Kanis JA, Vasikaran S, Kline WF, Matuszewski BK, Mccloskey E V., et al. Elimination and biochemical responses to intravenous alendronate in postmenopausal osteoporosis. J Bone Miner Res. 1997;12:1700–7.

183. Åkesson K. New approaches to pharmacological treatment of osteoporosis. Bull World Health Organ. 2003;81:657–63.

184. Fazil M, Baboota S, Sahni JK, Ameeduzzafar, Ali J. Bisphosphonates: Therapeutics potential and recent advances in drug delivery. Drug Deliv. 2015;22:1–9.

185. Tanvetyanon T, Stiff PJ. Management of the adverse effects associated with intravenous bisphosphonates. Ann Oncol. 2006;17:897–907.

186. John Camm A. Review of the cardiovascular safety of zoledronic acid and other bisphosphonates for the treatment of osteoporosis. Clin Ther. 2010;32:426–36.

187. Gertz BJ, Holland SD, Kline WF, Matuszewski BK, Freeman A, Quan H, et al. Studies of the oral bioavailability of alendronate. Clin Pharmacol Ther. 1995;58:288–98.

188. Felsenberg, Dieter; Hoffmeister B, Amling M. Onkologie: Kiefernekrosen nach hoch dosierter Bisphosphonattherapie. Vol. 103, Dtsch Arztebl. 2006.

189. Bamias A, Bamia C, Moulopoulos LA, Kastritis E, Moulopoulos LA, Melakopoulos I, et al. Osteonecrosis of the Jaw in Cancer After Treatment With Bisphosphonates: Incidence and Risk Factors Scintigraphic studies in Multiple Myeloma View project Cancer View project Osteonecrosis of the Jaw in Cancer After Treatment With Bisphosphonates: Inciden. Artic J Clin Oncol. 2005;23:8580–7.

190. Schilcher J, Michaëlsson K, Aspenberg P. Bisphosphonate Use and Atypical Fractures of the Femoral Shaft. N Engl J Med. 2011;364:1728–37.

191. Park-Wyllie LY, Mamdani MM, Juurlink DN, Hawker GA, Gunraj N, Austin PC, et al. Bisphosphonate use and the risk of subtrochanteric or femoral shaft fractures in older

women. JAMA - J Am Med Assoc. 2011;305:783–9.

192. Abrahamsen B, Eiken P, Eastell R. Subtrochanteric and diaphyseal femur fractures in patients treated with alendronate: A register-based national cohort study. J Bone Miner Res. 2009;24:1095–102.

193. Cao G. Nanostructures and Nanomaterials. 2nd editio. Nanostructures and Nanomaterials. Imperial College Press; 2004.

194. Silva GA. Introduction to nanotechnology and its applications to medicine. Surg Neurol. 2004;61:216–20.

195. Zhang L, Gu FX, Chan JM, Wang AZ, Langer RS, Farokhzad OC. Nanoparticles in medicine: Therapeutic applications and developments. Clin Pharmacol Ther. 2008;83:761–9.

196. Sanvicens N, Marco MP. Multifunctional nanoparticles - properties and prospects for their use in human medicine. Trends Biotechnol. 2008;26:425–33.

197. Nikalje AP. Nanotechnology and its Applications in Medicine. Nanotechnol its Appl Med Med chem. 2015;5:81–089.

198. Tinkle S, Mcneil SE, Mühlebach S, Bawa R, Borchard G, Barenholz YC, et al. Nanomedicines: Addressing the scientific and regulatory gap. Ann N Y Acad Sci. 2014;1313:35–56.

199. Bowman D, Marino A, Sylvester D. The patent landscape of nanomedicines. Med Res Arch. 2017;5.

200. Morigi V, Tocchio A, Bellavite Pellegrini C, Sakamoto JH, Arnone M, Tasciotti E. Nanotechnology in Medicine: From Inception to Market Domination. J Drug Deliv. 2012;2012:1–7.

201. Nanomedicine Market Size Worth $350.8 Billion By 2025 | CAGR: 11.2% [Internet]. 2017.

202. Shmeeda H, Amitay Y, Gorin J, Tzemach D, Mak L, Ogorka J, et al. Delivery of zoledronic acid encapsulated in folate-targeted liposome results in potent in vitro cytotoxic activity on tumor cells. J Control Release. 2010;146:76–83.

203. Shmeeda H, Amitay Y, Tzemach D, Gorin J, Gabizon A. Liposome encapsulation of zoledronic acid results in major changes in tissue distribution and increase in toxicity. J Control Release. 2013;167:265–75.

204. Hengst V, Oussoren C, Kissel T, Storm G. Bone targeting potential of bisphosphonate-targeted liposomes. Preparation, characterization and hydroxyapatite binding in vitro. Int J Pharm. 2007;331:224–7.

205. Dolatabadi JEN, Hamishehkar H, Eskandani M, Valizadeh H. Formulation, characterization and cytotoxicity studies of alendronate sodium-loaded solid lipid nanoparticles. Colloids Surfaces B Biointerfaces. 2014;117:21–8.

206. Abd El-Hamid BN, Swarnakar NK, Soliman GM, Attia MA, Pauletti GM. High payload nanostructured lipid carriers fabricated with alendronate/polyethyleneimine ion complexes. Int J Pharm. 2018;535:148–56.

207. Wang G, Mostafa NZ, Incani V, Kucharski C, Uludağ H. Bisphosphonate-decorated lipid nanoparticles designed as drug carriers for bone diseases. J Biomed Mater Res Part A. 2012;100A:684–93.

208. He Y, Huang Y, Huang Z, Jiang Y, Sun X, Shen Y, et al. Bisphosphonate-functionalized coordination polymer nanoparticles for the treatment of bone metastatic breast cancer. J Control Release. 2017;264:76–88.

209. Raichur V, Vemula KD, Bhadri N, Razdan R. Zolendronic Acid-Conjugated PLGA Ultrasmall Nanoparticle Loaded with Methotrexate as a Supercarrier for Bone-Targeted Drug Delivery. AAPS PharmSciTech. 2017;18:2227–39.

210. Hein CD, Liu X-M, Chen F, Cullen DM, Wang D. The Synthesis of a Multiblock Osteotropic Polyrotaxane by Copper(I)-Catalyzed Huisgen 1,3-Dipolar Cycloaddition. Macromol Biosci. 2010;10:1544–56.

211. Monteil M, Lecouvey M, Landy D, Ruellan S, Mallard I. Cyclodextrins: A promising drug delivery vehicle for bisphosphonate. Carbohydr Polym. 2017;156:285–93.

212. Yamashita S, Katsumi H, Sakane T, Yamamoto A. Bone-targeting dendrimer for the delivery of methotrexate and treatment of bone metastasis. J Drug Target. 2018;26:818–28.

213. Ma X, He Z, Han F, Zhong Z, Chen L, Li B. Preparation of collagen/hydroxyapatite/alendronate hybrid hydrogels as potential scaffolds for bone regeneration. Colloids Surfaces B Biointerfaces. 2016;143:81–7.

214. Posadowska U, Parizek M, Filova E, Wlodarczyk-Biegun M, Kamperman M, Bacakova L, et al. Injectable nanoparticle-loaded hydrogel system for local delivery of sodium alendronate. Int J Pharm. 2015;485:31–40.

215. Rawat P, Manglani K, Gupta S, Kalam A, Vohora D, Ahmad FJ, et al. Design and Development of Bioceramic Based Functionalized PLGA Nanoparticles of Risedronate for Bone Targeting: In-vitro Characterization and Pharmacodynamic Evaluation. Pharm Res. 2015;32:3149–58.

216. Cheng TL, Valtchev P, Murphy CM, Cantrill LC, Dehghani F, Little DG, et al. A sugar-based phase-transitioning delivery system for bone tissue engineering. Eur Cell Mater. 2013;26:208–21.

217. Cheng TL, Murphy CM, Ravarian R, Dehghani F, Little DG, Schindeler A. Bisphosphonate-adsorbed ceramic nanoparticles increase bone formation in an injectable carrier for bone tissue engineering. J Tissue Eng. 2015;6:1–9.

218. Ross RD, Roeder RK. Binding affinity of surface functionalized gold nanoparticles to hydroxyapatite. J Biomed Mater Res Part A. 2011;99A:58–66.

219. Lee D, Heo DN, Kim HJ, Ko WK, Lee SJ, Heo M, et al. Inhibition of Osteoclast Differentiation and Bone Resorption by Bisphosphonate-conjugated Gold Nanoparticles. Sci Rep. 2016;6.

220. Conners C. Bisphosphonate Functionalized Gold Nanoparticles for the Study and Treatment of Osteoporotic Disease. 2017.

221. Mirković M, Radović M, Stanković D, Milanović Z, Janković D, Matović M, et al. 99mTc–bisphosphonate–coated magnetic nanoparticles as potential theranostic nanoagent. Mater Sci Eng C. 2019;102:124–33.

222. Lalatonne Y, Monteil M, Jouni H, Serfaty JM, Sainte-Catherine O, Lièvre N, et al. Superparamagnetic Bifunctional Bisphosphonates Nanoparticles: A Potential MRI Contrast Agent for Osteoporosis Therapy and Diagnostic. J Osteoporos. 2010;2010:1–7.

223. Gonzalez KA, Wilson LJ, Wu W, Nancollas GH. Synthesis and in vitro characterization of a tissue-selective fullerene: Vectoring C60(OH)16AMBP to mineralized bone. Bioorganic Med Chem. 2002;10:1991–7.

224. Dlamini N, Mukaya HE, Van Zyl RL, Chen CT, Zeevaart RJ, Mbianda XY. Synthesis, characterization, kinetic drug release and anticancer activity of bisphosphonates multi-walled carbon nanotube conjugates. Mater Sci Eng C. 2019;104:109967.

225. Klajnert B, Bryszewska M. Dendrimers: properties and applications. 2001;48:199–208.

226. Kalepu S, Sunilkumar K, Sudheer B, Mohanvarma M. Liposomal drug delivery system - A Comprehensive Review | Insight Medical Publishing. Int J Drug Dev Res. 2013;5:62–75.

227. Dufès C, Uchegbu IF, Schätzlein AG. Dendrimers in gene delivery. Adv Drug Deliv Rev. 2005;57:2177–202.

228. Oliveira JM, Salgado AJ, Sousa N, Mano JF, Reis RL. Dendrimers and derivatives as a potential therapeutic tool in regenerative medicine strategies - A review. Prog Polym Sci. 2010;35:1163–94.

229. Singh P. Dendrimers and their applications in immunoassays and clinical diagnostics. Biotechnol Appl Biochem. 2007;48:1–9.

230. Torchilin VP. Recent advances with liposomes as pharmaceutical carriers. Nat Rev Drug Discov. 2005;4:145–60.

231. Puri A, Loomis K, Smith B, Lee JH, Yavlovich A, Heldman E, et al. Lipid-based nanoparticles as pharmaceutical drug carriers: From concepts to clinic. Crit Rev Ther Drug Carrier Syst. 2009;26:523–80.

232. Mishra DK, Shandilya R, Mishra PK. Lipid based nanocarriers: a translational perspective. Nanomedicine Nanotechnology, Biol Med. 2018;14:2023–50.

233. Khatak S, Dureja H. Recent Techniques and Patents on Solid Lipid Nanoparticles as Novel Carrier for Drug Delivery. Recent Pat Nanotechnol. 2015;9:150–77.

234. Pillai O, Panchagnula R. Polymers in drug delivery. Curr Opin Chem Biol. 2001;5:447–51.

235. Neuse EW. Synthetic polymers as drug-delivery vehicles in medicine. Met Based Drugs. 2008;2008:469531.

236. Yadav HKS, Almokdad AA, Shaluf SIM, Debe MS. Polymer-Based Nanomaterials for Drug-Delivery Carriers. In: Mohapatra S, Ranjan S, Dasgupta N, Mishra R, Thomas S, editors. Nanocarriers for Drug Delivery. Elsevier; 2019. p. 531–56.

237. Petros RA, DeSimone JM. Strategies in the design of nanoparticles for therapeutic applications. Nat Rev Drug Discov. 2010;9:615–27.

238. Crini G. Review: A history of cyclodextrins. Chem Rev. 2014;114:10940–75.

239. Szejtli J. Introduction and general overview of cyclodextrin chemistry. Chem Rev. 1998;98:1743–53.

240. Newkome GR, Yao ZQ, Baker GR, Gupta VK. Micelles. Part 1. Cascade Molecules: A New Approach to Micelles. A [27]-Arborol. Vol. 50, Journal of Organic Chemistry. 1985. p. 2003–4.

241. Tomalia DA, Baker H, Dewald J, Hall M, Kallos G, Martin S, et al. A new class of polymers: Starburst-dendritic macromolecules. Polym J. 1985;17:117–32.

242. Huang D, Wu D. Biodegradable dendrimers for drug delivery. Mater Sci Eng C. 2018;90:713–27.

243. Eichenbaum GM, Kiser PF, Simon SA, Needham D. pH and ion-triggered volume response of anionic hydrogel microspheres. Macromolecules. 1998;31:5084–93.

244. Seyfoori A, Koshkaki MR, Majidzadeh-A K. Nanohybrid Stimuli-Responsive Microgels: A New Approach in Cancer Therapy. In: Holban A, Grumezescu A, editors. Nanoarchitectonics for Smart Delivery and Drug Targeting. William Andrew Publishing; 2016. p. 715–42.

245. Peppas NA, editor. Hydrogels in Medicine and Pharmacy. Boca Raton, FL: CRC Press; 1987.

246. Ratner BD, Hoffman AS, Schoen FJ, Lemons JE, editors. Biomaterials Science: An Introduction to Materials. third. Biomaterials Science: An Introduction to Materials: Third Edition. Academic Press; 2013.

247. Kulinets I. Biomaterials and their applications in medicine. In: Amato S, Ezzell R, editors. Regulatory Affairs for Biomaterials and Medical Devices. Woodhead Publishing; 2015. p. 1–10.

248. Sokolova V, Epple M. Bioceramic nanoparticles for tissue engineering and drug delivery. In: Tissue Engineering Using Ceramics and Polymers: Second Edition. Elsevier Inc.; 2014. p. 633–47.

249. Daniel M-C, Astruc D. Gold Nanoparticles: Assembly, Supramolecular Chemistry, Quantum-Size-Related Properties, and Applications toward Biology, Catalysis, and Nanotechnology. Chem Rev. 2004;104:293–346.

250. Yeh YC, Creran B, Rotello VM. Gold nanoparticles: Preparation, properties, and applications in bionanotechnology. Nanoscale. 2012;4:1871–80.

251. Chen X, Li QW, Wang XM. Gold nanostructures for bioimaging, drug delivery and therapeutics. In: Precious Metals for Biomedical Applications. Elsevier Ltd; 2014. p. 163–76.

252. Ross RD, Cole LE, Roeder RK. Relative binding affinity of carboxylate-, phosphonate-, and bisphosphonate-functionalized gold nanoparticles targeted to damaged bone tissue. J Nanoparticle Res. 2012;14:1175.

253. Bauer JS, Link TM. Advances in osteoporosis imaging. Eur J Radiol. 2009;71:440–9.

254. Gu H, Xu K, Xu C, Xu B. Biofunctional magnetic nanoparticles for protein separation and pathogen detection. Chem Commun. 2006;941–9.

255. Akbarzadeh A, Samiei M, Davaran S. Magnetic nanoparticles: Preparation, physical properties, and applications in biomedicine. Nanoscale Res Lett. 2012;7:144.

256. Tartaj P, Morales MP, Gonzalez-Carreño T, Veintemillas-Verdaguer S, Bomati-Miguel O, Roca AG, et al. Biomedical Applications of Magnetic Nanoparticles. In: Reference Module in Materials Science and Materials Engineering. Elsevier; 2016.

257. Maiti D, Tong X, Mou X, Yang K. Carbon-Based Nanomaterials for Biomedical Applications: A Recent Study. Front Pharmacol. 2019;9:1401.

258. Cha C, Shin SR, Annabi N, Dokmeci MR, Khademhosseini A. Carbon-based nanomaterials: Multifunctional materials for biomedical engineering. ACS Nano. 2013;7:2891–7.

259. Tomás H, Alves CS, Rodrigues J. Laponite®: A key nanoplatform for biomedical applications? Nanomedicine Nanotechnology, Biol Med. 2018;14:2407–20.

260. Thompson DW, Butterworth JT. The nature of laponite and its aqueous dispersions. J Colloid Interface Sci. 1992;151:236–43.

261. Gaharwar AK, Mihaila SM, Swami A, Patel A, Sant S, Reis RL, et al. Bioactive silicate nanoplatelets for osteogenic differentiation of human mesenchymal stem cells. Adv Mater. 2013;25:3329–36.

262. Pavlidou S, Papaspyrides CD. A review on polymer-layered silicate nanocomposites. Prog Polym Sci. 2008;33:1119–98.

263. Reffitt DM, Ogston N, Jugdaohsingh R, Cheung HFJ, Evans BAJ, Thompson RPH, et al. Orthosilicic acid stimulates collagen type 1 synthesis and osteoblastic differentiation in human osteoblast-like cells in vitro. Bone. 2003;32:127–35.

264. Mihaila SM, Frias AM, Pirraco RP, Rada T, Reis RL, Gomes ME, et al. Human adipose tissue-derived ssea-4 subpopulation multi-differentiation potential towards the endothelial and osteogenic lineages. Tissue Eng - Part A. 2013;19:235–46.

265. Mihaila SM, Gaharwar AK, Reis RL, Khademhosseini A, Marques AP, Gomes ME. The osteogenic differentiation of SSEA-4 sub-population of human adipose derived stem cells using silicate nanoplatelets. Biomaterials. 2014;35:9087–99.

266. Wang C, Wang S, Li K, Ju Y, Li J, Zhang Y, et al. Preparation of laponite bioceramics for potential bone tissue engineering applications. PLoS One. 2014;9:e99585.

267. Thompson K, Rogers MJ, Coxon FP, Crockett JC. Cytosolic Entry of Bisphosphonate Drugs Requires Acidification of Vesicles after Fluid-Phase Endocytosis. Mol Pharmacol. 2006;69:1624–32.

268. Walash MI, Metwally ME-S, Eid M, El-Shaheny RN. Validated spectrophotometric methods for determination of Alendronate sodium in tablets through nucleophilic aromatic substitution reactions. Chem Cent J. 2012;6:25.

269. Wang D, Miller S, Kopecková P, Kopecek J. Bone-targeting macromolecular therapeutics. Adv Drug Deliv Rev. 2005;57:1049–76.

270. Bull B, Houwen B, Koepke J, Simson E. Reference and selected procedures for the quantitative determination of hemoglobin in blood. 3rd editio. Wayne, Pa: NCCLS; 2000.

271. Standard Practice for Assessment of Hemolytic Properties of Materials, ASTM International. In: ASTM F756-17. West Conshohocken, PA: ASTM International; 2017.

272. International Committee for Standardization in Haematology. Recommendations for reference method for haemoglobinometry in human blood (ICSH standard EP 6/2: 1977) and specifications for international haemiglobincyanide reference preparation (ICSH standard EP 6/3: 1977). J Clin Pathol. 1978;31:139–43.

273. Dominici M, Le Blanc K, Mueller I, Slaper-Cortenbach I, Marini F., Krause DS, et al. Minimal criteria for defining multipotent mesenchymal stromal cells. The International Society for Cellular Therapy position statement. Cytotherapy. 2006;8:315–7.

274. O'Brien J, Wilson I, Orton T, Pognan F. Investigation of the Alamar Blue (resazurin) fluorescent dye for the assessment of mammalian cell cytotoxicity. Eur J Biochem. 2000;267:5421–6.

275. Czekanska EM. Assessment of cell proliferation with resazurin-based fluorescent dye. Methods Mol Biol. 2011;740:27–32.

276. Jaiswal N, Haynesworth SE, Caplan AI, Bruder SP. Osteogenic differentiation of purified, culture-expanded human mesenchymal stem cells in vitro. J Cell Biochem. 1997;64:295–312.

277. Langenbach F, Handschel J. Effects of dexamethasone, ascorbic acid and β-glycerophosphate on the osteogenic differentiation of stem cells in vitro. Stem Cell Res Ther. 2013;4:117.

278. Aubin JE. Regulation of Osteoblast Formation and Function. Rev Endocr Metab Disord. 2001;2:81–94.

279. Liu F, Malaval L, Aubin JE. Global amplification polymerase chain reaction reveals novel transitional stages during osteoprogenitor differentiation. J Cell Sci. 2003;116:1787–96.

280. Lian JB, Roufosse AH, Reit B, Glimcher MJ. Concentrations of osteocalcin and phosphoprotein as a function of mineral content and age in cortical bone. Calcif Tissue Int. 1982;34 Suppl 2:S82-7.

281. Bills CE, Eisenberg H, Pallante SL. Complexes of organic acids with calcium phosphate: the Von Kossa stain as a clue to the composition of bone mineral. Johns Hopkins Med J. 1974;128:194–207.

282. Oddone N, Zambrana AI, Tassano M, Porcal W, Cabral P, Benech JC. Cell uptake mechanisms of PAMAM G4-FITC dendrimer in human myometrial cells. J Nanoparticle Res. 2013;15.

283. Guo L, Wang C, Yang C, Wang X, Zhang T, Zhang Z, et al. Morpholino-terminated dendrimer shows enhanced tumor pH-triggered cellular uptake, prolonged circulation time, and low cytotoxicity. Polymer (Guildf). 2016;84:189–97.

284. Ananchenko G, Novakovic J, Tikhomirova A. Alendronate Sodium. Profiles Drug Subst Excipients Relat Methodol. 2013;38:1–33.

285. Ishida O, Maruyama K, Sasaki K, Iwatsuru M. Size-dependent extravasation and interstitial localization of polyethyleneglycol liposomes in solid tumor-bearing mice. Int J Pharm. 1999;190:49–56.

286. Goldberg M, Langer R, Jia X. Nanostructured materials for applications in drug delivery and tissue engineering. J Biomater Sci Polym Ed. 2007;18:241–68.

287. Fu Y-C, Fu T-F, Wang H-J, Lin C-W, Lee G-H, Wu S-C, et al. Aspartic acid-based modified PLGA–PEG nanoparticles for bone targeting: In vitro and in vivo evaluation. Acta Biomater. 2014;10:4583–96.

288. Peppas NA, Bures P, Leobandung W, Ichikawa H. Hydrogels in pharmaceutical formulations. Eur J Pharm Biopharm. 2000;50:27–46.

289. Porstmann B, Jung K, Schmechta H, Evers U, Pergande M, Porstmann T, et al. Measurement of lysozyme in human body fluids: Comparison of various enzyme immunoassay techniques and their diagnostic application. Clin Biochem. 1989;22:349–55.

290. Brouwer J, van Leeuwen-Herberts T, de Ruit MO van. Determination of lysozyme in serum, urine, cerebrospinal fluid and feces by enzyme immunoassay. Clin Chim Acta.

1984;142:21–30.

291. Evani SJ, Ramasubramanian AK. Hemocompatibility of nanoparticles. In: Nanobiomaterials Handbook. CRC Press; 2016. p. 31.

292. Stadie WC. A method for the determination of methemoglobin in blood. J Biol Chem. 1920;41:237–41.

293. Drabkin DL, Austin HJ. Spectrophotometric studies: II. Preparations from washed blood cells; nitric oxide hemoglobin and sulfhemoglobin. J Biol Chem. 1935;112:51–6.

294. McMahon HT, Gallop JL. Membrane curvature and mechanisms of dynamic cell membrane remodelling. Nature. 2005;438:590–6.

295. Shi Y, Massagué J. Mechanisms of TGF-β signaling from cell membrane to the nucleus. Cell. 2003;113:685–700.

296. Brown D, Gluck S, Hartwig J. Structure of the novel membrane-coating material in proton-secreting epithelial cells and identification as an H+ATPase. J Cell Biol. 1987;105:1637–48.

297. Behzadi S, Serpooshan V, Tao W, Hamaly MA, Alkawareek MY, Dreaden EC, et al. Cellular uptake of nanoparticles: journey inside the cell. Chem Soc Rev. 2017;46:4218–44.

298. Barros D, Lima SAC, Cordeiro-Da-Silva A. Surface functionalization of polymeric nanospheres modulates macrophage activation: Relevance in Leishmaniasis therapy. Nanomedicine. 2015;10:387–403.

299. Yao D, Ehrlich M, Henis YI, Leof EB. Transforming growth factor-β receptors interact with AP2 by direct binding to β2 subunit. Mol Biol Cell. 2002;13:4001–12.

300. Cannon GJ, Swanson JA. The macrophage capacity for phagocytosis. J Cell Sci. 1992;101:907–13.

301. Vasquez RJ, Howell B, Yvon AMC, Wadsworth P, Cassimeris L. Nanomolar concentrations of nocodazole alter microtubule dynamic instability in vivo and in vitro. Mol Biol Cell. 1997;8:973–85.

302. Jin Y, Song Y, Zhu X, Zhou D, Chen C, Zhang Z, et al. Goblet cell-targeting nanoparticles for oral insulin delivery and the influence of mucus on insulin transport. Biomaterials. 2012;33:1573–82.

303. Pelkmans L, Helenius A. Endocytosis via caveolae. Traffic. 2002;3:311–20.

304. Kanlaya R, Sintiprungrat K, Chaiyarit S, Thongboonkerd V. Macropinocytosis is the major mechanism for endocytosis of calcium oxalate crystals into renal tubular cells. Cell Biochem Biophys. 2013;67:1171–9.

305. Hewlett LJ, Prescott AR, Watts C. The coated pit and macropinocytic pathways serve distinct endosome populations. J Cell Biol. 1994;124:689–703.

306. Swanson JA, Yoshida S. Macropinocytosis. In: Encyclopedia of Cell Biology. Elsevier Inc.; 2015. p. 758–65.

307. He C, Hu Y, Yin L, Tang C, Yin C. Effects of particle size and surface charge on cellular uptake and biodistribution of polymeric nanoparticles. Biomaterials. 2010;31:3657–66.

308. Steinrauf LK, Czerwinski EW, Pinkerton M. Comparison of the monovalent cation complexes of monensin, nigericin, and dianemycin. Biochem Biophys Res Commun.

1971;45:1279–83.

309. Ohkuma S, Poole B. Fluorescence probe measurement of the intralysosomal pH in living cells and the perturbation of pH by various agents. Proc Natl Acad Sci U S A. 1978;75:3327–31.

310. Grinde B. Effect of carboxylic ionophores on lysosomal protein degradation in rat hepatocytes. Exp Cell Res. 1983;149:27–35.

311. Huang Z, Nelson ER, Smith RL, Goodman SB. The Sequential Expression Profiles of Growth Factors from Osteroprogenitors to Osteoblasts *In Vitro*. Tissue Eng. 2007;13:2311–20.

312. Marom R, Shur I, Solomon R, Benayahu D. Characterization of adhesion and differentiation markers of osteogenic marrow stromal cells. J Cell Physiol. 2005;202:41–8.

313. Reffitt D., Ogston N, Jugdaohsingh R, Cheung HF., Evans BA., Thompson RP., et al. Orthosilicic acid stimulates collagen type 1 synthesis and osteoblastic differentiation in human osteoblast-like cells in vitro. Bone. 2003;32:127–35.

314. Wolf G. Function of the Bone Protein Osteocalcin: Definitive Evidence. Nutr Rev. 1996;54:332–3.

315. Neve A, Corrado A, Cantatore FP. Osteocalcin: Skeletal and extra-skeletal effects. J Cell Physiol. 2013;228:1149–53.

316. Quarles LD, Yohay DA, Lever LW, Caton R, Wenstrup RJ. Distinct proliferative and differentiated stages of murine MC3T3-E1 cells in culture: An in vitro model of osteoblast development. J Bone Miner Res. 2009;7:683–92.

317. Boskey AL, Robey PG. The Composition of Bone. In: Primer on the Metabolic Bone Diseases and Disorders of Mineral Metabolism. Wiley; 2018. p. 84–92.

7. ANNEXES

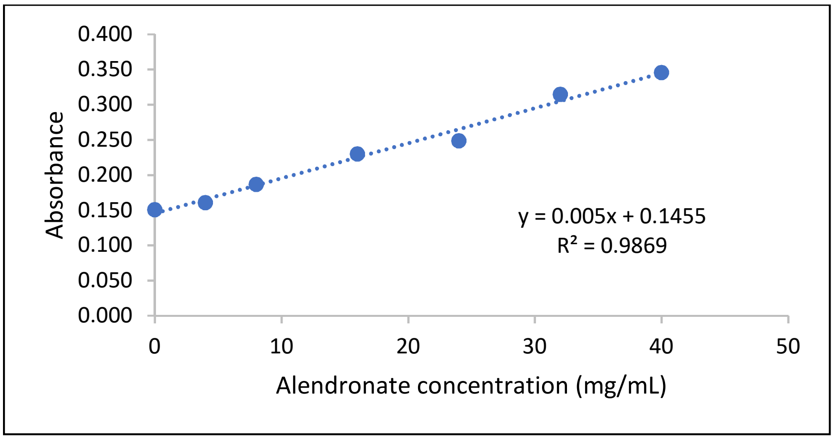

Figure 45 - Calibration curve with increasing alendronate concentrations used in the quantification of alendronate through the derivatization with DNFB method to determine its entrapment efficiency in the nanogel.

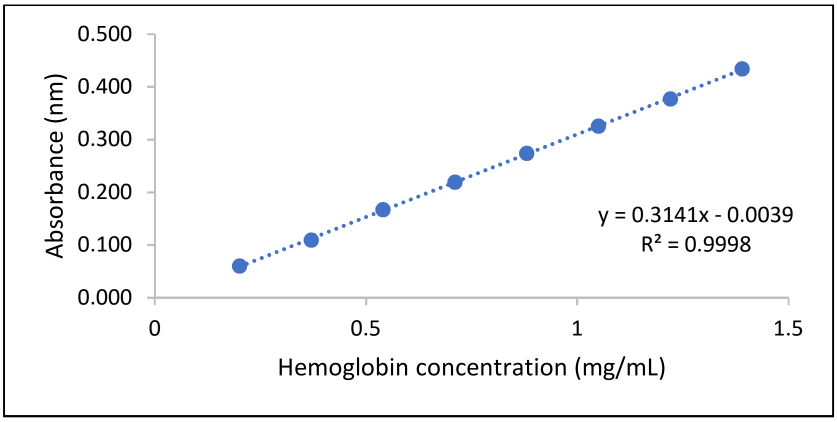

Figure 46 - Standard curve of the hemoglobin concentration

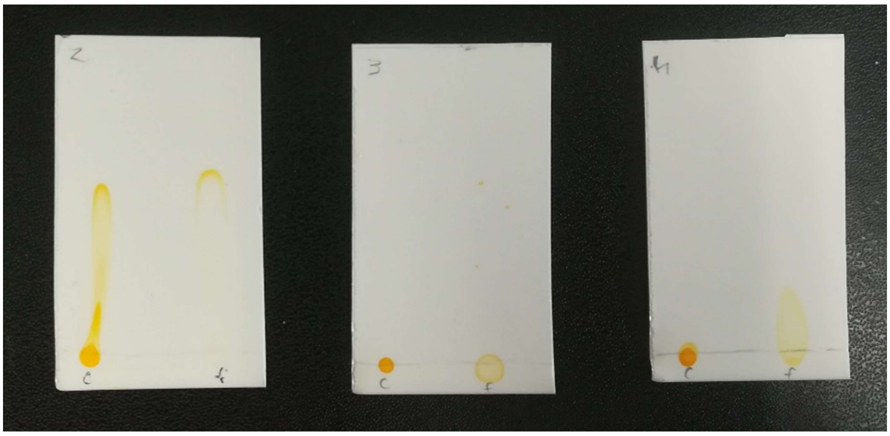

Figure 47 - Purification of the Alendronate-FITC conjugate by Thin layer chromatography on silica plates using various solvents as eluents: from left to right dichloromethane, hexane and a mix of dichloromethane and hexane in 1:1 volume ratio. The conjugate was applied on the life side of the plates and FITC was applied on the right side.

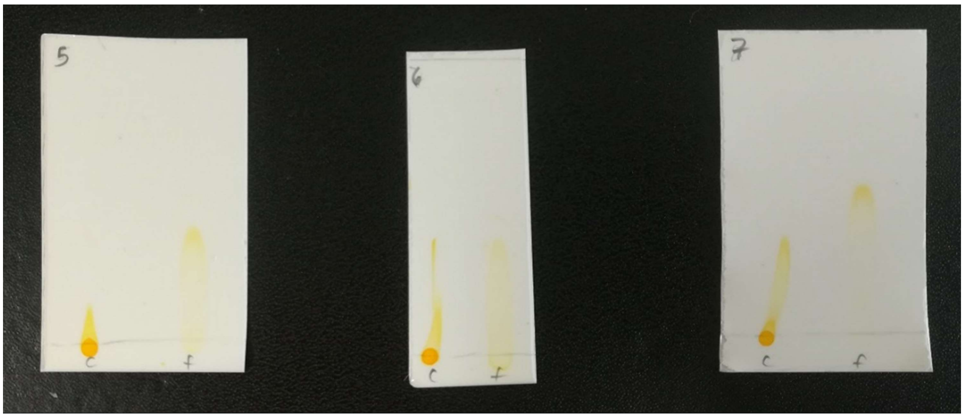

Figure 48 - Purification of the Alendronate-FITC conjugate by Thin layer chromatography on silica plates using as eluent a mix of dichloromethane and hexane in varying volume ratios. From left to right 1:2 ratio, 1:3 ratio and 1:5 ratio. The conjugate was applied on the life side of the plates and FITC was applied on the right side.

Figure 49 - Purification of the Alendronate-FITC conjugate by Thin layer chromatography on silica plate using as eluent a mix of tetrahydrofuran and methanol in 1:10 volume ratio. The conjugate was applied on the life side of the plates and FITC was applied on the right side.

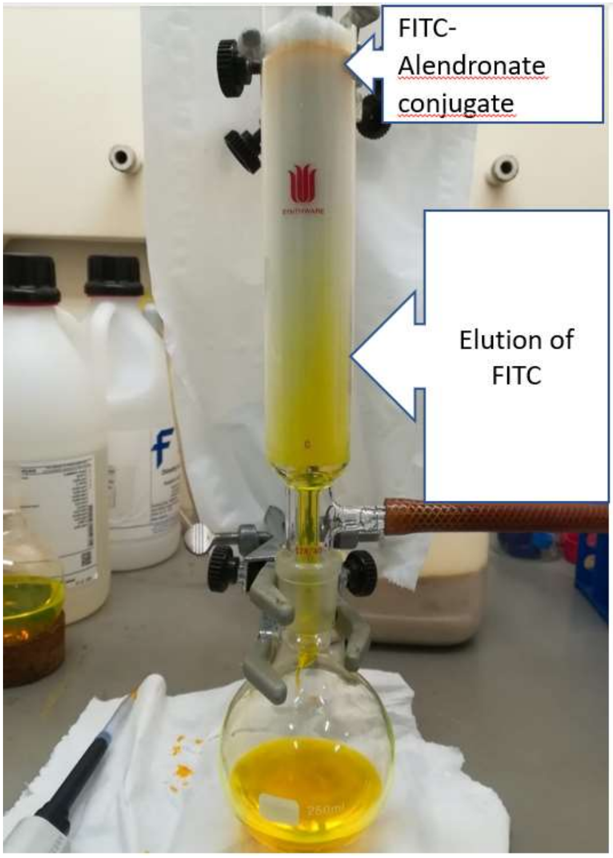

Figure 50 - Purification of the FITC-Alendronate conjugate by Flash Column Chromatography using THF:Methanol (1:10 volume ratio) as eluent. The elution of free FITC through the column is easily visible as well as the colored portion of silica at the top of the column, where the FITC-Alendronate conjugate is retained.

Projeto UID/QUI/00674/2019

Projeto M1420-01-0145-FEDER-000005